

**UNIVERSITÁ' DEGLI STUDI DI NAPOLI "FEDERICO II"**  
**FACOLTÁ DI INGEGNERIA**

*Dipartimento di Ingegneria Chimica, dei Materiali e  
della Produzione Industriale*



**DOTTORATO DI RICERCA**  
**IN**  
**INGEGNERIA DEI MATERIALI E DELLE STRUTTURE**

**XXIV CICLO**

**Effect of Halloysite nanotubes on properties of  
biodegradable PBAT/PHBV blend**

**Coordinatore**  
**Prof. Giuseppe Mensitieri**

**Dottoranda**  
**Ing. Barbara Vetrano**

**Tutor**  
**Ing. Pietro Russo**

# Index

<b>Abstract</b>	<b>5</b>
<b>Chapter I Introduction</b>	
1.1 General Introduction	7
1.2 Biodegradable polymers	9
1.2.1 Biodegradable polymer blends	10
1.3 Nanocomposites	11
1.4 Clay minerals	13
1.4.1 Modification of clays	15
Bibliography	19
<b>Chapter II Materials: Literature review</b>	
2.1 Aliphatic copolyesters: Poly(hydroxyalkanoates) (PHAs)	27
2.1.1 Synthesis	27
2.1.2 PHBV properties	30
2.1.3 PHBV composites	30
2.2 Aliphatic-aromatic copolyester: Poly(butylenes adipate-co-terephthalate) (PBAT)	31
2.2.1 PBAT composites	32
2.3 Halloysite nanotubes	34
2.3.1 Halloysite structure	34
2.3.2 Halloysite/ polymer composites	36
2.3.3 Modification of Halloysite nanotubes	37
Bibliography	39

## **Chapter II Film blowing process**

3.1 The process	46
3.2 Fundamental film blowing equations	50
Bibliography	53

## **Chapter IV Thermal and structural characterization of biodegradable blends filled with Halloysite nanotubes**

4.1 Introduction	55
4.2 Materials	57
4.2.1 Functionalization of HNTs	58
4.3 Preparation of nanocomposites and films	58
4.4 Characterization techniques	59
4.4.1 Fourier transform infrared spectroscopy (FTIR)	59
4.4.2 Thermogravimetric Analysis (TGA)	59
4.4.3 Differential scanning calorimetry (DSC)	59
4.4.4 Wide angle X ray diffraction (WAXD)	60
4.5 Results and discussion	61
4.6 Conclusions	78
Bibliography	80

## **Chapter V Rheological behavior of biodegradable nanocomposites filled with halloysite : effect of filler functionalization**

5.1 Introduction	85
5.2 Materials	86
5.3 Processing of biodegradable nanocomposites	87
5.4 Characterization techniques	88

5.4.1	Rheological characterization	88
5.4.1.1	Oscillatory measurements	90
5.4.1.2	Steady shear capillary measurements	91
5.5	Results and discussion	92
5.6	Conclusion	110
	Bibliography	112

## **Chapter VI Mechanical, Dynamic-Mechanical properties and morphological issues of PHBV based blown films containing Halloysite**

<b>6.1</b>	<b>Introduction</b>	<b>116</b>
<b>6.2</b>	<b>Materials</b>	<b>117</b>
<b>6.3</b>	<b>Preparation of bionanocomposite blown films</b>	<b>118</b>
<b>6.4</b>	<b>Characterization techniques</b>	<b>120</b>
6.4.1	Tensile test	120
6.4.2	Dynamic-mechanical analysis (DMA)	121
6.4.3	Morphological analysis	121
<b>6.5</b>	<b>Results and discussion</b>	<b>122</b>
	Bibliography	134

## **Chapter VII**

<b>Conclusion</b>	<b>137</b>
-------------------	------------

# Abstract

As an alternative for oil-based synthetic polymers (plastics) a lot of attention is paid nowadays to use biodegradable polymers. These polymers can be degraded upon disposal in bioactive environments by microorganisms, or by hydrolysis in buffer solutions or seawater.

The biodegradability depends on the polymer structure and it is independent of the origin of the raw materials, whether synthetic based or from natural resources[1]. These polymers degrade quickly in the natural environment and are not expected to produce any toxic component during their manufacture and disposal. Several applications of these polymers are in the fields of medicine, agriculture and packaging. Although studied and tested for decades, nowadays biodegradable plastics ("bioplastics" or "biopolymers") are gaining an important role in the market as a potential replacement of synthetic plastics, especially for pollution problems.

However, the biopolymer commercialization is still limited because of their fragility, their weak thermal stability and their high price.

Preparations of blends or composites are widely reported to be an efficient way of improving their performances. Tailoring composites with eco-friendly characteristics and specific properties incites researchers and industrials to develop materials produced from alternative resources to fossil fuel.

Incorporation of nano scale fillers can significantly enhance the mechanical, thermal and barrier performance in the biodegradable polymers [2].

The most widely used reinforcement is nanoclay due to its natural abundance and its very high aspect ratio.

The filler dispersion can be strongly affected by the type of clay, their pre-treatment and the way in which the polymer the compounding occurs. The nature of polymer-clay interface plays a very important role in the properties of polymer nanocomposites. Being naturally occurring clays generally highly hydrophilic species, they are naturally incompatible with a wide range of polymer types. A lot of researches has been conducted on organo-modified clays.

In this dissertation the processing and performances of a fully biodegradable and compostable blend and its nanocomposites have been investigated.

The specific materials used in the study include poly (butylene adipate-co-terephthalate) PBAT and poly(hydroxybutyrate-co-hydroxyvalerate) PHBV which are both biodegradable polymers. PBAT is an aliphatic-aromatic co-polyester and PHBV is a linear aliphatic co-polyester produced naturally by bacteria. These biodegradable nanocomposites can be used for packaging.

In order to enhance the properties of this blend, Halloysite nanotubes, a naturally occurring

aluminosilicate, have been added as fillers.

In an attempt to improve the dispersion of nanotubes within the polymer matrix, an organo-silane has been employed to modify the pristine surface of the clay.

Because of its unique hollow tubular structure, Halloysites can be used as delayed release mechanism for several purposes [3]. This adds value to the clay, expanding possible uses of the systems under investigation.

In fact, besides the protective function, the food packaging materials may extend food shelf life thanks to the addition of antibacterial, antifungal, antioxidant, antimicrobial constituents in the packaging applications [4].

The prepared composites have been filmed by melt blowing process. The blown film samples have been characterized in terms of thermal properties by differential scanning calorimetry (DSC) and thermogravimetry (TGA). Additionally, the crystalline properties data, obtained from the DSC study, and the orientation of the included nanotubes of clay have been verified using the X-ray diffraction (XRD). Dynamic shear rheological tests have been conducted using a rotational rheometer. Steady shear rheological data, instead, have been obtained from both rotational and capillary rheometer.

Modified Cross model was used to calculate the zero shear viscosity.

Finally, the mechanical behavior of blown films, analyzed via dynamic-mechanical analysis and tensile testing, has been correlated to the different orientation of the molecules and/or the halloysite nanotubes as well as their dispersion within the polymer matrix.

Globally, the best performances have been achieved with the use of modified Halloysite thanks to a more homogeneous distribution of filler within the polymer matrix as confirmed by the morphological analysis that was carried out by scanning electron microscope (SEM).

## **Bibliography**

- [1] Abraham JD, Kost J, Wiseman DM (1997) Handbook of biodegradable polymers, published by CRC Press Taylor & Francis Group
  
- [2] Someya Y, Nakazato T, Teramoto N, Shibata M J Appl Polym Sci 91,3,1463 (2004)
  
- [3] Han, J.H.. Innovations in Food Packaging. Elsevier Academic Press, London. 517 (2005).
  
- [4] Joussein, E.; Petit, S.; Churchman, J.; Theng, B.; Righi, D.; Delvaux, B., Halloysite Clay Minerals- A Review. Clay Minerals, 40, 383 (2005)

# Chapter I

---

## *Introduction*

## 1.1 General Introduction

Since the advent of synthetic polymer in the early 20th century, polymer and plastic products have been widely used every day in our life. In “The Graduate” (1967) Mike Nichols made a prophecy that “there’s a great future in plastics”. This was the truth, today plastics is used in sundry sectors like building, packaging, electronics, transportation etc., but its overexploitation constitutes the issue.

The increasingly limited availability and costs of fossil sources and the disposal after their life cycle are the main issues related to the petroleum-based plastics.

In the last few years, environmentalist concerns related to plastic dispersion into home waste have increased significantly. The strong and negative effect of the presence of indisposed plastic on the landscape and on the ecosystem is due to the nature of the plastic itself that makes it particularly resistant to degradation under normal ambient conditions.

A possible solution could be the recycling or incineration. Both the ways to dispose of waste plastic have disadvantages: plastics are often commingled with organic wastes making difficult and impractical the recycling of the underlying polymer without expensive cleaning and sanitizing procedures. Incineration is a waste treatment that involves the combustion of organic substances contained in waste materials [1]. The waste is converted into ash (formed by inorganic constituents that can take the form of solid lumps or particulates), fuel gas and heat (usable for producing electric power). This waste disposal technique can be dangerous if hazardous materials are not removed before incineration.

The *Year Book 2011 - Emerging issues in our global environment* of the United Nations Environment Programme analyze the impact of billion of plastic fragments into the oceans. The majority of plastics are hydrophobic but absorb nasty oils like pesticides and herbicides contained in the farm wastewater. The consumption of these plastic pieces by marine organisms as food by mistake begins poison pills in the whole food chain.

For more definitive solutions, it now aims to replace traditional plastics with degradable plastic. Research in this field is active worldwide in public and private institutions.

## 1.2 Biodegradable Polymer

Biodegradable polymers can be classified on the basis of their origin, which is naturally occurring or synthetic. However, the so called, “bio-plastics” are not in all cases biodegradable and compostable.

Only some bio-plastics, as well as some petroleum-based plastics, are compostable; this issue is often get muddled.

The biodegradability of plastics is dependent on the chemical structure of the material and on the constitution of the final product, but not on the resources used for its production.

The compostability is independent of the resources used as raw materials[2].

Compostable polymers are polymers which can be converted by micro-organisms into CO<sub>2</sub> and H<sub>2</sub>O in industrial composting plants and comply with standards, e.g. EN-13432 in Europe, ASTM-D-6400-04, ISO-17088, and DIN-V-54900. In Figure 1.1 the different classes of bio-polymers are summarized with some example.

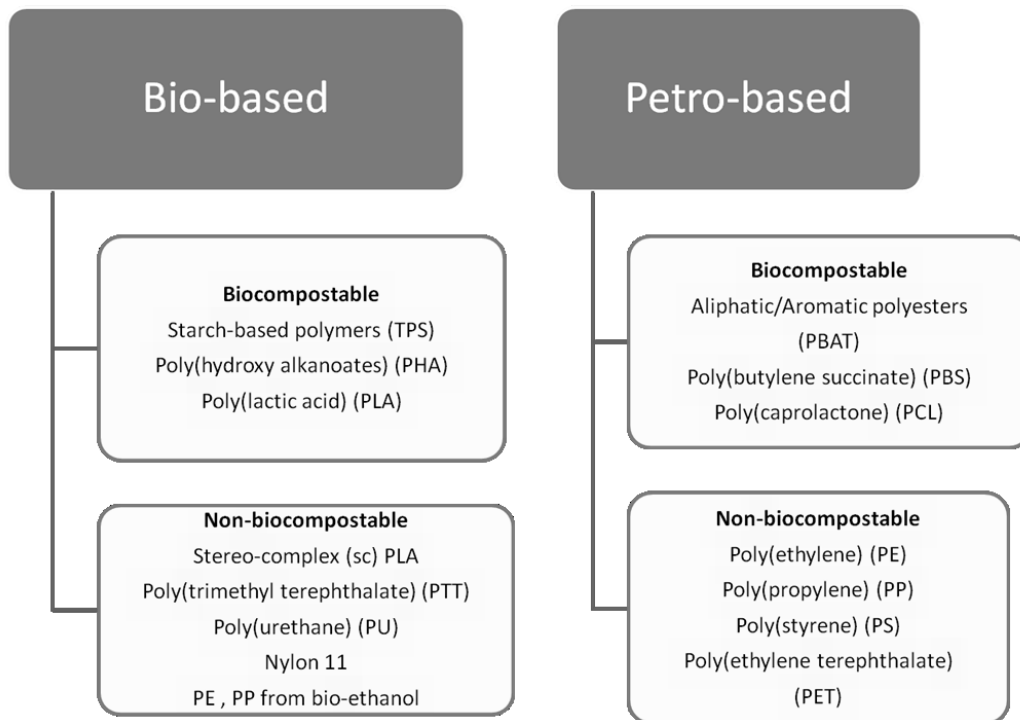


Fig. 1.1 Classification of petroleum-based and bio-based polymers [3]

In the short and medium term, the demand for bio-plastics may be appreciably enhanced if a positive dialogue among industry and the social movements concerned with the sustainability concept is established, emphasizing the benefits involved in the adoption of bio-plastic products. Governments at local and national levels can also promote the use of bio-plastics by passing legislation encompassing economic incentives to the adoption of bio-plastics in the industrial supply chain, and at the same time enforcing restrictions to the trade of environmental-unfriendly products[4]. However, some drawbacks to the expansion of the bio-plastic could be posed by their high costs, narrow processability window, and mechanical properties relatively inferior to those of other conventional polymers.

The improvements of these polymers are required in order to obtain more competitive materials preserving the biodegradability.

Different approaches have been studied to enhance the final materials properties:

- Blends with other suitable biodegradable polymers
- Introduction into the host matrix of small amounts of nanoparticle fillers.

## **1.2.1 Biodegradable polymer blends**

Biodegradable polymers can be classified according to their source [5]:

- polymers from renewable resource such as the agro-polymers from agro-resources (e.g., starch, cellulose),
- polymers obtained by microbial production, e.g., the polyhydroxyalkanoates,
- polymers chemically synthesized using monomers obtained from agro-resources, e.g., the poly(lactic acid),
- polymers obtained by chemical synthesis from fossil resources.

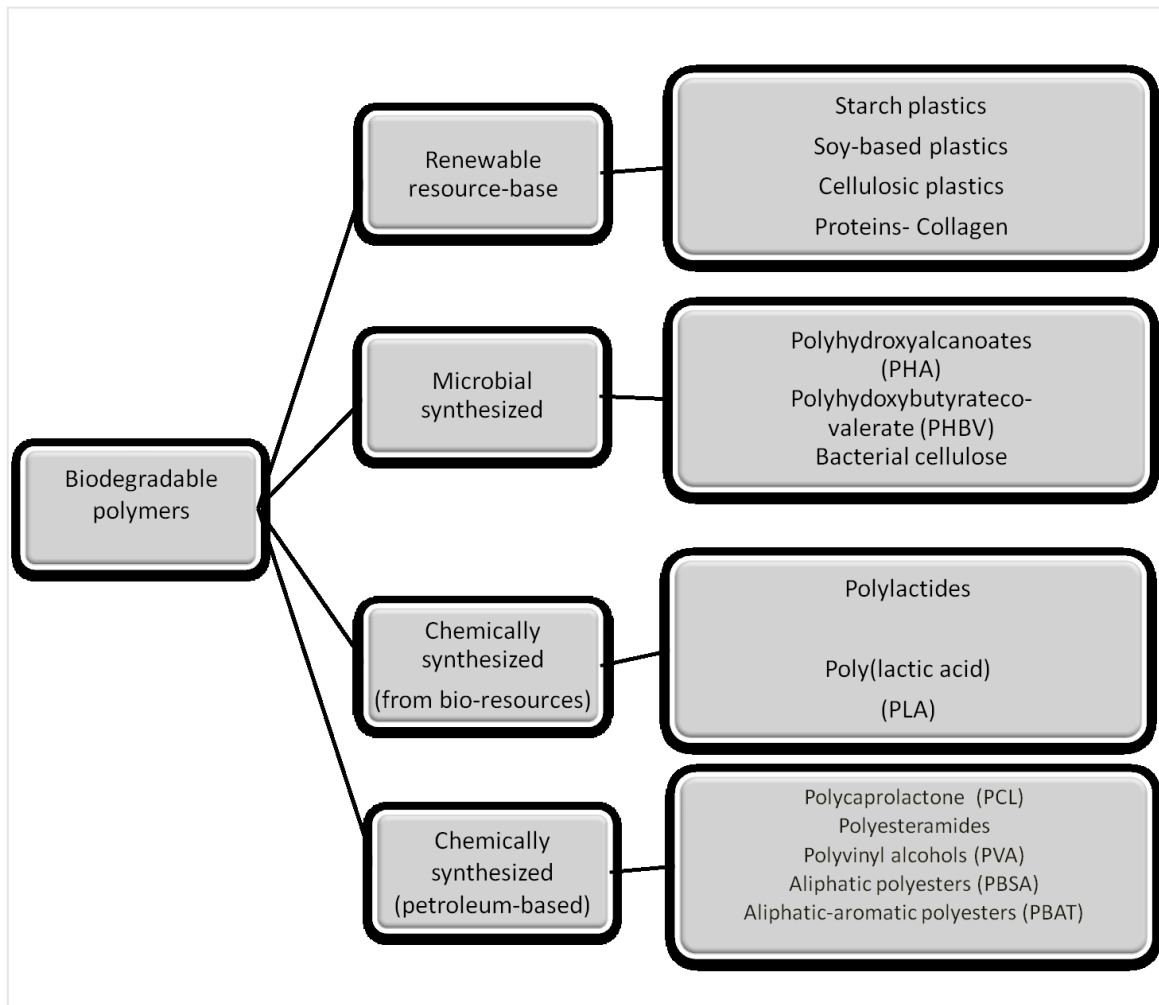


Fig.1.2 Schematic representation of biodegradable polymers

Polymer blending is a technique that allows to modify the properties using a conventional technology at low cost [6]. Polymer blends can be classified into several categories based on their miscibility which can be distinguished by their phase morphology and changes in glass transition temperatures.

Numerous biodegradable polymer blends have been developed in the last years. Today several biodegradable polymers are in the market especially Polylactic acid (PLA), the PHA's and thermoplastic starch based polymers[7,8].

PLA has been blended with plasticisers and a remarkable number of polymers such as poly( $\epsilon$ -caprolactone) (PCL) [9-12], polyhydroxy butyrate (PHB) [13,14], poly(butylene succinate) (PBS) [15], soy-bean oil (PSO) 16].

Blends with PLA or PCL bring about an improvement of PHA's processability [17-19] and polyhydroxy butyrate-co-valerate (PHBV) copolymers that belong to PHAs' family, was

modified by blending with many polymers such as poly vinyl chloride [20], poly(propylene carbonate) [21], poly(L-lactic) acid [22], poly(ethylene succinate) [23], polyolefins [24], and polycaprolactone [25].

TPS (thermoplastic starch) is used as a filler, lowering the price and enhancing the overall biodegradation rate. A completely biocompostable blend is obtained by adding it to PLA or PHBV[3]. Starch-based blends have been commercialized like Mater-Bi [26,27] (Novamont-Italy) or Bioplast [28] (Biotec-Germany) and different published works have shown the properties of TPS/PCL blends [27,29,30,31].

### 1.3. Nanocomposites

In contrast with traditional composites, where the reinforcements have dimensions in the order of micron, nanocomposites represent a new class of materials to which fillers with at least one of dimensions on the nano-scale are added. They have unique properties not shared by the conventional composites as well as the added value to use low filler percentages respect to composites ( up to 30-40 wt%), enabling easier processability.

The matrix/filler compatibility, the filler dispersion within the matrix and the aspect ratio (i.e. surface to volume or length to thickness with platelets) are critical aspects to obtain nanocomposite properties enhancement.

Advantages deriving from nanocomposites' use may include decreased gas permeability [32,33] and flammability [34], increased strength and heat resistance [35], high modulus [36,37], and increased biodegradability of biodegradable polymers [38].

Three types of fillers can be defined according to how many dimensions are in the nanometric scale:

- 1) three dimensional nanoparticles (pseudo-spherical), all dimensions are in the order of nanometres,
- 2) bi dimensional nanoparticles (nanotubes or whiskers), with the third dimension larger than nanometric one

- 3) mono dimensional (sheet-like) nanoparticles, only one dimension is in the order of nanometres.

Today the market has focused its attention on nanoclay fillers[39].

The concept of polymer–clay nanocomposites (PCN) was developed in the late 1980s and have received intense attention since the study published by the Toyota Central Research Laboratories[40,41].

Several technologies are used for the preparation of PCN and the most common used are:

- *In-situ polymerization*: filler and monomers are mixed to let the monomer enter into clay's layers, than polymerization reaction is promoted, allowing polymer to grow into clay's galleries. During the mixing step, the monomers spread in between the sheets of the clay and they are attracted for the high polarity of the surfaces of clay platelets. Then, the polymerization begins using heating, radiation, catalyst or organic initiator[42-44].
- *Intercalation from solution*: the nanoclay and the polymer are dissolved in a polar organic solvent that has to be able to solubilise the polymer and favor the clay dispersion. Then the solvent evaporates or precipitates adding non miscible solvent enabling layers to be reunited by entangling polymer macromolecules into them and forming an ordered structure. However, this technique is environmentally unfriendly and economically prohibitive[45,46].
- *Melt blending*: clays and polymer are mixed in molten condition.  
This process is of great interest for the industry because it is possible to use it with conventional technologies as extrusion, which is a cheap and rapid technology. Furthermore the use of harsh organic solvents is not necessary reducing environmental impact and economic cost.

It is necessary to consider different parameters that can influence the latter process such as shear devise, time residence, stress shear and organo-treatment of the clays. Moreover it is

worth noting that polymer-clay interaction mechanisms (miscibility between polymer and clay, hydrogen bonding, electrostatic, coordination, etc.) depends on the polarity, molecular weight, hydrophobicity, reactive groups, etc. of the polymer and clay mineral type [47].

## 1.4 Clay minerals

Clay minerals are part of the larger class of silicate minerals: the phyllosilicates. The phyllosilicates are composed by tetrahedral and octahedral building units and they are also known as *layered silicates* due to their stacked structure of 1-nm silicate sheets with a variable basal distance [47]. The structure of tetrahedral sheet is made up of individual tetrahedrons in which one silicon atom is surrounded by four oxygens. The arrangement is a hexagonal pattern in which the basal oxygens are linked; while the apical oxygens take part in the adjacent octahedral sheet and they point up/down [48].

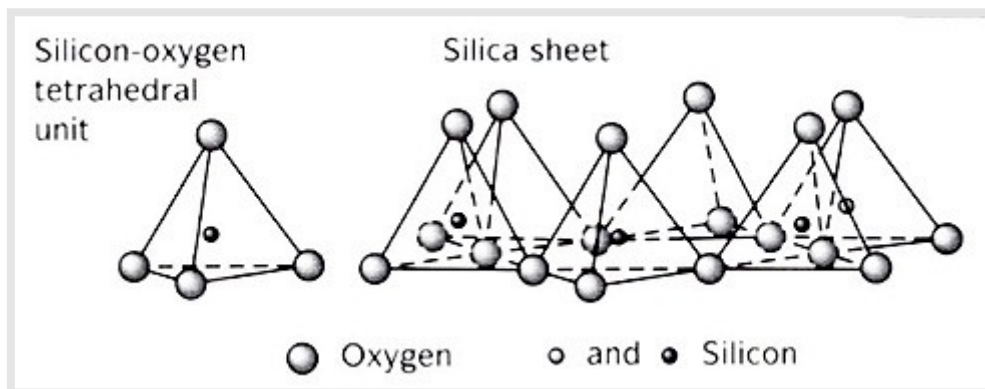


FIG.1.3 Silica tetrahedron and structure of tetrahedral sheet[49].

The alumina octahedral crystal structure consists of one aluminum atom tied to six oxygens and octahedral sheets are made up of individual octahedrons sharing edges composed of oxygen and hydroxyl anion groups coordinated by cations as Al, Mg,  $\text{Fe}^{3+}$  and  $\text{Fe}^{2+}$ . These octahedrons are arranged in a hexagonal pattern, too.

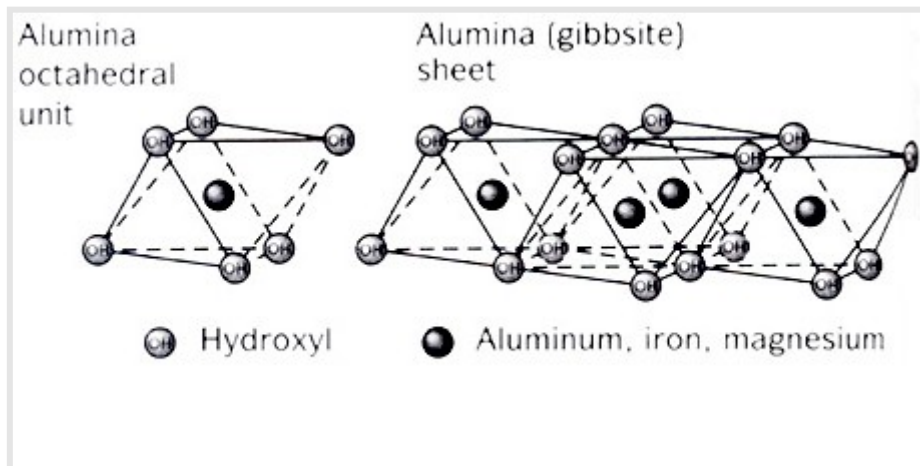


FIG.1.4 Alumina octahedron and structure of octahedral sheet[49].

There are two varieties of octahedral sheets: di-octahedral in which the cations are trivalent (i.e.  $\text{Al}^{3+}$ ) and the cation to oxygen ratio is 1:3 to maintain electric neutrality but one of the cation sites is vacant. When cations in octahedral sheet are divalent (+2) (usually Mg or  $\text{Fe}^{+2}$ ) then a tri-octahedral sheet is formed. In this case the cation to oxygen ratio is 1:2 and every lattice site is filled [50].

The classification of phyllosilicates is based on the number and the combination of tetrahedral, di- and tri-octahedral sheets. This family of clay minerals can be divided in two classes:

- *1:1 phyllosilicates* - one silica tetrahedral sheet and one alumina octahedral sheet combined to form a layer unit characterized by the fact that the apical oxygens of the tetrahedral sheet are also part of the octahedral sheet (e.g. Kaolinite) (Fig. 1.5 A)

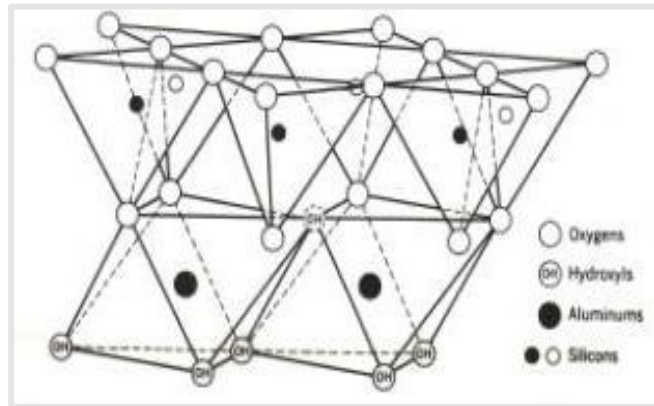


FIG. 1.5A Structure of 1:1 phyllosilicates [51]

- *2:1 phyllosilicates* - two silica tetrahedral sheets with a central alumina octahedral sheet (e.g. montmorillonite, saponite, etc.) (Fig.1.5 B)

The layered- silicates mainly used in nanocomposites belong to the latter family of phyllosilicates. The crystal structure is made up of two tetrahedral sheets of silica fused to an edge-shaped octahedral sheet of alumina or magnesia. The length of each layered sheet ranges from 30 nm to several micron and its thickness is about 1 nm. Layers stacking leads to a regular Van der Waals gap between the platelets called the *interlayer* or *the gallery*. With the exception of kaolinite, isomorphous substitutions is very common: a cation can be replaced by ions of lower valence ( $\text{Si}^{3+}$  in the tetrahedral sheet can be replaced by  $\text{Al}^{2+}$ , while  $\text{Al}^{2+}$  in the octahedral sheet may be replaced by  $\text{Li}^+$ ,  $\text{Mg}^{2+}$ ,  $\text{Fe}^{2+}$ ,  $\text{Fe}^{3+}$ ,  $\text{Zn}^{2+}$ , etc.). Isomorphous substitutions, as well as the presence of vacancies, can induce a negative charged surface of the clays layers. This negative charged surface is counterbalanced by alkali and alkaline earth cations ( $\text{Na}^+$ ,  $\text{Ca}^{++}$ ,  $\text{K}^+$ ) situated inside the galleries[42].

## Chapter I

---

The inorganic cations located in the galleries lead to an increase of the hydrophilic character of silicate surface and for this reason miscible with hydrophilic polymers such as poly(ethylene oxide) (PEO) [52] or poly(vinyl alcohol) (PVA) [53].

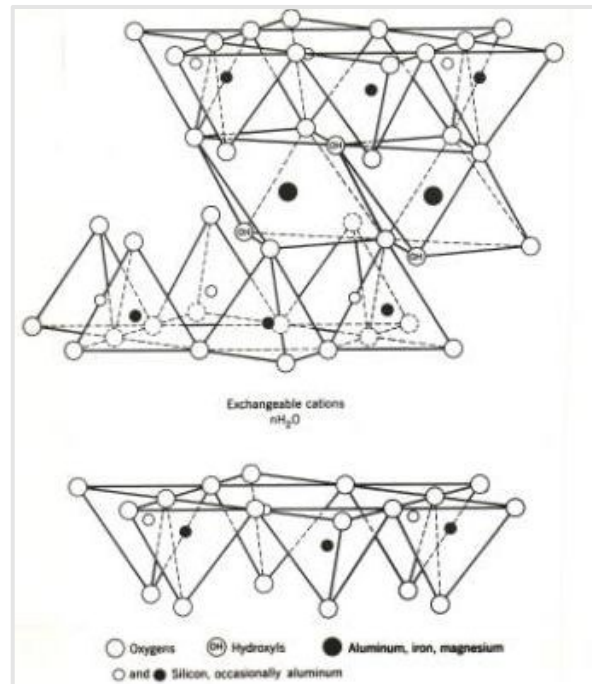


FIG. 1.5 B Structure of 2:1 phyllosilicates [51]

Thus, in order to make silicates miscible with organophilic polymers, it's required a chemical modification of the hydrophilic silicate surface.

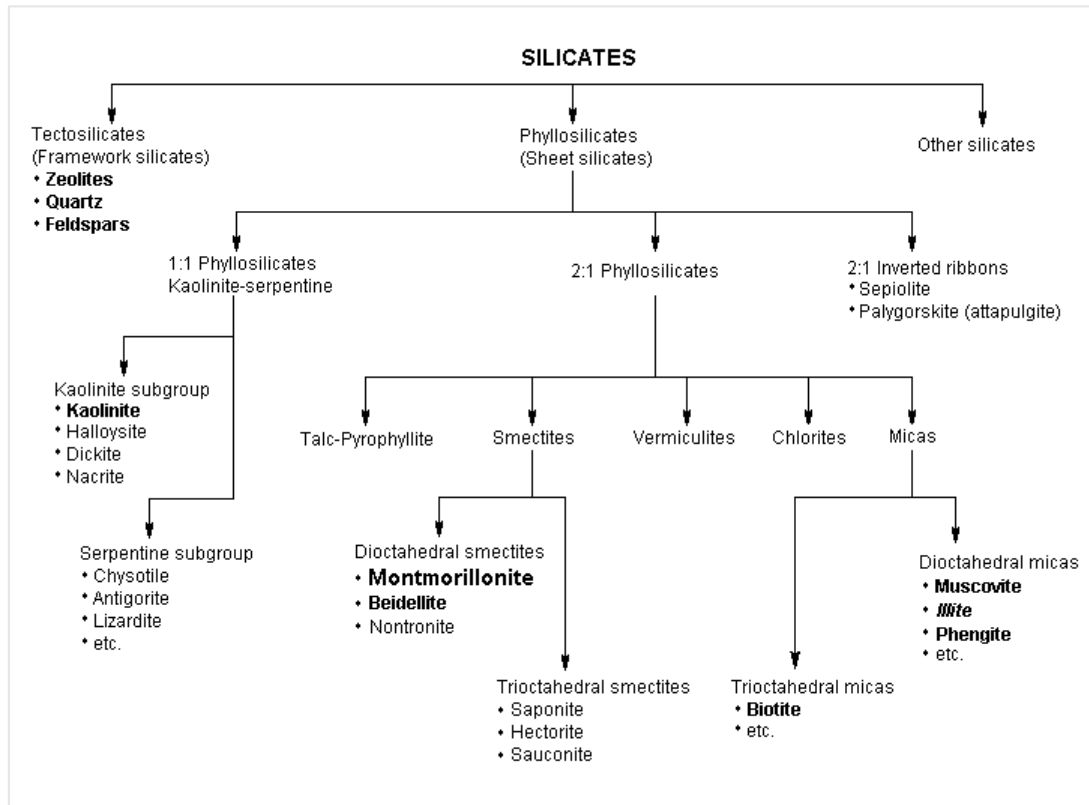


Table 1.1. Classification of clay minerals [54].

## 1.4.1 Modification of clays

The modification of the silicate surface to render layered silicates miscible with an organophilic polymer matrix is necessary to improve their dispersion into the matrix so as a nanocomposites can form. There are different procedures to modify the clays among which:

*Ion-exchange with organic cations:* small molecules can substitute the cations that are not strongly bound to the clay surface. The use of primary, secondary, tertiary, and quaternary alkylammonium or alkylphosphonium cations requires varied results; the surface energy of the clay platelets decreases easing the penetration of polymers or monomers into the clay galleries and they can provide functional groups that can react with the polymer matrix[42].

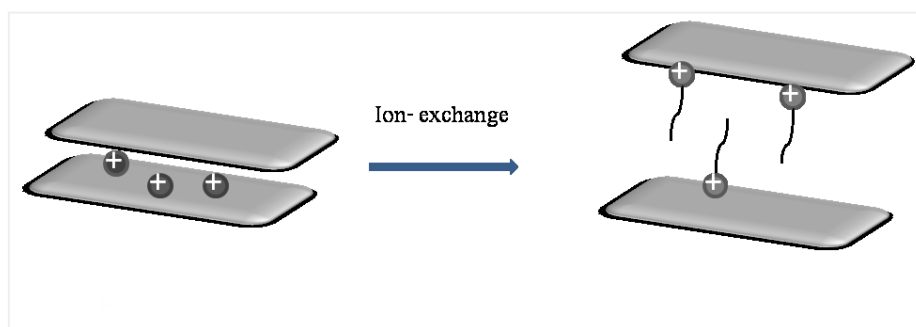


FIG. 1.6 Schematic representation of ion-exchange method

*Ion-dipole interaction* : The organic polar molecules can be absorbed by mineral clay by the formation of a coordination bond between the exchangeable cation and the organic molecules or by proton transfer from interlayer water to the organic molecules, or vice versa [55].

The partial negative charge of organic molecules allows the interaction with exchangeable cations by the formation of ion-dipole bonds. Glycols[56] and amides[57] have also been used as clays modifiers.

*Silylation reaction*: The grafting of silane onto clay surface [58] have been extensively investigated. The strategy of silylation is based on creation of covalent bonds between an organosilane and the hydroxyl groups located on the clay edge; via a condensation reaction can form siloxane bonds Si-O-Si [59]. If a silanol is chosen with a functional group able to react with the polymer, a covalent bond may be created between the clay filler and the polymer matrix [60].

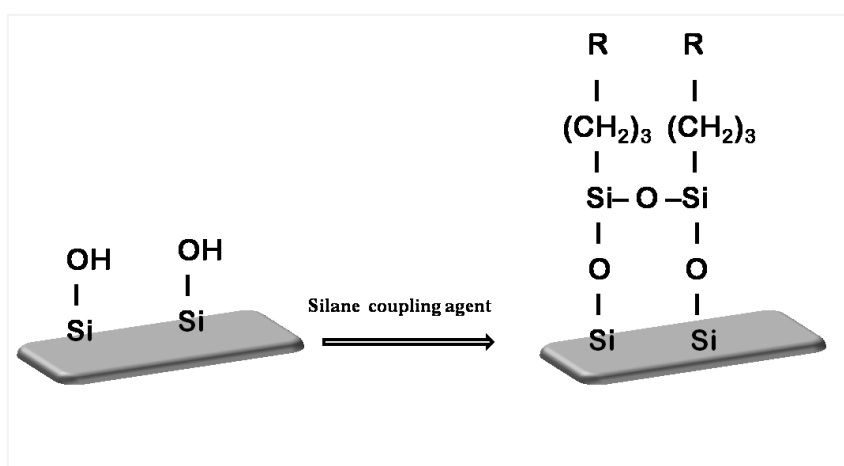


FIG. 1.7 Reaction between clay hydroxyl groups and organosilane

## Chapter I

---

One of the main issues in preparing nanocomposites with good properties is the uniform dispersion of the nanoparticles in the polymer matrix. Undoubtedly the possibility of organically modifying clays has partly contributed to overcome this problem.

## BibliographyI

---

- [1] Knox, Andrew (February 2005). "An overview of incineration and EFW Technology as applied to the management of municipal solid waste 9MSW". Univeristy of western Ontario. <http://www.oneia.ca/files/EFW0>
- [2] Mareschal F., Biodegradable Plastics Views of APME (Association of Plastic Manufactures in Europe) in E. Chiellini, R.Solaro eds. Biodegradable Polymers and Plastic, Kluwer Academic/Plenum Publishers NY, pp 67-71, 2003.
- [3] Piming Ma, Tailoring the properties of bio-based and biocompostable polymer blends, 2011-Ph. D Thesis
- [4] Antonio U. B. Queiroz and Fernanda P. Collares-Queiroz, Innovation and Industrial Trends in Bioplastics, Journal of Macromolecular Science R \_ , Part C: Polymer Reviews, 49:65–78, 2009
- [5] Averous, L., Boquillon, N. Carbohydrate Polymers, 56(2), 111, (2004).
- [6] Long Yu, Katherine Dean, Lin Li. Progress in Polymer Science 31, 6, 576 ( 2006),.
- [7] L. Avérous and E. Pollet (eds.), Environmental Silicate Nano-Biocomposites, Green Energy and Technology, \_ Springer-Verlag London 2012.
- [8] <http://www.polyone.com/enus/docs/Documents/Biomaterials%20Development%20in%20the%20Polymer%20Industry.pdf>
- [9] M.E. Broz, D.L. VanderHart, N.R. Washburn.. Biomaterials 24, 4181, (2003)
- [10] Takayama T., Todo M., Hideto T., and Arakawa K., Kobunshi Ronbunshu, 63,9, 626, (2006).
- [11] Dell’Erba, R.; Groeninckx, G.; Maglio, G.; Malincolino, M.; Migliozi, A. Polymer, 42, 7831, (2001).
- [12] Chen C.C. Biomaterials, 24 1167(2003)
- [13] Yu, L.; Dean, K.; Li, L.. Progress in Polymer Science, 31, 576 (2006).
- [14] Zhang, L.; Xiong, C.; Deng, X. *Polymer*, 37, 235 (1996).
- [15] Shibata, M.; Inoue, Y.; Miyoshi, M. *Polymer*, 47, 3557 (2006).
- [16] Robertson, M. L.; Chang, K.; Gramlich, W. M.; Hillmyer, M. A. *Macromolecules*, 43,1807 ( 2010).

## BibliographyI

---

- [17] Avella, M.; Martuscelli, E.; Raimo Copolymers. *Journal of Materials Science*, 35, 523 (2000).
- [18] Khemani, K.; Schmidt, H.; Hodson, S.K. U.S. Patent 7297394, 2007.
- [19] Noda, I.; Satkowski, M.M.; Dowrey, A.E.; Marcott, C. *Macromolecular Bioscience*, 4, 269- (2004).
- [20] A. Marcilla, J.C. Garcia-Quesada, and E. Gil, *J. Appl. Polym. Sci.* 110(4), 2102 (2008).
- [21] J. Tao, C. Song, M. Cao, D. Hu, L. Liu, N. Liu, and S. Wang, *Polym. Degrad. Stab.* 94(4), 575 (2009).
- [22] B.M.P. Ferreira, C.A.C. Zavaglia, and E.A.R. Duek, *J. Appl. Polym. Sci.* 86(11), 2898 (2002).
- [23] L. Miao, Z. Qiu, W. Yang, and T. Ikehara, *React. Funct. Polym.* 68(2), 446 (2008).
- [24] T. Sadik, V. Massardier, F. Becquart, and M. Taha, *J. Appl. Polym. Sci.* (2012) DOI: 10.1002/app.37957.
- [25] M.J. Jenkins, Y. Cao, L. Howell, and G.A. Leeke, *Polymer* 48(21), 6304 (2007).
- [26] Jasberg BK, Swanson CL, Shogren RL, Doane WM. *J Polym Mater*;9:163 (1992).
- [27] Bastioli C, Cerrutti A, Guanella I, Romano GC, Tosin M. *J Env Polym Deg*;3(2):81 (1995).
- [28] Bastioli C. *Polym Deg Stab*;59:263 (1998).
- [29] Amass W, Amass A, Tighe B. *Polym Int*;47:89 (1998).
- [30] Pranamuda H, Tokiwa Y, Tanaka H. *J Env Polym Deg*;4(1):1 (1996).
- [31] L. Averous, L. Moro, P. Dole, C. Fringant. *Polymer* 41 4157–4167 (2000).

## BibliographyI

---

- [32] Messersmith P.B, Giannelis E.P. J. Polym. Sci, Part A: Polym. Chem.33 1047-57 (1995).
- [33] Yano K., Usuki A., Okada A., Kurauchi T., Kamigaito O. J. Polym. Sci., Part A: Polym. Chem. 31, 2493, (1993)
- [34] Gilman J.W. Appl. Clay. Sci. 15 , 31, (1999)
- [35] Giannelis E.P. Polymer . Appl. Organomet. Chem. 12,675, (1998)
- [36] LeBaron P.C., Wang Z., Pinnavaia T.J. . Appl. Clay. Sci. 15, 11, (1999)
- [37] Giannelis E.P. Polymer layered silicate nanocomposites. Adv. Mater. 8, 29, (1996)
- [38] Sinha Ray S., Yamada K., Okamoto M., Ueda K. Nano Lett. 2, 1093, (2002)
- [39] Patent No.: US 7,888,419 B2, Feb.15,2011.
- [40] A. Usuki; M. Kawasumi; Y. Kojima; A. Okada; T. Kurauchi; O. Kaminogato, J. Mater. Res., , 8(5),1174, (1993)
- [41] A. Usuki; Y. Kojima; M. Kawasumi; A. Okada; Y. Fukushima; T. Kurauchi; O. Kaminogato, J. Mater. Res., , 8(1), 1185 (1993)
- [42] Ray, S.; Okamoto, M. Progress in Polymer Science, 28, 1539 (2003).
- [43] Lebaron, P. C.; Wang, Z.; Pinnavaia, T. J. Applied Clay Science, 15, 11 (1999)
- [44] Alexandre, M.; Dubois, P. Materials Science and Engineering: A 28, 1, (2000),
- [45] Okamoto, M. Rapra Review Reports, 14, 1-40( 2003)
- [46] Scott, M.A., Carrado, K.A. and Dutta, P.K. (eds).. Hand Book of Layered Materials. (2004)
- [47] Utracki, L. A.; Kamal, M. R. The Arabian Journal for Science and Engineering, 27, 43 (2002)
- [48] <http://www.swac.umn.edu/classes/soil2125/doc/s11ch1.htm>
- [49] <http://www.geol.umd.edu/~jmerck/geol342/lectures/07.html>
- [50] <http://classes.colgate.edu/rapril/geol201/summaries/silicates/phyllo.htm>

## BibliographyI

---

- [51] RE Grim, "Applied Clay Mineralogy. " McGraw-Hill Book Company, New York, (1968).
- [52] Aranda P, Ruiz-Hitzky E. Poly(ethylene oxide)-silicate intercalation materials. *Chem Mater*; 4:1395 (1992).
- [53] Greenland DJ. Adsorption of poly(vinyl alcohols) by montmorillonite. *J Colloid Sci*;18:647, (1963)
- [54] Bailey SW, chairman Summary of recommendations of AIPEA [Association Internationale Pour l'Étude des Argiles] nomenclature committee on clay. *AmMineral*, **65**:1-7.(1980b)  
[http://www.minsocam.org/msa/collectors\\_corner/arc/nomenclaturecl1.htm](http://www.minsocam.org/msa/collectors_corner/arc/nomenclaturecl1.htm).
- [55] Yariv, S.; Cross, H., *Organo-Clay Complexes and Interactions*. In Marcel Dekker, Inc: New York and Basel,; pp 1-101.( 2002)
- [56] Beall, G.W., Goss, M., *Appl. Clay Sci.* 27, 179 (2004)
- [57] Tahoun, S. A.; Mortland, M. M. *Soil Science*, 10, 314 (1966).
- [58] N.N. Herrera, J.M. Letoffe, J.L. Putaux, L. David, E. Bourgeat-Lami, *Langmuir* 20 1564. (2004)
- [59] M. Ogawa, S. Okumoto, K. Kuroda,. *Journ. Am. Chem. Soc.* 120 ,7361. (1998)
- [60] N.N. Herrera, J-L. Putaux, E. Bourgeat-Lami,. *Progr. In Solid State Chem.* 34 121,(2006)

## Chapter II

---

### *Materials : Literature review*

### 2.1 Aliphatic copolyesters : Poly(hydroxyalkanoates) (PHAs)

#### 2.1.1 Synthesis

Polyhydroxyalkanoates (PHAs) are synthesized through a fermentation process using bacteria, which generate the polymer, typically copolymers, as an energy reserve within the cell cytoplasm when the concentration of some nutrient, like nitrogen, phosphorous, magnesium, is limited [1]. The microorganisms will then utilize these storage polymers as carbon and energy source during conditions of starvation[2,3,4]. The fermenting step requires from 30 to 48 hours. The cells are isolated through a drying process, and the PHAs are usually recovered by a solvent extraction method using acetone or alcohols [5]. PHAs can be produced either by fed-batch or continuous fermentation; it depends on the type of bacteria. The mass production of PHAs is influenced by microorganism ability to utilize an inexpensive carbon source, growth rate, polymer synthesis rate, and the maximum extent of polymer accumulation[6]. The choose of bacteria and carbon source employed defines the structure of the final PHA[1,7].



FIG.2.1 Microorganism cell containing PHAs granules

In 1926 Maurice Lemoigne discovered that anaerobic degradation of *Bacillus megaterium* led to the excretion of poly-3-hydroxybutyrate (PHB) [8]. *Ralstonia eutrophia* (*R. eutropha*) is used for synthesizing poly(3- hydroxybutyrate) and 3-hydroxybutyrate copolymers [1, 5, 9]. Using glucose and propionate as the carbon feed source with *R. eutropha*, poly(3-hydroxybutyrate-co-3- hydroxyvalerate)(PHBV) is obtained with a concentration of the 3-hydroxyvalerate that can be adjusted by varying the ratio of glucose to propionate in the feedstock[9]. The increasingly use of *E. coli* to produce PHB- Poly(3-hydroxybutyrate) is

## Chapter II

due to its ability to synthesize extremely high intracellular levels of PHB, being easy genetically modifiable and its ability to use several inexpensive carbon sources. Moreover the utilization of mutants to metabolically engineer strains that produce P(3HB-co-3HV) copolymers [10,11]. Poly(3-hydroxybutyrate) (3HB) is the typical backbone of PHA copolymers[1, 8, 12, 13] and, depending on the number of methylene group in the backbone ( $m$  in figure 2.2) and the length of the side chain in the structure ( $R$  in figure 2.2), several PHAs can be formed.

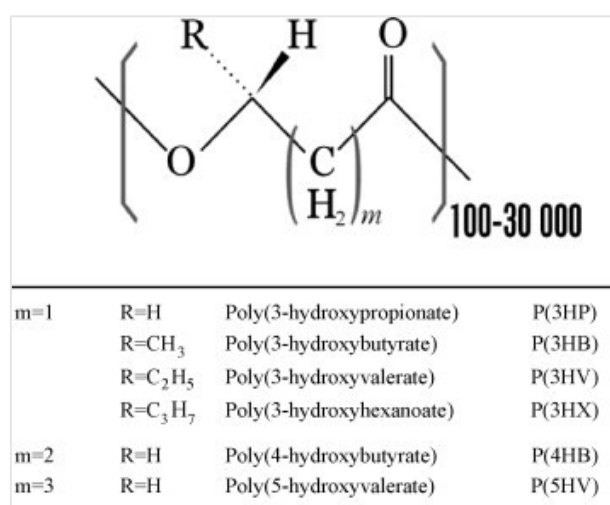


FIG 2.2 General structure of polyhydroxyalkanoates [14].

There are four main gene classes involved in the synthesis of PHAs[6, 15].

The most studied pathway is the synthesis of PHB using the bacterium *Ralstonia eutropha* in which the condensation of two acetyl-CoA molecules by a beta-ketothiolase produces acetoacetyl-CoA. NADPH-dependent acetoacetyl-CoA reductase then carries out its conversion to 3-hydroxybutyryl-CoA. The final step is the polymerization by PHB synthase[6].

The remaining pathways differ from the first for the catalytic functions carried out by the other classes of enzymes[16].

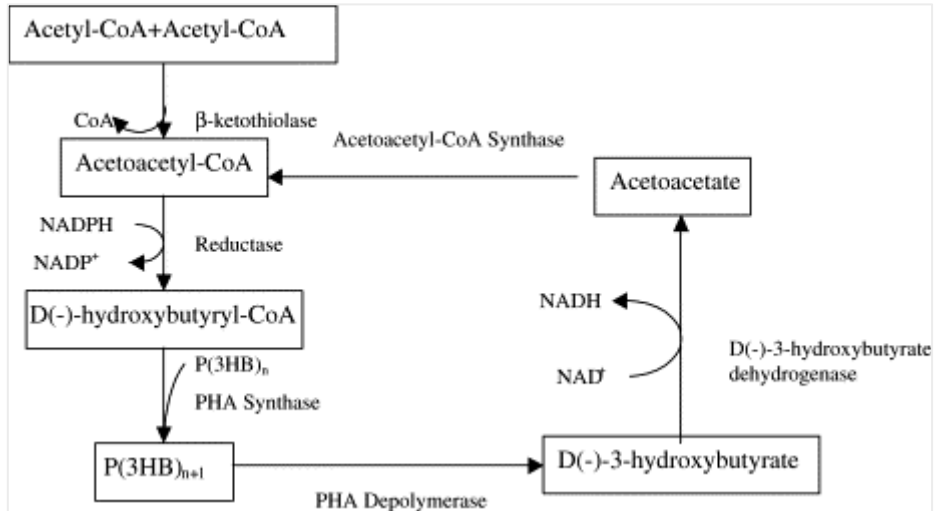


FIG.2.3 Enzymatic steps of PHB synthesis in *R. eutropha* [11]

The properties of the extract product can vary depending on the copolymer composition [1,8,12,13].

The most studied PHAs are PHBs and their copolymer PHBV.

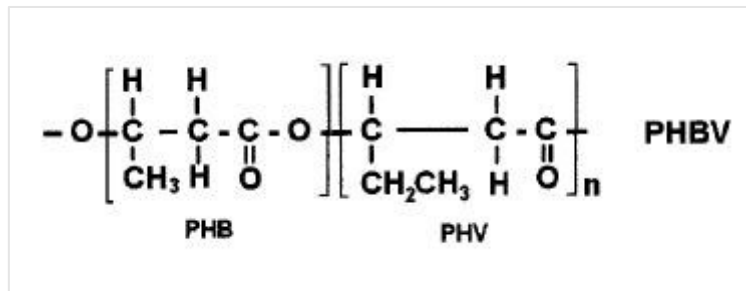


FIG.2.4 Chemical structure of copolymer PHBV

### 2.1.2 PHBV properties

Pure poly(3HB) is a stiff polymer due to its high crystallinity (a 60-80%)[13,17]; the low rate of crystallization related to the low heterogeneous nucleation density entails the growth of large spherulites that form inter-spherulitic cracks and cause brittle failure[17,18].

In order to improve the toughness of PHB, poly-(3-hydroxyvalerate) (HV) or (PHV) units are incorporated into PHB. A structural characteristic of PHBV is the isodimorphism. These resins display a melting temperature minimum for PHV content of 30 mol% and co-crystallization of the two monomer units in either of the homopolymer crystal lattices of PHB and PHV, depending on whether the (*R*)-PHV composition is above or below 40 mol%[6, 19].

The crystallinity of PHBV is about the same of PHB homo-polymer however the melting temperature is lower depending on the HV content[20]. The crystallinity and mechanical properties of PHBV can change with the variation of the percentage ratio of the respective monomers[21].

The rate of crystallization of PHA decreases with increasing structural complexity of the polymer. The bulky side groups in 3HV prevent crystallization due to steric effects[22].

Increasing HV content the melt stability is improved using lower processing temperatures[6, 23, 24]. Poly(3HB-co-3HV) has a good O<sub>2</sub>, CO<sub>2</sub>, and water vapor barrier, and it is suitable for some food packaging applications and containers for cosmetic products [5, 25].

The tensile strength of poly(3HB-co-3HV), on varying HV content, is about 20-40 MPa and the modulus decreases to 800- 2000 MPa with an increasing of elongation at break up to 20-30%[18, 26].

In table 2.1 some typical properties of PHBV with different HV content are shown.

### 2.1.3 PHBV composites

After the industrial production of PHBV under the trade name BIOPOL by Zeneca Bio Product for this polymer there was an attracting growing interest from researchers[27]. Choi and his group [28] showed results about PHBV/ Cloisite 30 B nanocomposites, prepared through a melt intercalation method. An intercalated structure was verified by XRD and TEM analyses. The temperature and rate of crystallization of PHBV increased with the

organo-clay acting as nucleating agent. Moreover, the nanocomposites showed significant increases in tensile strength and thermal stability[28]. The nucleation effect of the organophilic montmorillonite (OMMT) was studied by Chen *et al.*[29]. They showed that OMMT acted as a nucleating agent in the PHBV matrix but the nucleation and the overall crystallization rate decreased with the increase of clay content.

Wang and his co-workers[30] investigated the properties and the biodegradability of PHBV/OMMT nanocomposites.

They found that the biodegradability of PHBV/OMMT nanocomposites in soil suspension decreased with an increase in the amount of OMMT.

A comparison of morphology, thermal and mechanical properties of PHBV nanocomposites using two different types of silicates, organo-modified montmorillonite(C30B) and Halloysite nanotubes (HNTs), was evaluated in the work of Carli *et al.*[31].

Although the researches principally concern fillers with lamellar or layered structure for their availability and versatility, adding of nano-particles in PHBV like zinc oxide [32, 33], attapulgite [34], hydroxyapatite [35], fumed silica [36], calcium phosphate [37] or titanium dioxide[38] have also been reported. The effect of carbon nanotubes was analyzed by Lai *et al.*[39] and to develop completely biodegradable composites several types of natural fibers were utilized such as bamboo pulp[40], short abaca[41], jute [42] and kenaf fibers[43].

### **2.2 Aliphatic-Aromatic copolyesters: Poly(butylene adipate-co-terephthalate) (PBAT)**

The most important factors for the biodegradable plastics for commercial uses are price, performance and use of existing plant. In this regard, among the commercially available biodegradable polymers, synthetic aliphatic and aromatic biopolyesters such as poly(butylene adipate-*co*-terephthalate) (PBAT) show good thermal and mechanical properties with the added advantage of biocompatibility and biodegradability[44].

The introduction of terephthalate units into the main chains of aliphatic polyesters can improve the physical as well as biodegradable properties of the polymer[45].

PBAT, was commercialized by BASF under the trade name of Ecoflex® F BX 7011. It is an aliphatic-aromatic copolyester based on terephthalic acid, adipic acid, 1,4- butanediol and modular units as the statistical copolyester units, including 1,4-butanediol and the dicarbonic

acids, adipic acid and terephthalic acid, are linked.

These modular systems involve the incorporation of hydrophilic components of monomers with branching, leading to chain-lengthening, and thereby increasing the molecular weight to yield tailor-made products with totally different material properties[46].

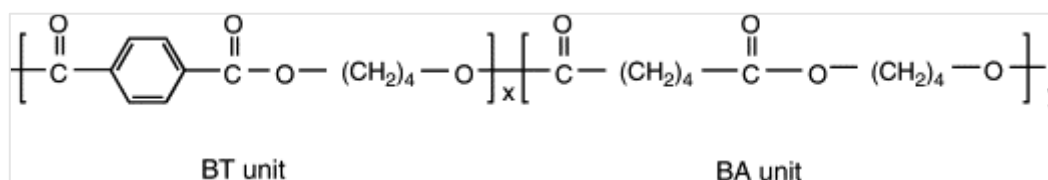


FIG.2.5 Chemical structure of PBAT[47].

Ecoflex® doesn't contain additives for decomposition and doesn't produce any negative consequences for environmental risk (ecotoxicity) if introduced into composting processes[48].

### 2.2.1 PBAT composites

Up to this time only few articles regarding PBAT/ clay nanocomposites have been published. Someya et al.[49,50] obtained certain level of clay intercalation and exfoliation in some compositions of PBAT- organically modified montmorillonites (OMMT) nanocomposites.

Chivrac et al. [51, 52] used various commercial organoclays as fillers in PBAT matrix by different preparation processes (i.e., solvent or melt intercalation). The higher intercalation degrees were obtained by solvent intercalation. The thermal and mechanical properties of composites system were also investigated.

Mohanty and Nayak [53] investigated the morphology and the properties of PBAT reinforced with different types of organoclays such as Cloisite30B (C30B), Cloisite20A (C20A), Bentonite (B109). Furthermore, they found an additional improvement of mechanical properties via functionalization of PBAT matrix upon grafting with maleic anhydride (MA).

An interesting study of soy protein concentrate (SPC) blended with poly(butylene adipate-co-terephthalate) (PBAT) was performed by Chen [58]. Using maleic anhydride grafted PBAT an overall improvement of the mechanical properties and the formation of percolated SPC network structure at high SPC concentrations was observed.

Recently, Fukushima and his co-workers[47] tried to improve the mechanical and thermal properties of PBAT by adding different types of nanoparticles, such as montmorillonites, hectorites and sepiolites, into the biodegradable matrix. They concluded that the best thermo-mechanical and physical properties of all nanocomposites studied were achieved with the addition of needle like sepiolite .

There is a growing interest in the field of biodegradable composites (biocomposites) , obtained by the combination of biodegradable polymers and biodegradable fillers (e.g., lignocellulosic fillers). Several studies are based on biodegradable polyesters matrices[54].

For example composites of PBAT with natural fiber have been studied.

Wu[55] in his work improved noticeably the mechanical properties of the neat polymer making composites with sisal fibers. The grafting of acrylic acid onto polymer matrix was carried out in order to enhance the compatibility between the two components.

Avèrous and F. Le Digabel [56] studied thermal and mechanical properties of biocomposites made of Poly(butylene adipate- co-terephthalate) (PBAT) and lignocellulosic fillers (LCF). The fibers increased the thermal degradation temperature of the matrix and, although the cristallinity didn't change, the fillers induced a nucleating effect. These biocomposites showed good mechanical properties. The addition of oil palm empty fruit bunch (EFB) fibers, chemical treated with succinic anhydride, in PBAT matrix improved thermal stability , tensile and flexural properties[57].

2.3 Halloysite nanotubes

2.3.1 Halloysite structure

Deposits of Halloysite are in several countries but most of which contain other clays like Kaolinite and some impurities. High purity deposits can be found in Utah (USA), in the Dragon mine, and in New Zealand.

Halloysite is a two-layered (1:1) natural aluminosilicate clay, chemically similar to kaolin, and with a stoichiometry  $Al_2(OH)_4Si_2O_5 \cdot nH_2O$  where n is 0 or 2 (Figure 2.6) depending on the two different polymorphs in which Halloysite can occur : the hydrated form (with interlayer spacing of 10 Å) and the anhydrous form (with interlayer spacing of 7 Å). The intercalated water is weakly bound and can be readily and irreversibly removed[59].

Aluminosilicates can occur in agglomerates, spheroids, sheets, or in hollow, tubular shapes. Halloysites exhibit a predominantly tubular morphology, but other shapes have been reported (scroll, glomerular or ‘onion-like’, platy)[59].

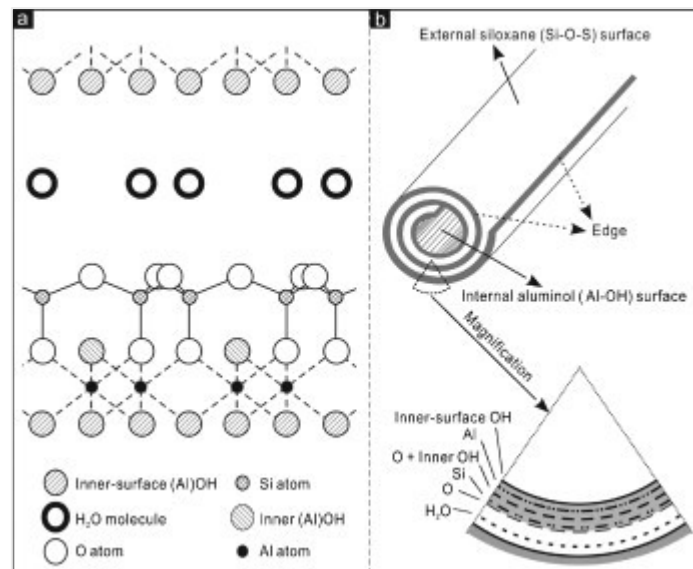


FIG. 2.6 Crystalline structure of Halloysite (a) and detail of nanotube(b) [60].

Halloysites have two different basal faces. The first one consist of a tetrahedral silicate surface Si-O-Si while the other basal surface has a di-octahedral layer (Al(OH)3) in which

only 2/3 of the existing octahedral sheet are filled by aluminium[61].

In Halloysites siloxane groups are bonded via only one oxygen atom to gibbsite octahedral rings at the outer part (figure 2.7), and the apical oxygen of tetrahedra becomes the vertices of octahedral[62].

According to Bates *et al.*[63] the cylindrical shape of clay is the effect of strain caused by mismatch in the two alignment of the tetrahedral sheet of silica bonded to the octahedral sheet of alumina.

The charge characteristics of Halloysite depend on pH value[64]. The clay presents negative charge at pH higher than 3 owing to the deprotonation of water and hydroxyl groups bound to aluminum and silicon at the edges.

The edges are considered to be positively charged at low pH, neutral at the isoelectric point (at around pH 3), and negatively charged at higher pH[65]. Halloysites are characterized by structural imperfections like substitutions of the  $\text{Al}^{3+}$  by  $\text{Fe}^{3+}$  in octahedral layer and  $\text{Si}^{4+}$  in the tetrahedral sheet is often replaced by  $\text{Al}^{3+}$ [59, 66]. These substitutions entail changes of the microstructure and the dimensions of tetrahedrons and octahedrons[66].

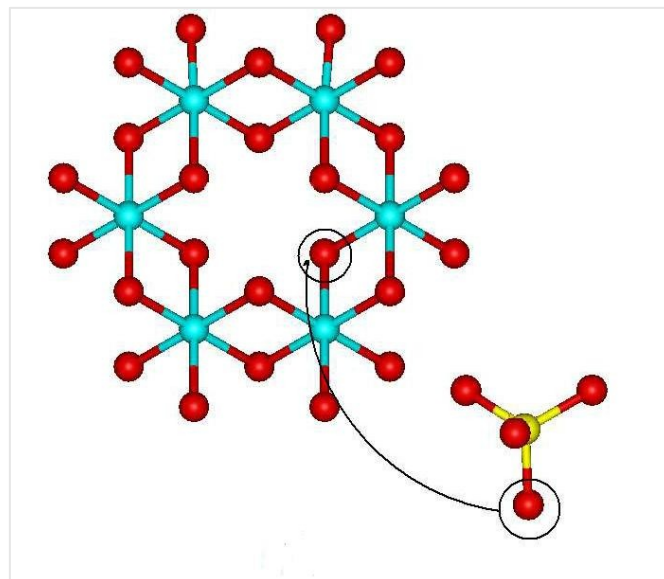


FIG. 2.7 Bonding of silicon atom to di-octahedral ring in Halloysite (7 Å)[61].

Dimensions of Halloysite particles vary from 50 to 70 nm in external diameter, ca. 15 nm diameter lumen and 1-1.5  $\mu\text{m}$  length[67].

The Young's modulus is between 230-340 GPa, depending on the orientation of overlapped nanotubes (armchair, zig-zag) and the number of layer defects compared to single-walled

ones[68].

Recently, Halloysite nanotubes, typically used in the manufacture of high quality ceramic white-ware, have received much attention. In fact, on one side, they have the potential to provide cheap alternatives to the expensive carbon nanotubes whereas, on the other hand, given their chemical similarity to lamellar clays as montmorillonites, they have the possibility to be further intercalated by chemical and/or physical ways[69].

These nanotubes have a wide range of applications considering interesting structure and properties such as widespread availability, large aspect ratio, high stiffness and their biocompatibility was demonstrated by Vergaro *et al.* (the nanotubes are not toxic for the cells)[70].

Their utilization as nanoscale container for the encapsulation of biologically active molecules (e.g., biocides, enzymes, and drugs), as a support for immobilization of catalyst molecules, controlled release, bioimplants, and for protective coating (e.g., anticorrosion or antimolding) has been also investigated[59, 70,71,72].

### 2.3.2 Halloysite/ polymer composites

Halloysite can be employed as nanofiller into polymer matrices to improve mechanical properties or fire performance [61].

Thermal stability and flame retardant effect of the Polypropylene/HNTs nanocomposites were investigated by Du *et al.*[73]. During the initial degradation stages of composite formulations, the degradation products, being entrapped into the lumen of HNTs, are delayed to diffuse and consequently an increased thermal stability is recorded.

Ye *et al.* [74] demonstrated that blending epoxies with an appropriate amount of HNTs could significantly increase impact strength without sacrificing flexural modulus, strength, and thermal stability.

Marney *et al.* [75] reported that nylon 6-halloysite composites show an improved fire behavior by a decrease of some fire properties parameters such as the peak of heat release rate (PHRR), the total heat released (THR), and the peak of mass loss rate (PMLR) with respect to the neat matrix by increasing the filler content. Moreover they reported about a thermal

insulation barrier that is developed at the surface of the composite during the burning acting as a flame retardant but without stopping the fire front.

Halloysite and ethylene propylene diene monomer (EPDM) nanocomposites were prepared by Ismail and his co-workers [76]. The increases in tensile strength, stiffness and ductility of EPDM/HNT nanocomposites were attributed to interfacial and inter-tubular interactions between HNTs and EPDM, and edge-to-edge and face-to-edge interactions between HNTs (zig-zag structure)[76].

Halloysites can also influence crystallization process of polypropylene as reported by Ning *et al.* [77]. They found that HNTs act as nucleating agents and enhance the overall crystallization rate. The HNTs also act as a nucleation point in isotactic polypropylene for both  $\alpha$ -PP and  $\beta$ -iPP, depending on the temperature and the processing conditions[78].

A study about polymorphism of PA6/HNTs nanocomposites was conducted by Guo *et al.* [79].

### 2.3.3 Modification of Halloysite nanotubes

In order to improve compatibility between clay nanotubes and polymer matrix, Halloysites have been functionalized with different silanes.

As described by Guo *et al.*[80] mechanical properties and heat distortion temperature were improved with addition of functionalized HNTs into PA6 matrix. Halloysites were modified with 3-(trimethoxysilyl)propyl methacrylate(MPS).

Pasbakhsh *et al.* modified HNTs with  $\gamma$ -methacryloxypropyl trimethoxysilane (MPS) to improve their dispersion in ethylene diene monomer (EPDM). The obtained nanocomposites showed tensile strength and tensile modulus at 100% elongation higher than those of EPDM/unmodified HNTs[81].

Halloysites modified with  $\gamma$ -glycidoxypropyltrimethoxy silane were incorporated into epoxy resin; the obtained nanocomposites exhibited improved flexural strength due to uniform dispersion of the nanotubes as TEM pointed out[82].

## Chapter II

---

A detailed study on modification of Halloysite clay nanotubes with  $\gamma$ -aminopropyltriethoxysilane (APTES) was done by Yuan *et al.*[83].

Recently, Phenylphosphonic acid (PPA) was used to unroll HNTs[84]. The unfolded and intercalated Halloysite increased fracture toughness of cured epoxies.

## Bibliography

---

- [1] Braunegg, G.; Lefebvre, G.; Genser, K.F. *Journal of Biotechnology*, 65, 127 (1998)
- [2] Anderson AJ, Dawes EA. *Microbiol Rev.* 54(4):450 (1990)
- [3] Bernd H. A. REHM. *Biochem. J.* 376, 15 (2003)
- [4] Verlinden RA, Hill DJ, Kenward MA, Williams CD, Radecka I. *J Appl Microbiol.* 102, 6,:1437 (2007).
- [5] Wolf, O. (Ed). *Techno-economic Feasibility of Large-scale Production of Bio-based Polymers in Europe*. Seville: Institute for Prospective Technological Studies: Technical Report Series, (2005).
- [6] Khanna, S., Srivastava, A.K. *Proc Biochem.* 40, 607 (2005)..
- [7] D'Haene P.;Remsen E.E.; Asrar, J. *Macromolecules*, , 32, 5229 (1999).
- [8] Lemoigne, M. *Bulletin de la Societe de Chimie Biologique*, 8, 770 (1926).
- [9] Holmes, P.A. *Physics in Technology*, 16, 32 (1985)
- [10] Fidler, S., Dennis, D. *FEMS Microbiol Rev.* 103, 231 (1992).
- [11] Hahn, S.K., Chang, Y.K., Lee, S.Y *Appl Environ Microbiol.* 61, 34. (1995).
- [12] Noda, I.; Green, P.R.; Satkowski, M.M.; Schectman, L.A. *Biomacromolecules*, 6, 580, (2005)
- [13] Philip, S.; Keshavarz, T.; Roy, I. *Journal of Chemical Technology and Biotechnology*, 82, 233 (2007)
- [14] Nicolas Jacquel, Chi-Wei Lo, Yu-Hong Wei, Ho-Shing Wu, Shaw S. Wang; *Biochemical Engineering Journal*, 39, 1, 15 (2008).
- [15] Aneja, KK. Ashby, RD. Solaiman, DKY. *Biotechnol Lett* ; 31: 1601 (2009)
- [16] Davis, R. Anilkumar, PK. Chandrashekar, A. Shamala, TR. Antonie Van Leeuwenhoek ; 94: 207 (2008).

## Bibliography

---

- [17] Barham, P.J. and Keller, A. *Journal of Polymer Science*, , 24, 69 (1986)
- [18] El-Hadi, A.; Schnabel, R.; Straube, E.; Muller, G.; Henning, S.. *Polymer Testing*, , 21, 665 (2002).
- [19] Sudesh, K., Abe, H., Doi, Y. *Prog Polym Sci.* 25, 1503 (2000).
- [20] Nair, L. S., and Laurencin, C. T. *Progress in Polymer Science*, 32(8-9).762 (2007).
- [21] Sabir, M. I., Xu, X., and Li, L, *Journal of Materials Science*, 44(21). 5713 (2009)
- [22] Kunioka, M.; Tamaki, A.; Doi, Y.. *Macromolecules*, 22, 694 ( 1989)
- [23] Ferreira, B.M.P., Zavaglia, C.A.C., Duek, E.A.R *J Appl Polym Sci.* 86, 2898 (2002)
- [24] Ramkumar, D.H.D., Bhattacharya. M. *Polym Eng Sci.* 38(9), 1426 (1998).
- [25] Miguel, O.; Fernandez-Berridi, M.J.; Iruin, J.J. *Journal of Applied Polymer Science*, , 64, 1849 (1997)
- [26] Avella, M.; Martuscelli, E.; Raimo, M. Review:. *Journal of Materials Science*, 35, 523 (2000).
- [27] Koning D, Can G. *J Microbiol*;41;303 (1995)
- [28] W. M. Choi, T. W. Kim, O. O. Park, Y. K. Chang, and J. W. Lee, *J. Appl. Polym. Sci.*, 90, 525 (2003).
- [29] Chen, G. X., Hao, G. J., Guo, T. Y., Song, M. D., Zhang, B. H. *Journal of Applied Polymer Science*, 93(2), 655 (2004).
- [30] Wang, S., Song, C., Chen, G., Guo, T., Liu, J., Zhang, B., Takeuchi, S. *Polymer Degradation and Stability*, 87(1), 69 (2005)
- [31] Larissa N. Carli; Janaina S. Crespo; Raquel S. Mauler *Composites Part A* 42 (11), 1601 (2011).
- [32] Yu W., Lan C-H., Wang S-J., Fang P-F., Sun Y-M.: *Polymer*, 51, 2403 (2010).
- [33] Naphade R., Jog J. *Fibers and Polymers*, 13, 692 (2012).
- [34] Thiré R. M. S. M., Arruda L. C., Barreto L. S.: *Materials Research*, 14, 340 (2011).

## Bibliography

---

- [35] Jack K. S., Velayudhan S., Luckman P., Trau M., Grøndahl L., Cooper-White J. *Acta Biomaterialia*, **5**, 2657 (2009).
- [36] Ma P. M., Wang R. Y., Wang S. F., Zhang Y., Zhang Y. X., Hristova D. *Journal of Applied Polymer Science*, **108**, 1770 (2008).
- [37] Duan B., Wang M., Zhou W. Y., Cheung W. L. *Applied Surface Science*, **255**, 529 (2008).
- [38] Buzarovska, A., Grozdanov, A., Avella, M., Gentile, G. and Errico, M., *Journal of Applied Polymer Science*, **114**: 3118 (2009)
- [39] Lai M., Li J., Yang J., Liu J., Tong X., Cheng H. *Polymer International*, **53**, 1479 (2004).
- [40] Jiang L., Huang J., Qian J., Chen F., Zhang J., Wolcott M. P., Zhu Y. *Journal of Polymers and the Environment*, **16**, 83 (2008).
- [41] Shibata, M., Takachiyo, K.-I., Ozawa, K., Yosomiya, R. and Takeishi, H., *J. Appl. Polym. Sci.*, **85**: 129 (2002)
- [42] Bledzki A. K., Jaszkwicz A. *Composites Science and Technology*, **70**, 1687 (2010).
- [43] Avella M., Gaceva G-B., Buz̄arovska A., Errico M. E., Gentile G., Grozdanov A. *Journal of Applied Polymer Science*, **104**, 3192 (2007).
- [44] F. Li, X. Xu, J. Yu, A. Cao, *Polym. Degrad. Stab.* **92** 1053 (2007)
- [45] Zhihua G, Kazuhiro K, Motonori Y, Hideki A, Yoshiharu D. *Polymer Degradation and Stability*; **83**:289, (2004)
- [46] MSc. Motonori Yamamoto, Dr. Uwe Witt, DI. Gabriel Skupin, Dr. Dieter Beimborn, Dr. Rolf-Joachim Müller. *Biodegradable Aliphatic- Aromatic Polyesters: <sup>TM</sup>Ecoflex*.
- [47] Kikku Fukushima, Meng-Hsiu Wu, Sergio Bocchini, Amaliya Rasyida, Ming-Chien Yang. *Materials Science and Engineering*; **C32 (6)**:1331,( 2012).
- [48] Witt, U.; Einig, T.; Yamamoto, M.; Kleeberg, I.; Deckwer, W.D.; Muller, R.J.. *Chemosphere*, **44 (2)**: 289 (2001).
- [49] Y. Someya, Y. Sugahara, M. Shibata, *J. Appl. Polym. Sci.* **95** 386 (2005)
- [50] Y. Someya, T. Nakazato, N. Teramoto, M. Shibata, *J. Appl. Polym. Sci.* **91** 1463 (2004)

## Bibliography

---

- [51] F. Chivrac, Z. Kadlecova, E. Pollet, L. Averous, J. Polym. Environ. 14 393 (2006)
- [52] F. Chivrac, E. Pollet, L. Averous, J. Polym. Sci. Polym. Phys. 45 1503 (2007).
- [53] Smita Mohanty, Sanjay Kumar Nayak. International Journal of Plastics Technology, 14 (2) , 192 (2010)
- [54] Mohanty, A. K., Misra, M., & Hinrichsen, G. Macromolecular Materials and Engineering . 1, 276. (2000)
- [55] Chin-San Wu Process, Characterization and Biodegradability of Aliphatic Aromatic Polyester/Sisal Fiber Composites. Journal of Polymers & the Environment; 19(3) , 706. (2011)
- [56] L. Avèrous, F. Le Digabel. Carbohydrate Polymers, 66 (4), 480 (2006).
- [57] Siyamak S, Ibrahim NA, Abdolmohammadi S, Yunus WM, Rahman MZ; Biocomposites. Int J Mol Sci. ;13(2):1327 (2012).
- [58] Feng Chen, Jinwen Zhang. Polymer 51( 8), 1812 (2010).
- [59] Joussein, E.; Petit, S.; Churchman, J.; Theng, B.; Righi, D.; Delvaux, B, 40, 383 ( 2005)
- [60] Yuan, P.; Southon, P. D.; Liu, Z.; Green, M.; Hook, J. M.; Antill, S. J.; Kepert, C. J., Journal of Physical Chemistry C, 112 (40), 15742 (2008).
- [61] Deepak Rawtani and Y.K. Agrawal.. Rev.Adv. Mater. Sci. 30 282 (2012)
- [62] Hélio A. Duarte, Maicon P. Lourenço, Thomas Heine and Luciana Guimarães:. Stability, Structure and Properties available at [www.intechopen.com](http://www.intechopen.com)
- [63] Bates, T.F., Hildebrand, F.A. & Swineford, A. American Mineralogist, 35, 463. (1950a).
- [64] Theng, B.K.G., Russell, M., Churchman, G.J. & Parfitt, R.L. Clays and Clay Minerals, 30, 143. (1982)
- [65] Braggs, B.; Fornasiero, D.; Ralston, J.; Stsmart, R. Clays Clay Min., 42, 123 (1994).
- [66] Balbir Singh Why does Halloysite roll?- A new Model. Clays and Clay Minerals, 44 (2), 191 (1996). .
- [67] Yin-Feng Shi, Zhong Tian, Yang Zhang, He-Bai Shen and Neng-Qin Jia. Nanoscale Research Letters, 6:608 (2011)

## Bibliography

---

- [68] Guimarães, L.; Enyashin, A. N.; Seifert, G.; Duarte, H. A. *Journal of Physical Chemistry C*, 114 (26), 11358 (2010)
- [69] H. Noro, Hexagonal platy Halloysite in an altered tuff bed, Komaki City, Aichi Prefecture, Central Japan *Clay Miner.* (1986) 21, 401
- [70] Viviana Vergaro, Elshad Abdullayev, Yuri M. Lvov, Andre Zeitoun, Roberto Cingolani, Ross Rinaldi, and Stefano Leporatti\*, *Biomacromolecules*, 11, 820. (2010)
- [71] Price RR, Gaber BP, Lvov Y: *J Microencapsulation*, 18:713 (2001).
- [72] Abdullayev E, Price R, Shchukin D, Lvov Y. *Appl Mater Interfaces*, 1:1437 (2009).
- [73] Mingliang Du, Baochun Guo, Demin Jia. *European Polymer Journal* 42 (6): 1362. (2006)
- [74] Y. Ye, H. Chen, J.S. Wu, and L. Ye, *Polymer* 48(21): 6426 (2007).
- [75] Marney, D. C. O., Yang, W., Russell, L. J., Shen, S. Z., Nguyen, T., Yuan, Q., Varley, R. and Li, S. *Polym. Adv. Technol*, 23: 1564.(2012).
- [76] Ismail H., Pasbakhsh P., Fauzi M. N. A., Abu Bakar A.: *Polymer Testing*,. 27, 841. (2008)
- [77] Nan-ying Ning, Qin-jian Yin, Feng Luo, Qin Zhang, Rongni Du, Qiang Fu, *Polymer* 48 ( 25): 7374 (2007).
- [78] Liu, M.; Guo, B.; Du, M.; Chen, F.; Jia, D.*Polymer*, 50 (13):3022 (2009).
- [79] Baochun Guo, Quanliang Zou, Yanda Lei, Mingliang Du, Mingxian Liu, Demin Jia, *Thermochimica Acta*, 484, 1–2( 20): 48 (2009)
- [80] Baochun Guo, Quanliang Zou, Yanda Lei and Demin Jia *Polymer Journal*,41 : 835. (2009)
- [81] Pooria Pasbakhsh, H Ismail, M N Ahmad Fauzi, A Abu Bakar. *Applied Clay Science* 48 (3): 405 (2010).
- [82] Liu, M.; Guo, B.; Du, M.; Lei, Y.; Jia, D. *Journal of Polymer Research*, 15 (3): 205. (2007)

## Bibliography

---

- [83] Peng Yuan, Peter D. Southon, Zongwen Liu, Malcolm E. R. Green, James M. Hook, Sarah J. Antill and Cameron J. Kepert. *J. Phys. Chem. C*, , 112 (40):15742 (2008).
- [84] Tang, Y.; Deng, S.; Ye, L.; Yang, C.; Yuan, Q.; Zhang, J.; Zhao, C. *Composites Part A: Applied Science and Manufacturing*, 42 (4):345.(2011)

## Chapter III

---

### *Film blowing process*

### 3.1 The process

The blown film extrusion (film blowing) is an important industrial process to manufacture thin and biaxially oriented polymeric films.

This process consists in extruding a polymer melt from an annular die and a biaxial orientation is achieved by continuously inflating it and axial drawing to form a thin tubular product. The equipment is provided with air jets to cool down the bubble. Figure 3.1 shows a scheme of the film blowing process.

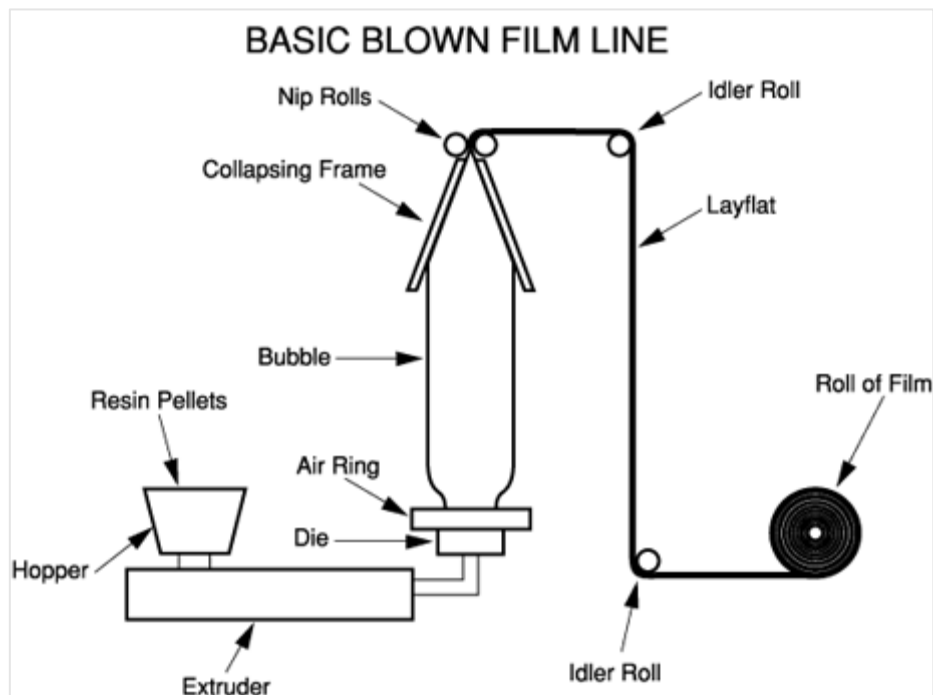


FIG. 3.1 Schematic of film blowing process[1].

More in details, polymer melt is extruded through an annular slit die, usually vertically, to form a thin walled tube. The inflation of bubble is actuated by introducing air into the bubble through a hole in the centre of the die. The tube then is pulled upwards, continually cooling, towards the nip rollers which seal it to create what is known as a 'lay-flat' tube of film.

In the molten state the film is stretched in two directions.

When air is blown into the tube by the orifice in the annular die the film is being stretched in

the radial (transverse) direction, while the elongation along the axial (machine) direction is achieved by controlling the velocity of the nip rollers and the mass flow rate at the die. These two stretchings occur simultaneously and are controlled by changing the volume of air inside the bubble and by altering the haul off speed.

Extension of the melt in both the radial and axial direction stops at the “freeze line ” (frost line) due to the cooling air which is blown outside the bubble and determine the crystallization of the melt. This is not a sharp line but a narrow zone over which solidification occurs. In fact, the solidification occurs first at the cooled surface, at the melt-solid interface, and then moves away from this surface through the thickness of the film. The height of the freeze line can be controlled through the air flow rate and negligible deformation occurs beyond the freeze line in most process[2, 3].

The main advantages in using this process are the following:

- Regulation of film width and thickness by control of the volume of air in the bubble, the output of the extruder and the speed of the haul -off
- Eliminate end effects such as edge bead trim and non uniform temperature that can result from flat die film extrusion
- Very high productivity
- Permits the combination of a number of different materials and properties

Blown films can be used either in tube form (e.g. for plastic bags and sacks) or the tube can be slit to form a sheet. Typical applications include industrial packaging (e.g. shrink film, stretch film, bag film or container liners), consumer packaging (e.g. packaging film for frozen products, shrink film for transport, food wrap film, packaging bags, or form, fill and seal packaging film), laminating film (e.g. laminating of aluminium or paper used for packaging for example milk or coffee), barrier film (e.g. film made of raw materials such as polyamides and EVOH acting as an aroma or oxygen barrier used for packaging food, e. g. cold meats and cheese), films for the packaging of medical products, agricultural films (e.g. greenhouse film, crop forcing film, silage film, silage stretch films.

This process is used extensively with polyesters and polyolefins. These-materials do not get together, so a multi -layer film would delaminate. To overcome this, small layers of special

## Chapter III

---

adhesive resins, best known as “tie layers”, are used in between.

The final film dimensions are determined by a number of process variables: the “blow up ratio” (BUR), which is a ratio of the bubble radius at the freeze line to the radius of the die, and the machine direction draw down ratio (DDR), which is the ratio of the velocity at the nip rollers to the velocity of the polymer melt exiting the die.

Typically, the blow up ratio ranges between 1,5 and 4. The solidified film is flattened into a double-layered sheet by the nip rollers forming an almost airtight seal at the top of the bubble. After the flat film is reeled up under constant tension either as tubular film or after slitting into sheet film. The width of the flattened tube is called the “layflat width” and this is equal to  $p$  times the final bubble radius.

Rheological properties play a fundamental role in film blowing. They govern the shape and the stability of the bubble and the onset of sharkskin (surface roughness). Because of the complexity of the involved flows, it is generally impossible to establish simple quantitative correlations between these phenomena and easy- measured rheological properties.

However, an understanding of how variations in the rheological behavior of melts can affect the process and the properties of blown films is essential to achieve optimum results from this process.

The objective of the film blowing process is to produce a thin film having a uniform gauge and good optical and mechanical properties. Since the film is quite thin, it is especially important to avoid the presence in the extrudate of unmelted material, gels or foreign matter, as these will be readily visible in the final product. In order to achieve good mechanical properties it is often advantageous, particularly in the case of packaging films, to have molecular orientation in the film that is as much as possible “balanced” in the machine and transverse directions.

Ultimate film properties are controlled by molecular orientation and stress induced crystallization[4].

A stable bubble in the film blowing process is a requirement for the continuous operation of the process and the production of an acceptable film [5]. In general there are three forms of instabilities or combinations of these reported in literature:

1. Axisymmetric periodic variations of the bubble diameter, known as bubble instability (BI).
2. Helical motions of the bubble, described as helical instability (HI).
3. Variations in the position of the frost line height (FLHI).

## Chapter III

---

BI and HI have been reported by a number of researchers [6–10], however, FLHI was only reported by Ghaneh-Fard et al. [6,10], after previous authors were using the term “meta stable” [3] which was misleading for time -dependent oscillations in FLH. Results on bubble stability have generally been qualitative until recently when Sweeney et al. [11] utilized a video analysis system as an effective non-contact, real time device for quantifying instabilities during film blowing. Sweeney and his co-workers al. [11] first proposed the diameter range ( $D_r$ ) concept for measuring the degree of helical instability.

The average diameter,  $D$ , and the degree of helical instability (DHI) are then derived from the following equations:

$$D = P_l - P_r \quad (3.1.1)$$

$$D_{\max} = P_{l,\max} \cdot P_{r,\min} \quad (3.1.2)$$

$$D_{\min} = P_{l,\min} \cdot P_{r,\max} \quad (3.1.3)$$

$$D_r = D_{\max} \cdot D_{\min} \quad (3.1.4)$$

$$DHI = \frac{D_r}{D} \times 100 \quad (3.1.5)$$

where  $D$  is the average diameter of the bubble and  $P$  is the average distance of the bubble from a reference line.

The subscript r denotes the distance of the right bubble edge and l the distance of the left bubble edge from the reference line. The bubble was defined as stable if the DHI was less than 20%, partially helically stable if the DHI was between 20 and 40% and helically unstable if the DHI was greater than 40%.

The analysis of bubble stability in film blowing has largely focused on PEs (HDPE, LLDPE and LDPE), mainly due to their superior melt strength in comparison to other polymers such

as PP. Only recently have been reported results on the bubble stability of PP [10]. Ghaneh-Fard et al. [10] studied the bubble stability of PPs and they found that these resins have a

much smaller stable operating window in comparison to PEs.

### 3.2 Fundamental film blowing equations

Pearson and Petrie [12,13] first developed in detail the kinematic and dynamic equations describing fluid flow in film blowing. This was based on the thin shell theory where the thickness of the bubble was small in comparison to the bubble diameter. The kinematic and dynamic analysis of the bubble is discussed below and has provided the theoretical framework for most subsequent studies.

For the continuous steady state operation of an incompressible fluid, the law of conservation of mass at any point along the bubble yields the following relationship for volumetric throughput:

$$Q = 2\pi aHv_s = \text{constant}, \quad (3.2.1)$$

where  $v_s$  is the meridional (machine direction) velocity component,  $Q$  the total volumetric flow rate through the die,  $a$  the local bubble radius and  $H$  the local film thickness. Since the problem is axisymmetric,  $v_t$  (velocity in the transverse direction) is zero and  $v_n$  (velocity in the normal direction) is not exactly zero since the film is changing thickness[14], but is negligible, similar to fibre spinning and lubricating flows.

The derivative of Eq. (3.2.1) with respect to,  $s$ , the distance along the film yields a relation between the deformation rates in film blowing[15]:

$$\frac{dv_s}{ds} = -\frac{1}{H} \frac{dH}{ds} - \frac{1}{a} v_s \frac{da}{ds} \quad (3.2.2)$$

where  $\frac{dv_s}{ds}$ ,  $-\frac{1}{H} \frac{dH}{ds}$ ,  $-\frac{1}{a} v_s \frac{da}{ds}$  represent the rate of stretching along the machine, normal and transverse direction, respectively.

## Chapter III

Considering the thin film bubble membrane[12,13] , a small element of the material is in equilibrium under a set of membrane forces (Figure 3.2 a).  $\sigma_t$  and  $\sigma_s$  are the tangential and meridional stresses, respectively.

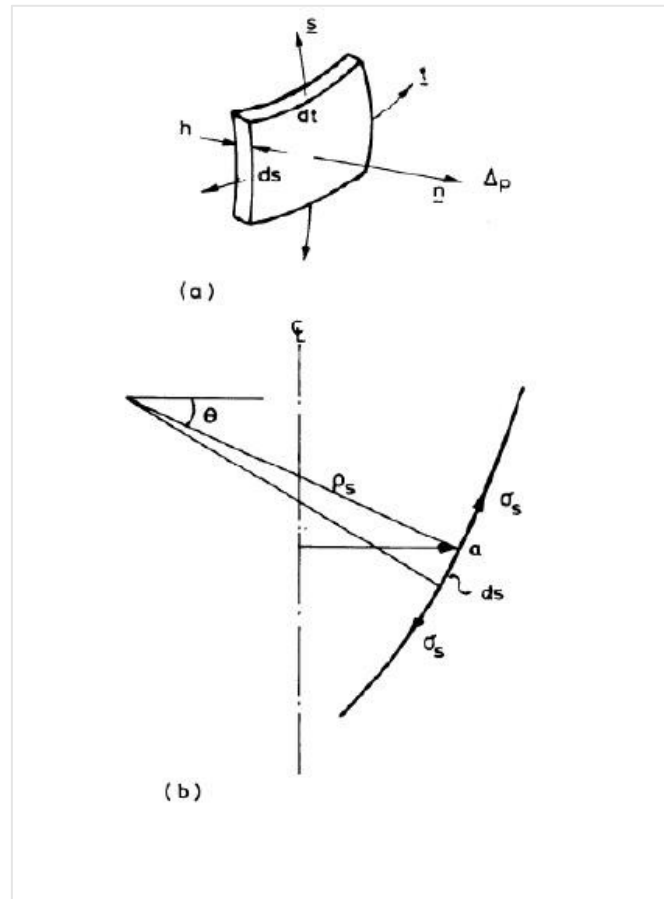


FIG.3.2 Film geometry (a) Element of the film with force and  
(b) Curvature of the film[14]

The equilibrium force balance in the normal direction yields

$$\frac{\Delta P}{H} = \frac{\sigma_s}{\rho_s} + \frac{\sigma_t}{\rho_t} \quad (3.2.3 \text{ a})$$

where  $\rho_s$  and  $\rho_t$  are the principal radii of curvature in the two directions and  $\Delta P$  is the internal pressure measured relative to the external (atmospheric) pressure.

Considering figure 3.2 b

$$\rho_s = \frac{[1+(da/dz)^2]^{3/2}}{\frac{d^2a}{dz^2}} \quad (3.2.3 \text{ b})$$

$$\rho_t = [1 + (da/dz)^2]^{1/2} \quad (3.2.3 \text{ c})$$

where  $a$  is the bubble radius.

A force balance in the direction of the axis of symmetry,  $z$ , yields

$$F_z = -\Delta P \pi a^2 + 2\pi a H \sigma_s \cos \theta \quad (3.2.4)$$

$F_z$  is the (constant) total force on the shell and

$$\cos \theta = \left[ 1 + \left( \frac{da}{dz} \right)^2 \right]^{-1/2} \quad (3.2.4)$$

In the analysis of Pearson and Petrie [12,13] inertia, gravity, surface tension and air drag effects are neglected. These are generally realistic assumptions due to the thin film bubble membrane and the viscous forces dominating the process for polymer melts. The governing equations can be easily extended to include these effects by incorporating appropriate physical data. These equations combined with a rheological constitutive equation, relating the stresses to the strains or strain rates in the bubble, result in a series of equations which are solved to yield predictions for various film blowing process characteristics (film temperature, bubble radius and velocity profiles).

## Bibliography

---

- [1] <http://www.layfieldflexpack.com/pages/plastics101/extrusionprocess.aspx>
- [2] J.F. Agassant, P. Avenas, J.Ph. Sergent, P.J. Carreau, *Polymer Processing Principles and Modeling*, Carl Hanser, Munich,(1991).
- [3] C.D. Han, *Rheology in Polymer Processing*, Academic Press, New York, 1976
- [4] J.M. Dealy, K.F. Wissbrun, *Melt Rheology and its Role in Plastics Processing*, Van Nostrand Reinhold, New York, (1990).
- [5] M. Fleissner, *Int. Polym. Process.* 2, 229(1988).
- [6] A. Ghaneh-Fard, P.J. Carreau, P.G. Lafleur. 37,1148 (1997).
- [7] T. Kanai, J.L. White, *J. Polym. Eng.* 5,135 (1985).
- [8] T. Kanai, J.L. White, *Polym Eng Sci* 24,1185 (1984).
- [9] C.D. Han, J.Y. Park, *J. Appl. Polym. Sci.* 19,3291,138 (1975)
- [10] A. Ghaneh-Fard, P.J. Carreau, P.G. Lafleur, *Am. Inst. Chem. Eng. J.* 42, 1388 (1996).
- [11] P.A. Sweeney, G.A. Campbell, F.A. Feeney, *Int. Polym Process.* 7, 229 (1992).
- [12] J.R. Pearson, C.J.S. Petrie, *J. Fluid Mech.* 42, 60 (1970).
- [13] J.R.A. Pearson, C.J.S. Petrie, *J. Fluid Mech.* 40, 1 (1970).
- [14] Luo, X.L., Tanner, R. I. *J. Polym Eng & Sci*, 25, 620 (1985)
- [15] Muke, S., Connell H., Sbarski I. & Bhattacharya S. N. *J. Non newtonian Fluid Mech.*, 116, 113 (2003)

***Thermal and Structural  
Characterization  
of Biodegradable Blends Filled With  
Halloysite Nanotubes***

### 4.1 Introduction

In recent decades, environmental aspects, especially related to the increasing widespread use of plastics from several industrial applications, have gained ever more interest as to encourage research in the study and the development of the so called eco-materials.

In this context, as witnessed by a large amount of literature, much effort has been spent to emphasize potentialities of these resins, often less efficient and more expensive than traditional ones derived from petroleum, considering also the use of natural fillers as reinforcements [1-7].

Biodegradable resins can be derived from renewable resources, synthesized by microbes or coming from petroleum but intrinsically biodegradable owing to some specific structural features which helps their environmental degradation. Among the ones coming from microbial synthesis, a relevant role is played by poly hydroxy alkanoates (PHAs), which family belongs to polyhydroxy butyrate-co-valerate (PHBV) copolymers. These materials are attractive candidates for many applications owing to their biodegradability and biocompatibility [8, 9] but their use is still limited by some drawbacks such as slow crystallization rate, relatively difficult processing, low elongation at break, and very high degree of crystallinity. At this aim, a huge amount of articles report about modification of PHBV resins by blending with many polymers such as poly vinyl chloride [10], poly(propylene carbonate) [11], poly(L-lactic) acid [12], poly(ethylene succinate) [13], polyolefins [14], and polycaprolactone [15]. In this context, the matrix used in this research, currently supplied by a Chinese firm, involves two biodegradable resins:

PHBV and poly butylene adipate-co-terephthalate (PBAT) in a blend with a weight ratio equal to 30:70, respectively.

Javadi et al. [16], investigating solid and microcellular components based on PHBV/PBAT blends with different weight ratios, demonstrated that an increasing inclusion of PBAT strongly influence the morphology of microcellular items by increasing the cell sizes and simultaneously reducing the cell density of foamed products. Moreover, a relevant improvement of mechanical properties, especially in terms of toughness and elongation at break, and variation of thermal properties by reduction of the degree of crystallinity was observed in all components with the increase of the PBAT loading.

Further available results about the same formulations refer to investigations carried out on composite systems filled with recycled wood fibers (RWF) and nanoclay. Specifically, again Javadi et al. [17] demonstrated that at constant content of PBAT, the wood fibers reduces the size of the cells and increase their density while the clay particles do not seem to have any effect on this morphological aspect.

Further applications of these blends could be provided in the food packaging field maybe by improving their mechanical and/or barrier properties, even by the inclusion of nanofillers. In this regard, interesting perspectives have been proven by composite systems containing nanoclays as widely reported in the literature [18–20].

In this frame, in order to verify potential applications of the PHBV/PBAT blends in the packaging field and with the aim to further enhance the mechanical properties of films based on, the focus of this research has been devoted to clay materials with needle-like or tubular-like structure as reinforcement. This filler, best known as halloysites ( $\text{Al}_2\text{Si}_2\text{O}_5(\text{OH})_4 \times n\text{H}_2\text{O}$ ), is a two-layered (1:1) natural aluminosilicate clay, chemically similar to kaolin but exhibiting a predominantly tubular morphology.

From a structural point of view, tubes of halloysite (HNTs), naturally available with an aspect ratio up to almost 100, are characterized by 15–20 aluminosilicate layers rolled in the multiplayer tubule walls with a layer spacing of 0.72 nm for the dehydrated halloysite. In particular, the  $\text{SiO}_2$  layer is relevant to the outer surface of the tube and it is negatively charged above pH 4, whereas the  $\text{Al}_2\text{O}_3$  layer is relevant to the inner lumen surface, resulting in a positively charged interior of the tubes at pH less than 8.5 [21,22].

Recently, halloysites, typically used in the manufacture of high quality ceramic white-ware, have received much attention. In fact, on one side, they have the potential to provide cheap alternatives to the expensive carbon nanotubes whereas, on the other hand, given their chemical similarity to lamellar clays as montmorillonites, they have the possibility to be further intercalated by chemical and/ or physical ways [23].

Halloysite nanotubes (HNTs) are a new type of additive for enhancing the mechanical, thermal and fire-retardant performance of polymers[24-34].

Other potential applications of HNTs, considered by now, regards drug-delivery systems [35, 36], nanotemplates or nanoscale reaction vessels instead of carbon nanotubes or boron nitride nanotubes [37–41], and treatment of contaminated waters by removing of dyes [42– 44] widely used in various fields.

In this chapter, the influence of inclusions of as received or chemically modified tubular clays

on thermal behavior and structural aspects of a commercial PHBV/PBAT blend have been investigated.

Furthermore, in order to simulate the effect of processing conditions on the same thermal and structural issues, the investigation of any effects related to the application of various cooling rates has been also considered for all examined film samples.

## Experimental

### 4.2 Materials

A commercial PHBV/PBAT 30/70 wt/wt blend was used as the matrix. This blend, purchased in pellet form from Ningbo Tianan Biologic Material Co. Ltd. (Tinan- ENMAT) (China) under the trade name 6010P, in the following is simply coded as Enmat.

About the filler, clay nanotubes best known as halloysites (HNTs) with average sizes equal to: 0.25–4 nm (length), 30 nm (diameter), and 64 m<sup>2</sup>/g (surface area) were supplied by Sigma Aldrich. As will be discussed later, X-ray diffraction analysis confirmed that the halloysite was in the dehydrated state showing a diffraction signal at 12.138 corresponding to a (001) basal spacing of approximately 7.3Å.

3-(Trimethoxysilyl)-propyl methacrylate (MPS), chemically 98% pure grade, was purchased from Sigma Aldrich.

#### 4.2.1 Functionalization of HNTs

For the purpose of modification of Halloysite clay, 3-(trimethoxysilyl) propyl methacrylate (MPS), was added to an ethanol solution with pH 4.5, obtained dropping acetic acid and mildly stirred for 5 min. Halloysite nanotubes were then gradually added into the solution and stirred for 15 min. The mixture was left at ambient temperature for roughly 2 hours and then under vacuum at 70° to complete the removal of residual traces of solvent[33].

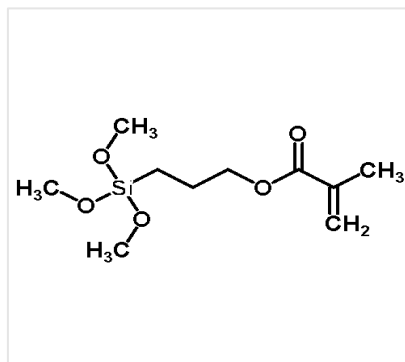


FIG.4.1 Chemical structure of MPS

### 4.3 Preparation of Nanocomposites and Films

Formulations based on Enmat, containing as received or chemically modified clay nanotubes, were prepared by melt compounding. The matrix and the fillers, opportunely pre-dried in a vacuum oven at 70°C for 12 hr, were hand-mixed prior to extrusion. Each formulation was fed by a hopper to a HAAKE PolyLab twin-screw extruder (L/D = 40), employing the following temperature profile 150–155–160–165–165–160–160–160°C from the hopper to the die and a screw speed equal to 100 rpm.

All the extruded materials were dried under the same conditions of the starting materials and processed by the traditional technology of film blowing. At this purpose, a COLLIN single screw extruder (25:1 L/D) equipped with a COLLIN TEACH LINE BL50T with a diameter of 30 mm, a die-gap of 0.8 mm was used. The screw rotation speed was 27 rpm and the temperature profile equal to 160–175–175–165–160°C from the hopper to the die. Films having a thickness approximately equal to 35 µm were manufactured with a blow up ratio (BUR) of 3.3 and maintaining the longitudinal draw ratio (DR) of 7. The homogeneity of the thickness of the film were quantitatively measured by cutting a 1m long film for all materials and measuring the thickness on at least five positions every 20 cm.

### 4.4 Characterization Techniques

#### 4.4.1 Fourier Transform Infrared Spectroscopy (FTIR)

The chemical interaction of silane with nanotube surface was verified by infrared spectroscopy. The FTIR-ATR instrument used was a Nicolet 6700 (Thermo Scientific) operating in the wavenumber range of 650 to 4000  $\text{cm}^{-1}$ , with ZnSe crystal, 32 scans and 4  $\text{cm}^{-1}$  resolution.

#### 4.4.2 Thermogravimetric Analysis (TGA)

TGA was conducted under nitrogen atmosphere with TGA Q 5000 by TA Instruments at a heating rate of 10°C/min from 30°C to 700°C.

Average weight of each sample was about 6 mg. This test was done in order to study changes in the onset of degradation temperature after nanofiller addition.

#### 4.4.3 Differential Scanning Calorimetry (DSC)

All tests were made by using a Mettler Differential Scanning Microscopy 1 instrument in nitrogen atmosphere with a sample weight about 8–10 mg. For each test, sample was first heated from 25°C to 200°C at a rate of 10°/min, and kept at the end temperature for 1 min, in order to erase the thermal history of the samples (I run). The specimen was subsequently cooled at constant rates of 2, 5, and 10°/min up to -60°C (II run) and, finally, reheated up to 200°C with a heating rate of 10°/min (III run).

Thermal tests have been performed within 3 days from the film fabrication in order to avoid that physical ageing phenomena, given the low Tg of the matrix (-32°C), might influence the results. The degree of crystallinity ( $x_c$ ) of the PHBV phase and nanocomposites was evaluated using the following equation:

$$x_c = \frac{\Delta H_m}{\Delta H_m^0} \frac{100}{(1 - w)}$$

where  $\Delta H_m^0$  is the enthalpy of melting per gram of the 100% crystalline of the single copolymers (109 J/g and 114 J/g for PHBV and PBAT respectively)[45,46],  $\Delta H_m$  is the measured enthalpy of melting determined from the DSC endotherms, and  $w$  the weight fraction of filler.

#### 4.4.4 Wide-angle X-ray diffraction (WAXD)

Wide-angle X-ray diffraction (WAXD) measurements were obtained by an automatic Bruker D8 Advance diffractometer, in reflection, at 35 kV and 40 mA, using the nickel filtered Cu-Ka radiation (1.5418 Å). The WAXD patterns were recorded on both film samples and crystallized DSC specimens for  $2\theta$  values from 5 to 40°, with a step size of 0.007° and an acquisition time of 1 sec. The observed integral breadths ( $B_{hkl}$ ) were determined by a fit with a Lorentzian function of the intensity corrected diffraction patterns. The instrumental broadening ( $b$ ) was also determined by fitting of Lorentzian function to line profiles of a standard silicon powder 325 mesh (99%). For each observed reflection, the corrected integral breadths were determined by subtracting the instrumental broadening of the closest silicon reflection from the observed integral breadths,  $\beta_{hkl} = B_{hkl} - b$ . The correlation lengths perpendicular to  $hkl$  planes ( $D_{hkl}$ ) were determined using Scherrer's equation, assuming the Scherrer's constant  $K = 0.9$ .

$$D_{hkl} = \frac{K\lambda}{\beta_{hkl} \cos \theta_{hkl}}$$

where  $\lambda$  is the wavelength of the incident X-rays and  $\theta_{hkl}$  the diffraction angle.

WAXD measurements were also obtained with an automatic Philips powder diffractometer, in transmission, by using a cylindrical camera (radius = 57.3 mm). The WAXD patterns were recorded on a BAS-MS imaging plate (FUJIFILM) and processed with a digital imaging reader (FUJIBAS 1800). In particular, to recognize the kind of crystalline orientation present

in the samples, photographic X-ray diffraction patterns were taken by placing the film sample parallel to the axis of the cylindrical camera and by sending the X-ray beam parallel to the film surface.

### 4.5 RESULTS AND DISCUSSION

#### 4.5.1 Fourier Transform Infrared Spectroscopy (FTIR)

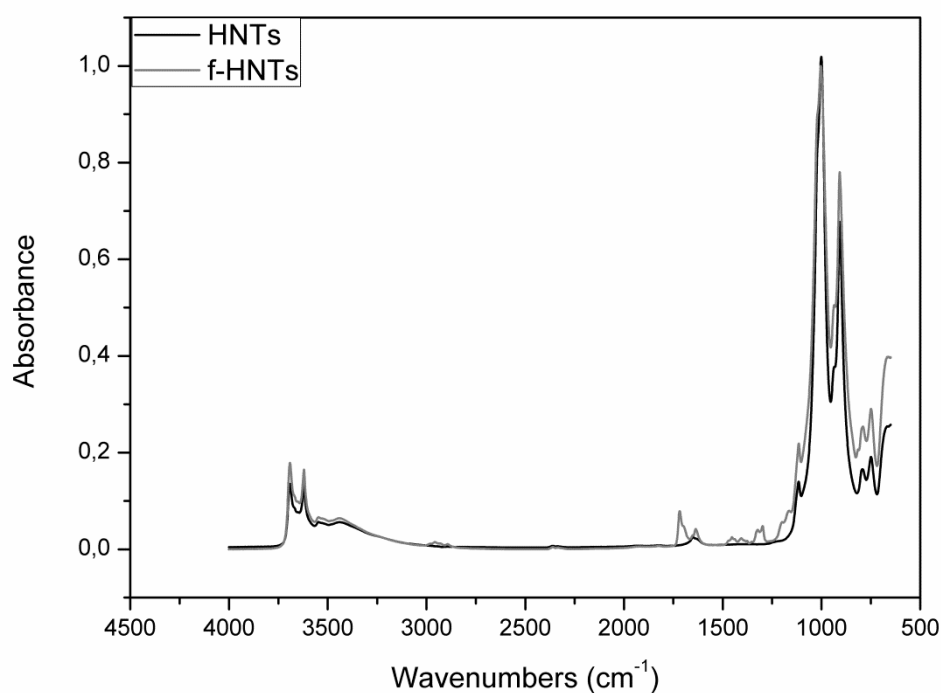


FIG.4.2 FTIR spectra of as received and modified Halloysite

The infrared spectra of halloysite in the hydroxyl stretching region show two bands at  $3690\text{ cm}^{-1}$ , which is attributed to the hydroxyl stretching of the inner surface hydroxyl and band at  $3619\text{ cm}^{-1}$  assigned to the inner hydroxyls. The absorption bands at  $1470$ ,  $1720$  and  $2958\text{ cm}^{-1}$  are attributed to the  $\text{CH}_2$  scissoring, C-O and C-H stretching vibration while the C-C adsorption band is shown at  $1637\text{ cm}^{-1}$ .

The increasing of the intensity of the band at  $909\text{ cm}^{-1}$  from HNTs to f-HNTs and the slightly intensifying of the band at  $1110\text{ cm}^{-1}$  may be indicative of the possibility of RSi–O–Si and RSi–O–Al bonds between RSi–OCH<sub>3</sub> and RSi–OH groups of MPS with Si–O groups at the surface and Al–OH groups at the edges of the HNTs[47].

The absorption bands at  $1023\text{ cm}^{-1}$  related to Si–O–Si stretching bands become sharper due to some silane groups were linked to the surface of the tubes forming Si–O–Si bonds.

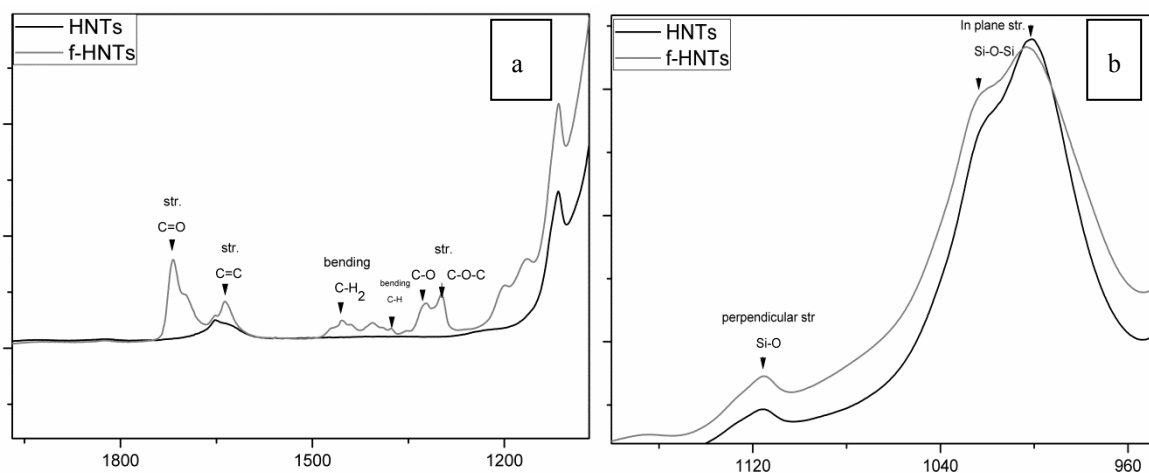


FIG.4.3 Infrared spectra (a) in the  $2000\text{--}1100\text{cm}^{-1}$  and (b) in the  $1200\text{--}900\text{cm}^{-1}$ .

### 4.5.2 Thermogravimetric Analysis (TGA)

The effect of the clay content on the thermal stability of Enmat and its composites were examined by TGA. Weight loss curves and their derivative (DTG), figure 4.4-4.5, for all the samples, show two major weight loss steps, attributable to PHBV and PBAT respectively[48,49].

The initial degradation temperatures, the maximum degradation rate temperatures obtained by

DTG, and the ash content at 700°C are reported in Table 4.1.

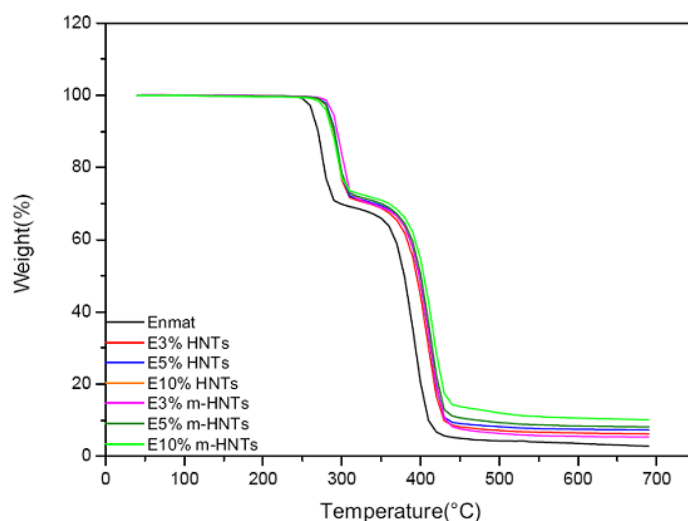


FIG.4.4 Weight loss of Enmat and its HNT composites

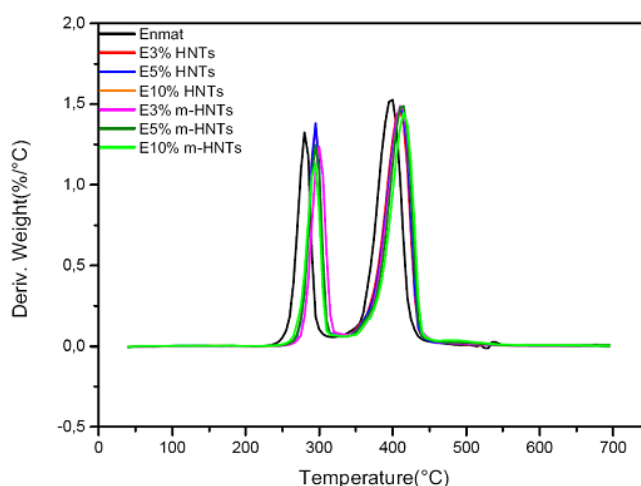


FIG.4.5 Derivative TGA

Results show that the addition of Halloysite nanotubes affect the thermal decomposition behaviour of the matrix. The thermal stability is increased, the onset temperature of PBAT is shifted to higher temperatures, indicating a stabilization effect of filler. In the first decomposition step, related to PHBV an increase of onset temperatures occurs, too.

In all cases, the residual weights are close to that of the nominal loadings.

In the composite systems an increase in the tortuosity of gas molecules is less plausible due to its tubular structure, instead the limited diffusion of degradation products is more likely

related to extensive molecular interaction between the polymer and the filler[50].

Another explanation of the increase of thermal stability could be found in the entrapment of degradation product inside the lumen of nanotubes, as reported by Du *et al.*[33] in their study on PP/HNT nanocomposites.

The thermal stability can be partly ascribed to the presence of a relatively low amount of iron oxides ( $\text{Fe}_2\text{O}_3$ ) [51] in the HNTs.

Filler content (%)	Initial degradation temperature (°C)		DTG peak temperature (°C)		Residue (%)
	PHBV	PBAT	PHBV	PBAT	
0	273	344	285	403	2,9
3%HNTs	284	360	295	409	5,9
5%HNTs	285	363	295	411	7,4
10%HNTs	283	362	295	410	10,1
3% m-HNTs	288	365	299	411	5,6
5% m-HNTs	285	368	295	412	8,1
10% m-HNTs	282	376	294	415	10,8

TAB.4.1 Thermal decomposition of all of the formulations

### 4.5.3 Differential Scanning Calorimetry (DSC)

Figures 4.6 (a) and (b) compare the DSC heating thermograms of composite film samples containing neat HNTs and silanized HNTs, respectively, with the thermal behavior of film samples of the neat matrix. From these picture a slight endothermic signal centered at about 125°C, typical of the PBAT phase, and a strong signal approximately centered at 172°C relative to the PHBV phase are always detected.

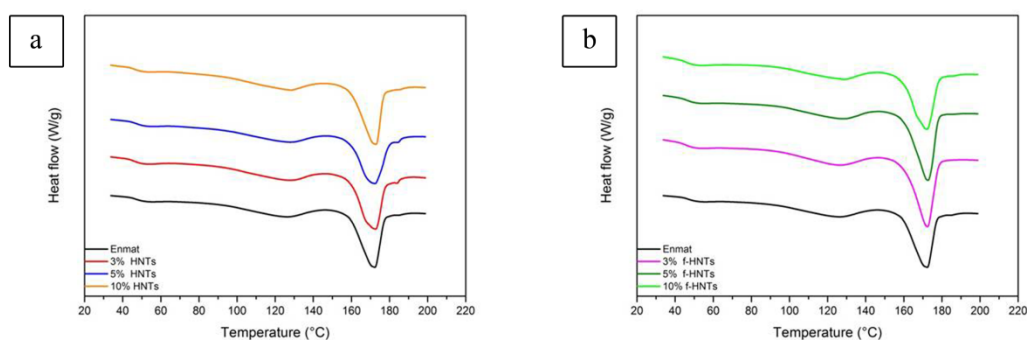


FIG.4.6 Comparison of DSC 1<sup>st</sup> heating run of composite films containing pure HNTs(a) and silanized HNTs (b)

As shown in Table 4.2, the inclusion of the nanotubes of HNTs does not significantly influence neither the shape nor the position of the weak signal associated to the PBAT phase. On the contrary, although the position of the strongest signal related to the PHBV phase seems to remain almost unchanged, deformations and broadening effects are always evident. Moreover, an increase of the melting enthalpies of the PHBV phase is recorded indicating the increase of its degree of crystallinity with the filler loading especially in the presence of unmodified clay nanotubes.

Filler content (wt%)	$T_{mPBAT}$ (°C)	$\Delta H_{mPBAT}$ (J·g <sup>-1</sup> )	$T_{mPHBV}$ (°C)	$\Delta H_{mPHBV}$ (J·g <sup>-1</sup> )
0	125,3	6,1	172,3	18,2
3% HNT <sub>s</sub>	125,8	6,2	172,8	20,2
5% HNT <sub>s</sub>	126,4	5,9	172,5	20,3
10% HNT <sub>s</sub>	126,3	6,2	172,9	21,1
3% f- HNT <sub>s</sub>	125,4	6,5	172,4	20,6
5% f- HNT <sub>s</sub>	126,2	6,7	172,6	20,8
10% f- HNT <sub>s</sub>	126,0	6,5	172,1	20,9

TAB. 4.2 Melting temperatures ( $T_m$ ) and hentalpies ( $\Delta H_m$ ) of the main phases constituting the investigated materials.

About the cooling step, in order to simulate different processing conditions, the effect of different crystallization rates (CR) on thermal and structural aspects of the examined systems has been considered. In details, the cooling has been performed at 2, 5 and 10 °C/min. As expected, the increase of the rate of cooling broaden and shifts crystallization signals to lower temperatures. In fact, the faster is the cooling the greater is the likelihood that crystals are formed uneven in terms of both size and shape (broadening of the signal). In addition, usually the macromolecular chains constituting the material, having a mean relaxation rate slower than the cooling one, starts to crystallize at temperatures much lower as quickly lowers their temperature.

These results, evident for the neat matrix in Figure 4.7, are enhanced by the filler loading (see Figure 4.8) but they are significantly reduced, under the same cooling rate, for samples containing silanized clay nanotubes (see Figure 4.9). This behavior may be interpreted assuming that the unevenness of PHBV crystals can be reduced by improving the interactions at the filler-matrix interface.

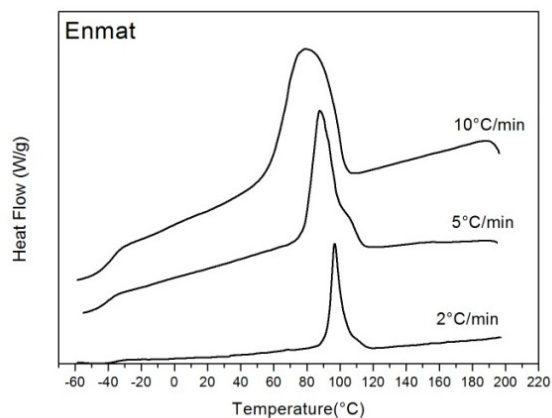


FIG. 4.7 DSC cooling curves of the matrix at various cooling rates

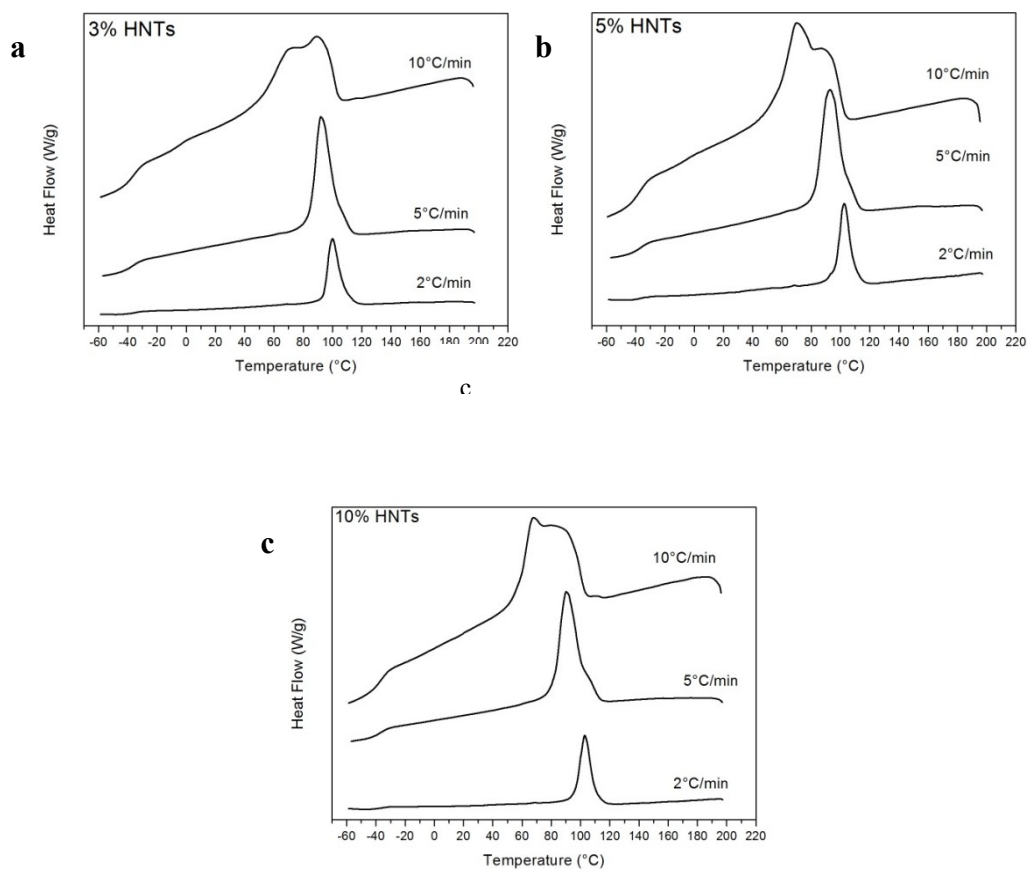


FIG 4.8 DSC cooling curves of nanocomposites containing 3 wt% (a), 5 wt% (b) and 10 wt% (c) of pure halloysites at various cooling rates

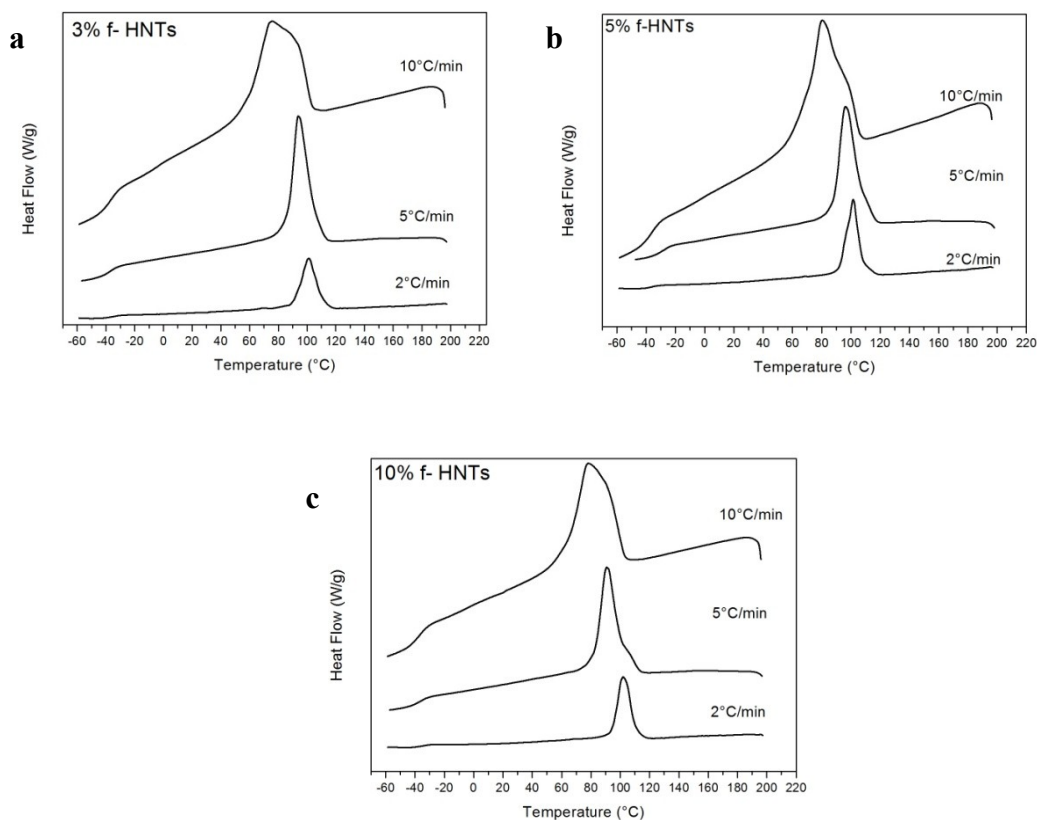


FIG.4.9 DSC cooling curves of nanocomposites containing 3 wt% (a), 5 wt% (b) and 10 wt% (c) of modified halloysites at various cooling rates

Figure 4.10 collects heating thermograms of all studied film samples, previously crystallized at 2 °C/min, taking the neat matrix based films as the reference for each of the two families of examined composite systems.

In all cases, on the contrary to what observed in the first heating step, it is evident a splitting of the melting signal of the PHBV phase in a low-temperature (L) and a high-temperature signal (H) and, again, no effect on the slight PBAT signal.

Analogous considerations, although with different extent, may be drawn from Figures 4.11 and 4.12 comparing second heating thermograms of samples crystallized at 5 and 10 °/min, respectively, with respect to the reference sample.

Recently, the existence of a double-melting signal for PHBV based systems, widely investigated by calorimetric and diffraction methods, has been explained in different ways. The behavior is mainly ascribed assuming melting and recrystallization of thin, unstable crystals during the calorimetric scan [52-54]. Owen et al. [55] attribute the reason of the

splitting to the HV units acting as defects of the PHB lattice. According to this assumption, given the reduced cohesion of molecules in the crystals of PHBV with respect to PHB, HV units could diffuse out of the crystal during the reorganization, increasing the internal cohesion of crystals and increasing the melting parameters.

Wang et al. [56], investigating PHBV based films containing montmorillonites associated the presence of two endothermic signals just to the inclusion of lamellar clays. They considered the low-temperature peak as the main peak of pure PHBV and they ascribed the high-temperature melting peak to a new polymorphic structure growing on the MMT layers (heterogeneous nucleation).

As better highlighted from Table 4.3, the peak crystallization temperature decreases with increasing the cooling rate (CR) while the melting temperatures are only slightly affected by this variable. Moreover, an increase of the crystallization temperature with the filler content is always observed at least up to 5% by weight of filler as a sign of a dominant heterogeneous nucleation on the homogeneous crystallization phenomena of the PHBV phase. This effect, confirmed by the increase of the overall degree of crystallinity, is reduced in presence of silanized halloysites for which the improved adhesion at the interface with the matrix could decrease the filler surface available for heterogeneous nucleation.

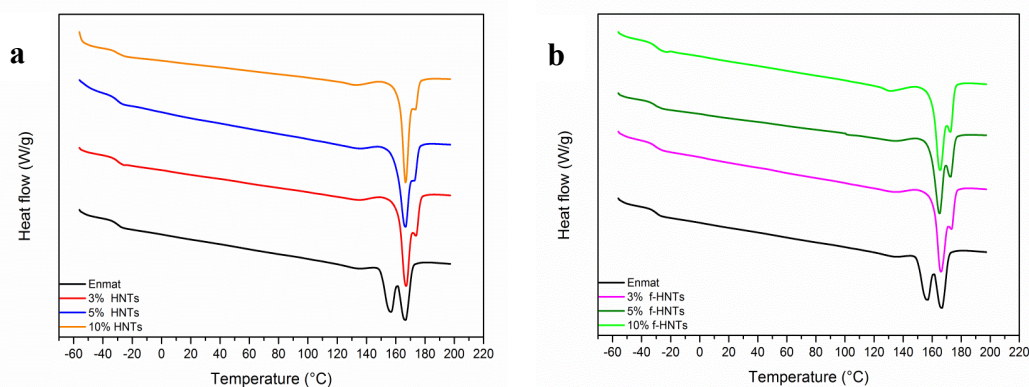


FIG. 4.10. Comparison of thermograms of specimens containing as received (a) and modified (b) halloysites, all crystallized at 2 °C/min

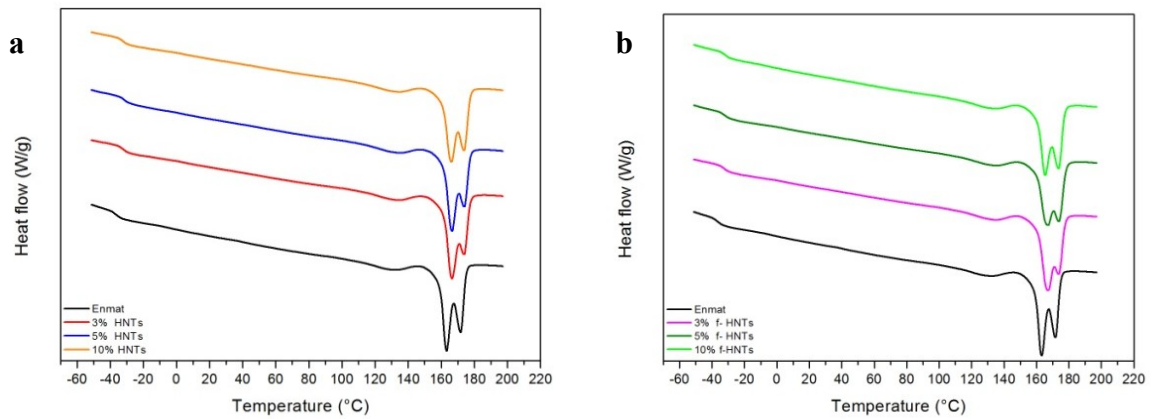


FIG. 4.11. Comparison of thermograms of specimens containing as received (a) and modified (b) halloysites, all crystallized at 2 °C/min

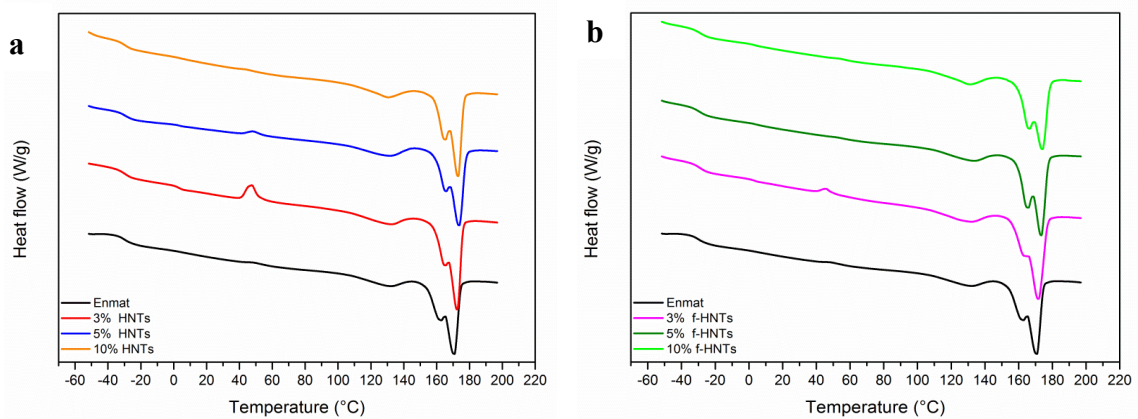


FIG. 4.12 Comparison of thermograms of specimens containing as received (a) and modified (b) halloysites, all crystallized at 10 °C/min

## Chapter IV

CR (°C min <sup>-1</sup> )	2						5						10					
	LT <sub>m</sub> (°C)	HT <sub>m</sub> (°C)	ΔH <sub>m</sub> (J g <sup>-1</sup> )	x (%)	T <sub>c</sub> (°C)	ΔH <sub>c</sub> (J g <sup>-1</sup> )	LT <sub>m</sub> (°C)	HT <sub>m</sub> (°C)	ΔH <sub>m</sub> (J g <sup>-1</sup> )	x (%)	T <sub>c</sub> (°C)	ΔH <sub>c</sub> (J g <sup>-1</sup> )	LT <sub>m</sub> (°C)	HT <sub>m</sub> (°C)	ΔH <sub>m</sub> (J g <sup>-1</sup> )	x (%)	T <sub>c</sub> (°C)	ΔH <sub>c</sub> (J g <sup>-1</sup> )
0	156.5	166.8	17.5	16.1	96.7	23.9	165.0	173.3	17.6	16.1	87.7	26.4	162.9	170.8	18.1	16.6	78.5	25.2
3 HNTs	167.1	173.9	19.0	18.0	100.0	25.3	166.4	173.9	21.4	20.2	90.0	27.3	164.6	172.4	22.2	21.0	88.7	20.6
5 HNTs	166.6	172.8	18.9	18.3	102.7	27.0	165.3	173.5	22.6	21.8	92.7	27.8	165.4	173.5	24.3	23.5	89.1	22.7
10 HNTs	166.5	173.4	17.3	17.6	103.0	25.1	166.7	174.3	21.6	22.0	89.1	27.5	165.1	172.9	22.9	23.3	85.4	24.5
3 f-HNTs	166.1	173.6	18.9	17.9	101.2	25.9	164.5	173.1	20.6	19.5	90.2	27.6	162.9	171.6	20.8	19.7	75.7	25.4
5 f-HNTs	165.1	172.8	18.1	17.5	101.6	26.4	165.9	173.3	22.0	21.2	91.3	28.5	165.8	173.2	22.8	22.0	80.1	24.7
10 f-HNTs	165.4	172.5	19.9	20.3	101.9	29.8	165.8	173.5	19.6	20.0	92.9	24.3	165.8	173.9	21.3	21.7	78.1	24.8

TAB. 4.3 DSC thermal parameters of all investigated materials.

In order to gain further insights into double-melting behavior, the PHBV endothermic signals were analyzed remotely using a deconvolution route that, in all cases, allowed the evaluation of melting enthalpies and some geometric parameters as the Full Width at Medium Height (FWMH) of both low- and high-temperature peaks.

For example, the deconvolution of the double-melting signal related to composite films containing 3% by weight of pure HNTs is shown in Fig.4.13.

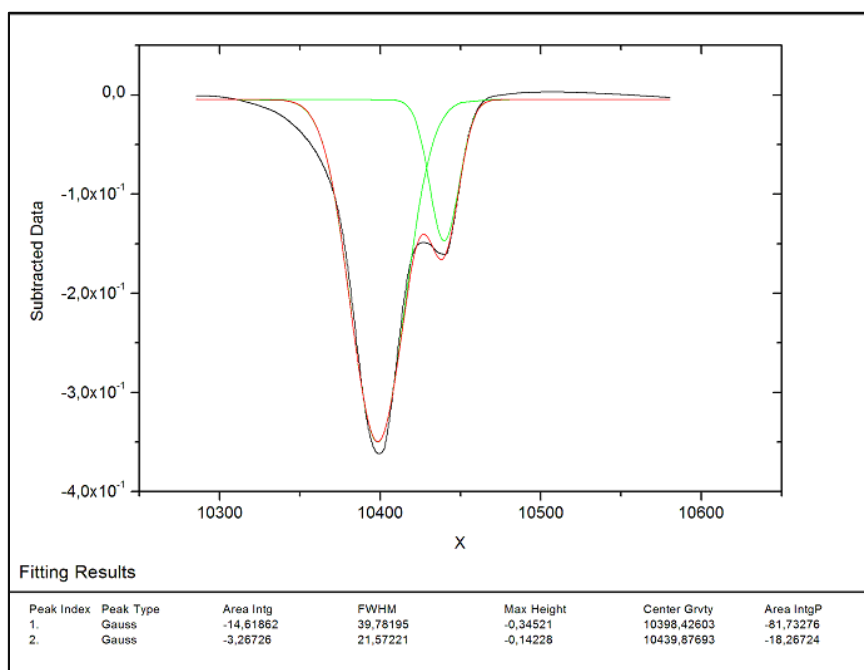


FIG 4.13 Example of deconvolution of the melting signals

Results, in terms of enthalpy values (Table 4.4), show that, at the lowest crystallization rate, composite films, compared with unfilled ones, display higher melting enthalpies and crystallization temperatures which proved the crystallization-promoting effect of halloysite. This effect disappears by increasing the cooling rates probably due to the prevalence of the homogeneous crystallization phenomena.

CR (°C/min)	2		5		10	
Enthalpies (J/g)	$\Delta H_L$	$\Delta H_H$	$\Delta H_L$	$\Delta H_H$	$\Delta H_L$	$\Delta H_M$
<b>Enmat</b>	8.9	9.1	12.3	7.1	9.7	8.3
<b>3 wt% HNTs</b>	14.6	3.3	13.5	5.1	10.6	8.3
<b>5 wt% HNTs</b>	15.7	1.8	12.5	5.3	9.2	8.7
<b>10 wt% HNTs</b>	13.1	2.5	12.0	6.1	9.4	9.0
<b>3 wt% f-HNTs</b>	14.4	3.3	14.5	5.0	9.3	11.4
<b>5 wt% f-HNTs</b>	13.4	3.8	13.9	5.6	9.9	9.4
<b>10 wt% f-HNTs</b>	15.1	3.9	11.0	7.1	10.1	7.9

TAB.4.4 Enthalpies of low-temperature (L) and high-temperature (H) melting signals

Moreover, besides the matrix, for which it seems that there isn't a well-defined trend for enthalpies of the signals at low and high temperature with the cooling rate, in the case of nanocomposites it is clear that with increasing the crystallization rate, the area of the peak at low temperature decreases while the area of the peak at high temperature increases.

At this regard, it is plausible to assume that the low-temperature signal is related to the melting of uneven crystals produced by the homogeneous crystallization of the PHBV phase while high-temperature one is due to the melting of more perfect crystals coming from the nucleation action of the included filler nanoparticles. Thus, given the simultaneous occurrence of both crystallization phenomena in all investigated systems, results show that the higher the cooling rate the more pronounced is the effect of the heterogeneous nucleation. In other words, given the extremely low crystallization rate of the PHBV phase, at high cooling rates heterogeneous crystallization phenomena induced by the filler prevail on homogeneous ones giving rise to more stable films, at least in terms of thermal properties.

As far as the Full Width at Medium Height (FWMH) is concerned, again composite films has shown narrower melting signals and more symmetrical melting and crystallization curves, with respect to the neat matrix suggesting a narrower crystal size distribution in the nanocomposites then in the pure PHBV. This effect is enhanced by increasing the filler content. Regarding the influence of cooling rate, instead, under the same filler content, the increasing of this parameter leads to a narrowing of the low-temperature melting signals and a

broadening of the high-temperature ones (see Table 4.5). This behavior is in line with the ever more enhanced effect of heterogeneous nucleation phenomena with respect to homogeneous one, by increasing the rate at which film samples are cooled.

CR (°C/min)	2		5		10	
Sample	FWMH <sub>L</sub> (°C)	FWMH <sub>H</sub> (°C)	FWMH <sub>L</sub> (°C)	FWMH <sub>H</sub> (°C)	FWMH <sub>L</sub> (°C)	FWMH <sub>H</sub> (°C)
<b>Enmat</b>	44.3	36.8	40.7	27.5	64.2	31.6
<b>3 wt% HNTs</b>	39.8	21.6	44.4	25.1	59.4	27.1
<b>5 wt% HNTs</b>	36.0	17.8	42.1	25.9	57.9	31.6
<b>10 wt% HNTs</b>	33.2	11.6	44.9	26.9	51.6	28.6
<b>3 wt% f-HNTs</b>	42.1	22.1	50.9	25.1	61.0	37.9
<b>5 wt% f-HNTs</b>	43.4	23.2	53.6	28.6	49.7	31.0
<b>10 wt% f-HNTs</b>	43.2	22.1	42.8	29.2	56.0	31.6

TAB 4.5 Full Width at Medium Height (FWMH) of low-temperature (L) and high-temperature (H) melting signals

#### 4.5.4 X-Ray Diffraction Analysis

Structural features of both film samples and specimens, crystallized during DSC cooling scans, have been studied by X-ray diffraction analysis. The diffraction patterns of ENMAT in pellet (curve A) and in film form (curve B) have been reported in Fig. 4.14 indicating reflections of PHBV and PBAT phases with filled circles and filled squares, respectively [57-60]. The diffraction pattern B of of Figure 4.14 shows that during the film blowing process both PHBV and PBAT phases crystallize.

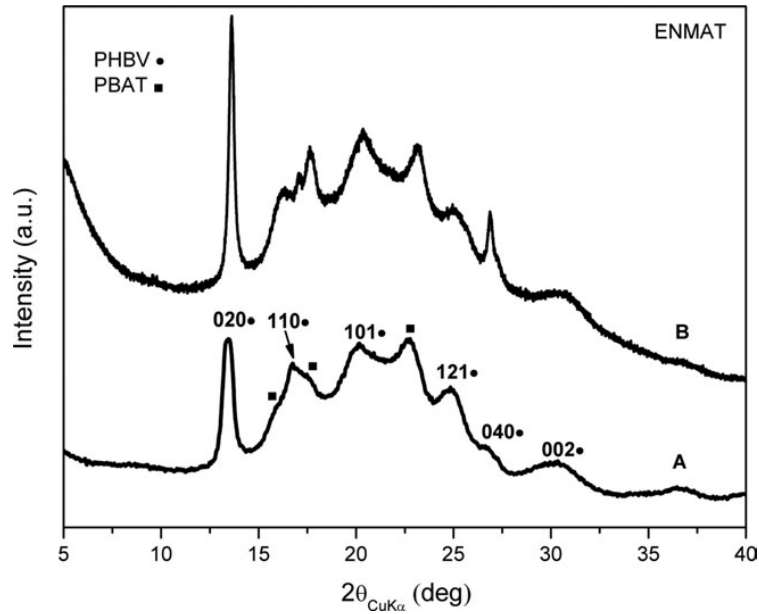


FIG.4.14 X-ray diffraction patterns of ENMAT in pellet form (A) and in film form (B): (filled circles) reflections of PHBV phase; (filled squares) reflections of PBAT phase.

Moreover, narrower reflections of pattern B with respect to the ones characterizing pattern A, suggest the presence of more perfect crystals in the film form (e. g. for PHBV orthorhombic crystals  $D_{020}$  increases from 14,5 to 30,1 nm). Diffraction patterns of composites containing as received and modified HNTs have been reported in Figures 4.15 and 4.16. In both figures the diffraction patterns of the polymer matrix and the filler have been reported. In these pictures, reflections characterizing the PHBV and PBAT crystalline phases have been highlighted with filled symbols, while reflections of the HNTs crystalline phases have been indicated as empty triangles [61].

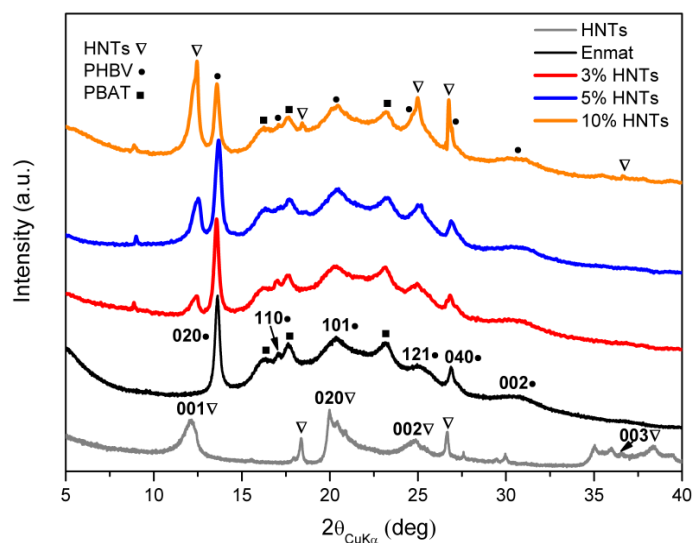


FIG. 4.15 X-ray diffraction patterns for films containing pure HNTs: (filled symbols) reflections of PHBV and PBAT crystalline phases; (empty triangles) reflections of HNTs crystalline phase.

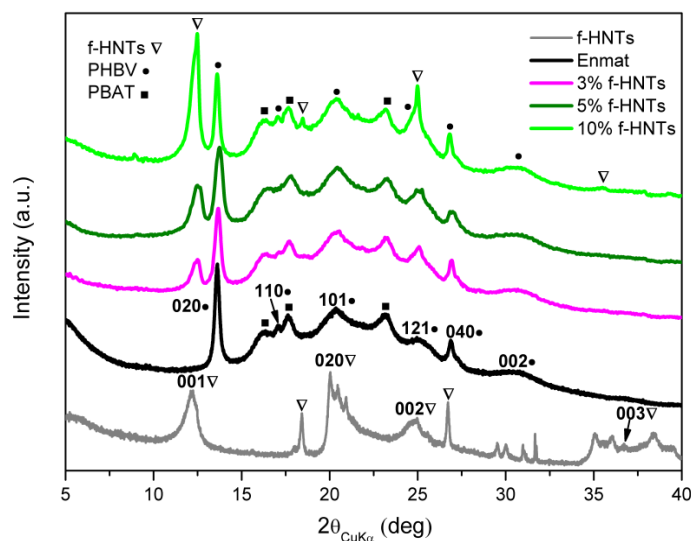


FIG.4.16 X-ray diffraction patterns for films containing modified HNTs: (filled symbols) reflections of PHBV and PBAT crystalline phases; (empty triangles) reflections of modified HNTs crystalline phase.

In these cases, in line with calorimetric results, the presence of the filler, although it may alter the kinetics and mechanisms of crystallization, does not seem to affect the degree of crystallinity of the PBAT phase. The intensity ratio between the reflections of the HNTs

phase is strongly altered in composite films, while the positions remain unchanged. In particular, 001 and 002 reflections are much more intense and the 020 reflection is negligible. This indicates a preferred orientation of the HNTs basal planes parallel to the film plane. Such orientation has been confirmed by X-ray diffraction patterns, taken with beam parallel to the film plane and collected on a photographic cylindrical camera. In this respect, the diffraction pattern of the composite film containing 10 %wt. of HNTs, reported in Figure 4.17, shows intense 001 reflection arcs centered on the equatorial line.

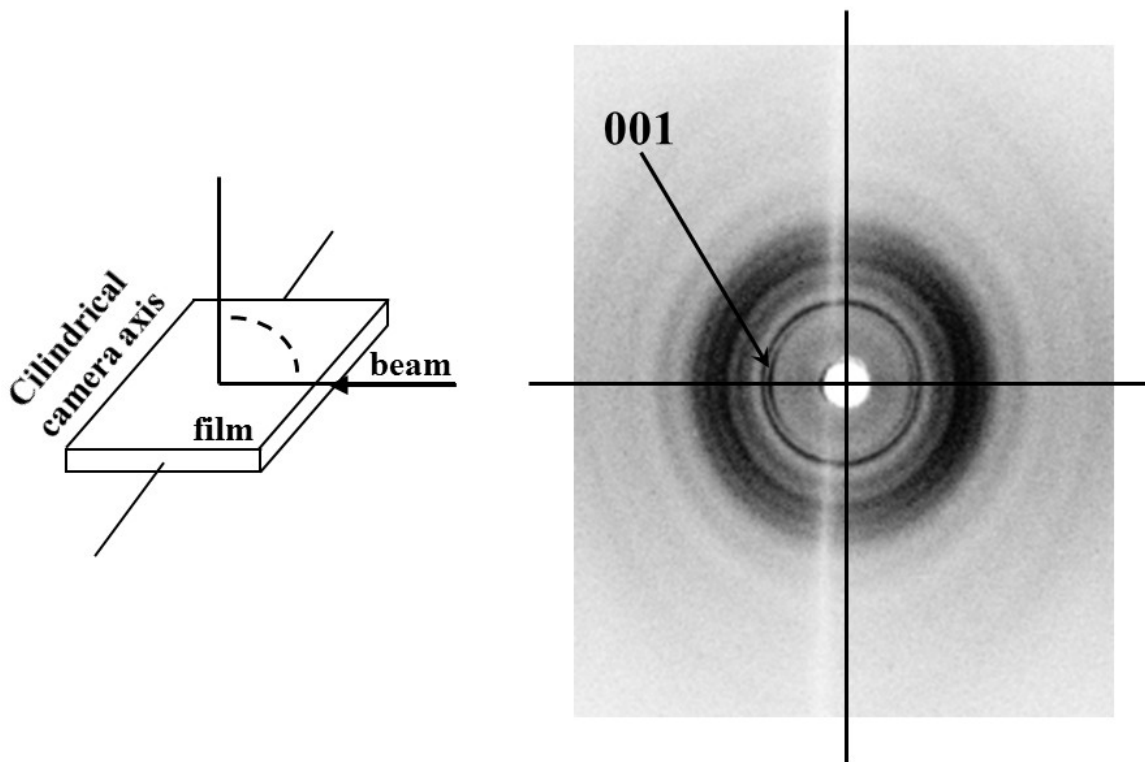


FIG. 4.17 X-ray diffraction pattern, taken with beam parallel to the film plane and collected on a photographic cylindrical camera, for the composite film containing 10 %wt. of HNTs.

In Figure 4.18 diffraction patterns of specimens containing HNTs, all crystallized at 5 °C/min during DSC cooling scans, have been compared. For all specimens, PHBV phase crystallizes, while PBAT phase is essentially amorphous. HNTs basal reflections are only slightly visible even for composites with 10 %wt. of filler. Such results have been confirmed by X-ray

diffraction patterns, collected on a photographic cylindrical camera, of specimens crystallized at 5 °C/min during DSC cooling scans. Actually, in the diffraction pattern of the specimen with 10 %wt. of HNTs the 001 reflection becomes negligible. This behavior can be attributed to the occurrence of a complete disorientation of the added halloysites associated with the polymer melting.

Strictly similar results have been obtained for specimens crystallized at cooling rates of 2 and 10 °C/min.

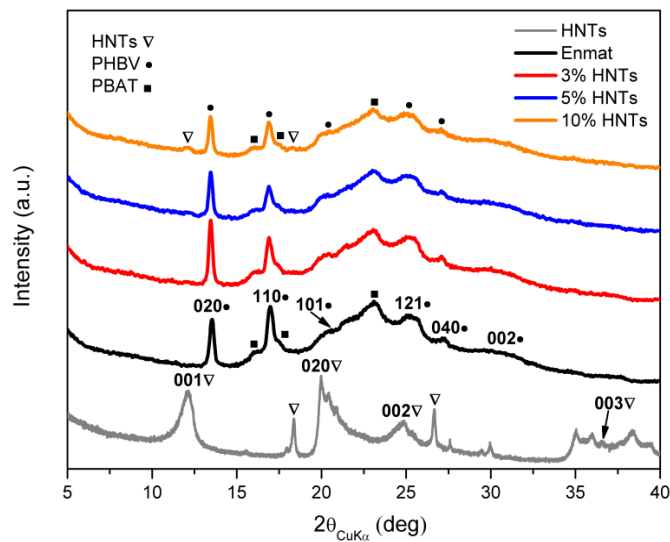


FIG.4.18 X-ray diffraction patterns for specimens containing HNTs all crystallized at 5 °C/min: (filled symbols) reflections of PHBV and PBAT phases; (empty triangles) reflections of HNTs crystalline phase.

## Conclusions

Bio-composites, based on a commercial PHBV/PBAT blend and loaded with natural or chemically functionalised halloysite nanotubes, have been analysed and interpreted in terms of calorimetric and structural tests.

Results showed the crystallization of both phases constituting the matrix with a dominant contribution from the copolymer PHBV. Such crystallinity, improved by orientations, induced by the film technology, that may, among other things, facilitate the formation of more perfect

## Chapter IV

---

crystals, is not homogeneously influenced by the inclusion of halloysites. In particular, although the filler may influence the kinetics and mechanisms of crystallization, the investigations demonstrated that, for composite films, the slight crystallization of PBAT remained unchanged, while there was an increase of the degree of crystallinity of the PHBV phase.

The analysis of samples crystallized at a controlled rate showed the splitting of the PHBV melting signal attributed to simultaneous phenomena of homogeneous crystallization and heterogeneous nucleation of PHBV phase.

## Bibliography

---

- [1] A.K. Bledzki and J. Gassan, *Prog. Polym. Sci.* 24(2), 221m(1999).
- [2] K.-K. Yang, X.-L. Wang, and Y.-Z. Wang, *J. Ind. Eng. Chem.* 13(4), 485 (2007).
- [3] Q. Zhang, Q. Liu, J.E. Mark, and I. Noda, *Appl. Clay Sci.* 46, 51 (2009).
- [4] S. Bhuyan, S. Sundararajan, Y. Lu, and R.C. Larock, *Wear* 268(5–6), 797 (2010).
- [5] I. Armentano, M. Dottori, E. Fortunati, S. Mattioli, and J.M. Kenny, *Polym. Degrad. Stab.* 95(11), 2126 (2010).
- [6] P. Russo, C. Carfagna, F. Cimino, D. Acierno, and P. Persico, *Adv. Polym. Technol.* (2012) DOI: 10.1002/adv.21282.
- [7] J.K. Pandey, S.H. Ahn, C.S. Lee, A.K. Mohanty, and M. Misra, *Macromol. Mater. Eng.* 295, 975 (2010).
- [8] C.J. Song, S.F. Wang, S. Ono, B.H. Zhang, C. Shimasaki, and M. Inoue, *Polym. Adv. Technol.* 14, 184 (2003).
- [9] L.L. Madison and G.W. Huisman, *Mol. Biol. Rev.* 63, 21 (1999).
- [10] A. Marcilla, J.C. Garcia-Quesada, and E. Gil, *J. Appl. Polym. Sci.* 110(4), 2102 (2008).
- [11] J. Tao, C. Song, M. Cao, D. Hu, L. Liu, N. Liu, and S. Wang, *Polym. Degrad. Stab.* 94(4), 575 (2009).
- [12] B.M.P. Ferreira, C.A.C. Zavaglia, and E.A.R. Duek, *J. Appl. Polym. Sci.* 86(11), 2898 (2002).
- [13] L. Miao, Z. Qiu, W. Yang, and T. Ikehara, *React. Funct. Polym.* 68(2), 446 (2008).
- [14] T. Sadik, V. Massardier, F. Becquart, and M. Taha, *J. Appl. Polym. Sci.* (2012) DOI: 10.1002/app.37957.
- [15] M.J. Jenkins, Y. Cao, L. Howell, and G.A. Leeke, *Polymer* 48(21), 6304 (2007).
- [16] A. Javadi, A.J. Kramschuster, S. Pilla, J. Lee, S. Gong, and L.-S. Tung, *Polym. Eng. Sci.* 50(7), 1440 (2010).
- [17] A. Javadi, Y. Srithep, J. Lee, S. Pilla, C. Clemons, S. Gong, and L.-S. Turng, *Compos Part A: Appl. Sci. Manuf.* 41(8), 982 (2010).
- [18] H.M. Cordeiro de Azeredo, L.H. Caparelli Mattoso, and T.H. McHugh, “Nanocomposites in Food Packaging—A Review” in *Advances in Diverse Industrial Applications of Nanocomposites*, B. Reddy, Ed., InTech, (2011). ISBN: 978- 953-307-202-9. Rijeka, Croatia, pp. 57–78.

## Bibliography

---

- [19] L. Incarnato, P. Scarfato, G.M. Russo, L. Di Maio, P. Iannelli, and D. Acierno, *Polymer* **44**, 4625 (2003).
- [20] L. Incarnato, L. Di Maio, E. Garofalo, and P. Scarfato, ‘‘Polylactide nanocomposites as a new solution for eco-compatible packaging materials’’ in 5th International Conference on Times of Polymers (TOP) and Composites. AIP Conference Proceedings Vol. 1255, Ischia (Italy), June 20–23, 364 (2010).
- [21] G. Tari, I. Bobos, C. Gomes, and J. Ferreira, *J. Colloids Interface Sci.* **210**, 360 (1999).
- [22] N. Veerabadran, Y. Lvov, and R. Price, *Macromol. Rapid Commun.* **30**, 94 (2009).
- [23] H. Noro, *Clay Miner.* **21**, 401 (1986).
- [24] Guo B., Lei Y., Chen F., Liu X., Du M., Jia D.: *Applied Surface Science*, **255**, 2715–2722 (2008).
- [25] Liu M., Guo B., Zou Q., Du M., Jia D. *Nanotechnology*, **19**, 205709 (2008).
- [26] Du M., Guo B., Lei Y., Liu M., Jia D. *Polymer*, **49**, 4871–4876 (2008).
- [27] Ye Y., Chen H., Wu J., Ye L. *Polymer*, **48**, 6426–6433 (2007).
- [28] Deng S., Zhang J., Ye L., Wu J. *Polymer*, **49**, 5119–5127 (2008).
- [29] Marney D. C. O., Russell L. J., Wu D. Y., Nguyen T., Cramm D., Rigopoulos N., Wright N., Greaves M. *Polymer Degradation and Stability*, **93**, 1971–1978 (2008).
- [30] Ismail H., Pasbakhsh P., Fauzi M. N. A., Abu Bakar A. *Polymer Testing*, **27**, 841–850 (2008).
- [31] Hedicke-Höchstötter K., Lim G. T., Altstädt V. *Composites Science and Technology*, **69**, 330–334 (2009).
- [32] Liu M., Guo B., Du M., Chen F., Jia D. *Polymer*, **50**, 3022–3030 (2009).
- [33] Du M., Guo B., Jia D. *European Polymer Journal*, **42**, 1362–1369 (2006).
- [34] Ning N-Y., Yin Q-J., Luo F., Zhang Q., Du R., Fu Q. *Polymer*, **48**, 7374–7384 (2007).
- [35] S.R. Levis and P.B. Deasy, *Int. J. Pharm.* **253**, 145 (2003).
- [36] H.M. Kelly, P.B. Deasy, E. Ziaka, and N. Claffey, *Int. J. Pharm.* **274**, 167 (2004).
- [37] S.J. Antill, *Aust. J. Chem.* **56**(7), 723 (2003).
- [38] D.G. Shchukin, G.B. Sukhorukov, R.R. Price, and Y.M. Lvov, *Small* **1**(5), 510 (2005).

## Bibliography

---

- [39] S. Barrientos-Ramirez, E.V. Ramos-Fernandez, J. Silvestre-Albero, A. Sepulveda-Escribano, M.M. Pastor-Blas, and A. Gonzalez-Montiel, *Micropor. Mesopor. Mater.* 120, 132 (2009).
- [40] A.P. Wang, F.Y. Kang, and Z.H. Huang, *Micropor. Mesopor. Mater.* 108(1–3) 318 (2008).
- [41] P. Liu and M. Zhao, *Appl. Surf. Sci.* 255, 3989 (2009).
- [42] M. Zhao and P. Liu, *Micropor. Mesopor. Mater.* 112, 419 (2008).
- [43] M.T. Viseras, C. Aguzzi, P. Cerezo, C. Viseras, and C. Valenzuela, *Micropor. Mesopor. Mater.* 108, 112 (2008).
- [44] P. Luo, Y. Zhao, B. Zhang, J. Liu, Y. Yang, and J. Liu, *Water Res.* 44, 1489 (2010).
- [45] P.J. Barham, A. Keller, E.L. Otun, and P.A. Holmes, *J. Mater. Sci.* 19(9), 2781 (1984).
- [46] Chivrac, F., Kadlecova, Z., Pollet, E., Averous, L.. *Journal of Polymers and the Environment*, 14(4), 393 (2006)
- [47] Pooria Pasbakhsh, H. Ismail, M.N Ahmad Fauzi, A. Abu Bakar *Applied Clay Science* 48 ,405–413 (2010)
- [48] Shufang Wang, Cunjiang Songb, Guangxin Chena, Tianying Guoa, Jing Liub, Banghua Zhang, Shigeiya Takeuchi, *Polymer Degradation and Stability* 77 69 (2005)
- [49] Mohanty, S. and Nayak, S. K..*Polym Compos*, 31: 1194 (2010)
- [50] Larissa N. Carli,Janaina S. Crespo,Raquel S. Mauler. *Composites Part A: Applied Science and Manufacturing*, 42, 11, 1601 (2011).
- [51] Technical report of Imerys Tableware Asia Limited available from:<http://www.imerys-tableware.com/halloy.html>.
- [52] Y. Lee and R.S. Porter, *Macromolecules* 20, 1336 (1986).
- [53] M. Yasuniwa, S. Tsubakihara, Y. Sugimoto, and C. Nakafuku, *J. Polym. Sci. Part B: Polym. Phys.* 42(1), 25 (2004).
- [54] Z.B. Qiu, T. Ikehara, and T. Nishi, *Polymer* 44, 3095 (2003).

## Bibliography

---

- [55] A.J. Owen, J. Heinzl, Z. Skrbic, and V. Divjakovic, *Polymer* 33(7), 1563 (1992).
- [56] S. Wang, C. Song, G. Chen, T. Guo, J. Liu, B. Zhang, and S. Takeuchi, *Polym. Degrad. Stab.* 87, 69 (2005).
- [57] M. Kunioka, A. Tamaki, and Y. Doi, *Macromolecules* 22, 694 (1989).
- [58] Z. Skrbic and V. Divjakovic, *Polymer* 37(3), 505 (1996).
- [59] M. Lai, J. Li, J. Yang, J. Liu, X. Tong, and H. Cheng, *Polym. Int.* 53, 1479 (2004).
- [60] F. Yang and Z. Qiu, *J. Appl. Polym. Sci.* 119, 1426, (2011).
- [61] I. Bobos, J. Duplay, J. Rocha, and C. Gomes, *Clay Clay Miner.* 48(6), 596 (2001).

## Chapter V

---

***Rheological behavior of  
biodegradable nanocomposites filled  
with Halloysite: effect of filler  
functionalization***

### 5.1 Introduction

Today manufactures of plastic products and packages have to meet several requests, such as low cost, improved mechanical and barrier performance. In line with this trend, in the last decades a huge effort of the research has been focused on the reinforcement of polymers by the addition of nanofillers such as clay minerals or carbon nanotubes[1-10].

An appropriate dispersion, distribution, and compatibility between the nanofillers and the polymeric matrix are key features to obtain an enhancement on biodegradability [11,12] and flammability [13,14] besides an improvement of mechanical [15,16], thermal [17,18] and barrier [19,20] properties.

Silicate nanoplatelets, e.g., montmorillonite and carbon nanotubes are the most used fillers in polymer nanocomposites [21-23].

However, Halloysite nanotubes (HNTs), a naturally occurring clay mineral, is attracting interest for fabrication of high performance materials based on polymers. Halloysite( $\text{Al}_2\text{Si}_2\text{O}_5(\text{OH})_4 \cdot n\text{H}_2\text{O}$ ), is a mineral chemically similar to kaolin but exhibiting a predominantly tubular morphology.

This clay consists of hollow tubes with dimensions that generally vary from 50 to 70 nm in external diameter, a *ca.* 15-nm diameter lumen, and 0.5 to 2  $\mu\text{m}$  in length [24].

HNT nanotubes represent an alternative to carbon nanotubes(CNT) because its costs competitiveness, natural availability and biocompatibility.

HNTs are a new type of additive for enhancing the mechanical properties, thermal stability and anti-flammability characteristics of polymer matrices [25-29].

Recently HNTs have been incorporated into various biopolymers[30-32].

In recent decades, a large amount of researches have been made on biodegradable polymers to overcome environmental problems associated with conventional plastic waste.

Aliphatic polyesters such as poly(-hydroxybutyrate-*co*-hydroxybutyrate) PHBV, which have higher flexibility and lower processing temperatures than the homo-polymer Poly(3-hydroxybutyrate) (PHB), are attractive candidates for many applications owing to their biodegradability and biocompatibility[33,34]. However the use of PHBV is still limited by some drawbacks such as slow crystallization rate, relatively difficult processing, low elongation at break, and very high degree of crystallinity. Blending

PHBV with other biodegradable polymers such as PLA[35], PCL,[36] or cellulose and starch derivatives [37,38] is a way of obtaining new materials with improved properties, which can overcome the drawbacks of the PHBV.

Poly- (butylenedipate-co-terephthalate) (PBAT) is an aliphatic-aromatic co-polyester with high toughness but it is also biodegradable and compostable. Accordingly, PBAT is an excellent candidate for toughening PHBV.

The matrix used in this research, currently supplied by a Chinese firm, involves these two biodegradable resins:

PHBV and PBAT in a blend with a weight ratio equal to 30:70, respectively.

There are few research reports showing properties of this blend[39-43], but HNTs reinforced PBAT/ PHBV nanocomposites have never been reported.

Polymer nanocomposites with functional properties, including biocompatibility, compostability, and mechanical properties may be designed by using HNTs as filler in PBAT/PHBV matrix.

The investigation of the effect of Halloysite nanotubes loading, nanotubes functionalization and temperature on the rheological behavior of the nanocomposites was the main objective of this chapter.

### **Experimental section**

#### **5.2 Materials and surface modification of the clay.**

A blend of PBAT/PHBV with 70:30 weight ratio, was supplied, in pellet form, from Ningbo Tianan Biologic Material Co. Ltd. (Tianan-ENMAT) (China) under commercial name 6010P and in this study denoted as Enmat. Halloysite nanotubes (HNTs), used as filler, with average sizes equal to: 0.25-4 nm (length), 30 nm (diameter), 64 m<sup>2</sup>/g (surface area) and a specific gravity 2.53 g/cm<sup>3</sup> were provided by Sigma-Aldrich.

As confirmed by X-ray diffraction analysis Halloysite was in the dehydrated state s

showing a diffraction signal at 12.138 corresponding to a (001) basal spacing of approximately 7.3Å.

Modification of Halloysite clay was made according to a well established procedure reported elsewhere [26]

The successful functionalization of Halloysite particles was verified by ATR-FTIR spectroscopy.

The pellet(Enmat) and the clay nanotubes , unmodified (HNTs) and chemically modified (f-HNTs) were dried under vacuum at 70°C for at least 12 hrs prior to use.

### **5.3 Processing of biodegradable nanocomposites**

The nanocomposites of Enmat with Halloysite ,as received and modified, were prepared using melt compounding technique in a co-rotating twin screw extruder (HAAKE PolyLab, L/D=40).

The bio-polymer were melt mixed with the filler at different weight percentage (3, 5, 10 wt%) maintaining the processing temperature at 150-155-160-165-165-160-160-160 °C from feed to die zone of extruder and setting the screw speed at 100 rpm. Pure Enmat was also extruded under the same conditions to use as reference material. Subsequently the extruded materials was pelletized to granules and dried overnight at 70 °C to remove the water absorbed after extrusion.

Systematic thermogravimetric measurements, shown in previous chapter , confirmed a good agreement between nominal and actual filler contents.

Formulation	Abbreviation
PBAT/PHBV	Enmat
PBAT/PHBV+3% Halloysite	3%HNTs
PBAT/PHBV+5%Halloysite	5%HNTs
PBAT/PHBV+10%Halloysite	10%HNTs
PBAT/PHBV+3% silanized Halloysite	3% f-HNTs
PBAT/PHBV+5% silanized Halloysite	5% f-HNTs
PBAT/PHBV+10%silanized Halloysite	10% f-HNTs

### 5.4 Characterization Techniques

#### 5.4.1 Fourier Transform Infrared Spectroscopy (FTIR)

To confirm the chemical interaction of silane with nanotube surface the nanoparticles were analyzed by infrared spectroscopy. The FTIR-ATR instrument used was a Nicolet 6700 (Thermo Scientific) operating in the wavenumber range of 650 to 4000  $\text{cm}^{-1}$ , with ZnSe crystal, 32 scans and 4  $\text{cm}^{-1}$  resolution.

#### 5.4.2 Rheological characterization

Shear rheology of the polymer melt is a useful tool to characterize the materials and to determine their processing performance.

There are two techniques normally utilized to determine the shear rheological behavior of a material:

- Dynamic shear rheology
- Steady shear rheology

Shear rheological techniques are used to determine the flow behavior and structure evolution of a material under the influence of a steady-state deformation.

## Chapter V

---

Dynamic rheology is a structural analysis tool because it uses a frequency excitation method to determine the molecular-level structure of a polymeric system[43].

Small strain dynamic shear rheological properties are generally considered to obtain the elastic and viscous response of the materials, while the processing properties are estimated analyzing rheological behavior at high frequencies.

In order to verify the processability of nanocomposite samples and to establish the nanodispersion structure, capillary and parallel plate rheometers have been considered in this study to characterize the rheological properties of the investigated nanocomposite systems.

### 5.4.3 Oscillatory measurements

Dynamic and steady-state tests were carried out on a controlled stress rheometer (*SR 500*, *Rheometric Scientific*) equipped with a parallel plate geometry (25 mm diameter, gap ~1 mm) at 160°, 170° and 180°C. The samples were directly melted for 5 min between preheated parallel plates to erase thermal history and to avoid any further rearrangement and/or failure of brittle clay nanotubes. The dynamic experiments were run setting an angular frequency from 0,01 to 100 rad/s under a constant amplitude of 5%. In advance a strain sweep test were performed to assure that the tests were in the linear viscoelasticity region. All measurements were conducted under a nitrogen atmosphere to minimize oxidative degradation of matrix.

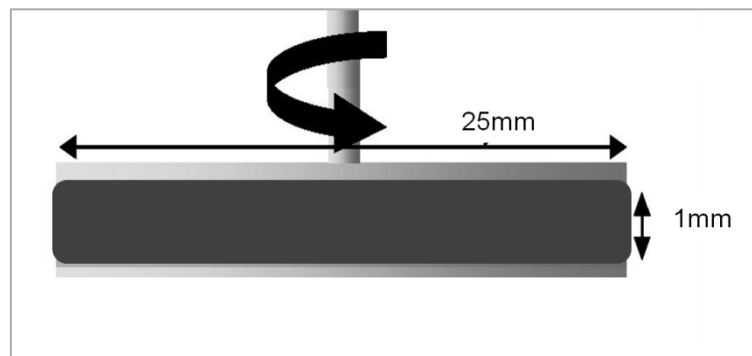


FIG.5.1 Schematic of a parallel plate rheometer

### 5.4.4 Steady shear capillary measurements

All the investigated compounds and the neat matrix, taken as the reference material, were subjected to capillary extrusion. At this purpose an instrument (*ACER 2000, Rheometric Scientific*) having a barrel diameter of 20 mm and a capillary die ( $D=1\text{ mm} - L/D=30$ ) was used.

Measurements on predried pellets were conducted at 160, 170 and 180°C.

Results reported as viscosity vs shear rate, on the range  $30-10^3 \text{ s}^{-1}$ , were corrected according to the Moony-Rabinovitch approach but neglecting Bagley corrections.

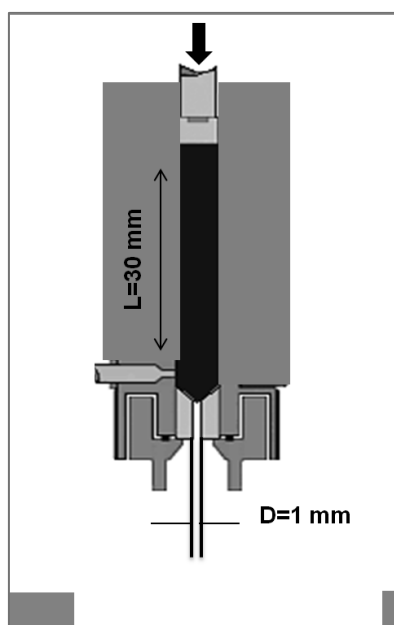


FIG 5.2 Schematic of capillary rheometer

## 5.4 Results and discussion

### 5.4.1 Fourier Transform Infrared Spectroscopy (FTIR)

As discussed in chapter IV, the absorption bands at 1720 and 1635  $\text{cm}^{-1}$  are associated to the stretching vibrations of C- O and C- C groups.

The band at 1470 is attributed to deformation vibrations of C-H in CH<sub>2</sub> bonds . The asymmetric and symmetric stretching vibrations of C-O of C-O-C bonds are attributed to bands at 1320 and 1296  $\text{cm}^{-1}$ , respectively. All those bands are related with the non-hydrolyzable part of the MPS molecule [44]. In fact the first step of the silanization process was hydrolysis of the silane in ethanol under stirring at room temperature.

This process can be represented:

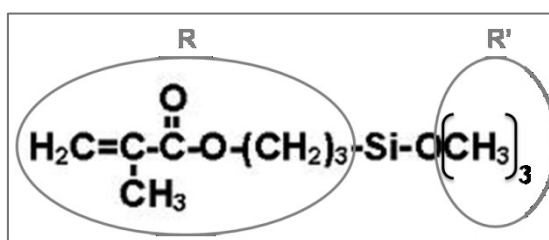
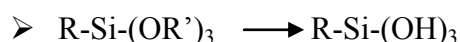


FIG. 5.3 Molecular structure of MPS

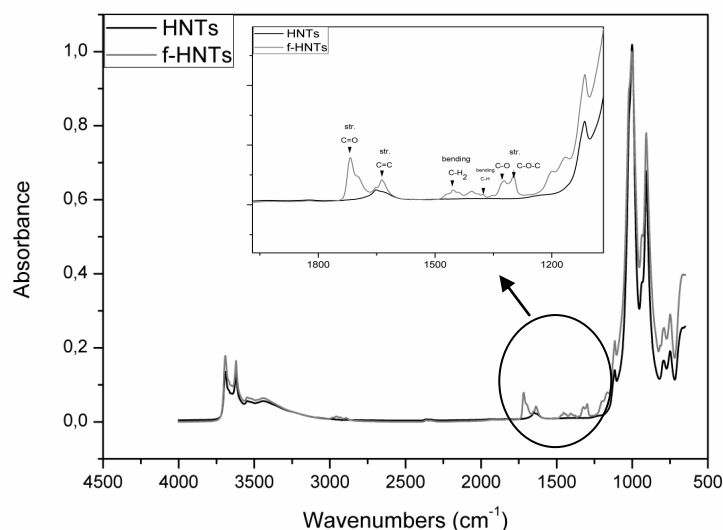


FIG.5.4 FTIR spectra of as received and modified Halloysite

## 5.4.2 Rheological characterization

### 5.4.2.1 Dynamic tests

The linear viscoelastic response as measured by the storage and loss moduli ( $G'$  and  $G''$ ), for systems containing as received Halloysite and silanized one, at 160°, 170° and 180°C are shown in fig 5.5-5.8.

$G'$  and  $G''$  represent the elastic and viscous responses of the studied systems, respectively. However, when nanocomposites with functionalized Halloysite were tested, they displayed an extremely high viscosity at 160°C, beyond the equipment limit. Therefore it was impossible to carry out the test at this temperature.

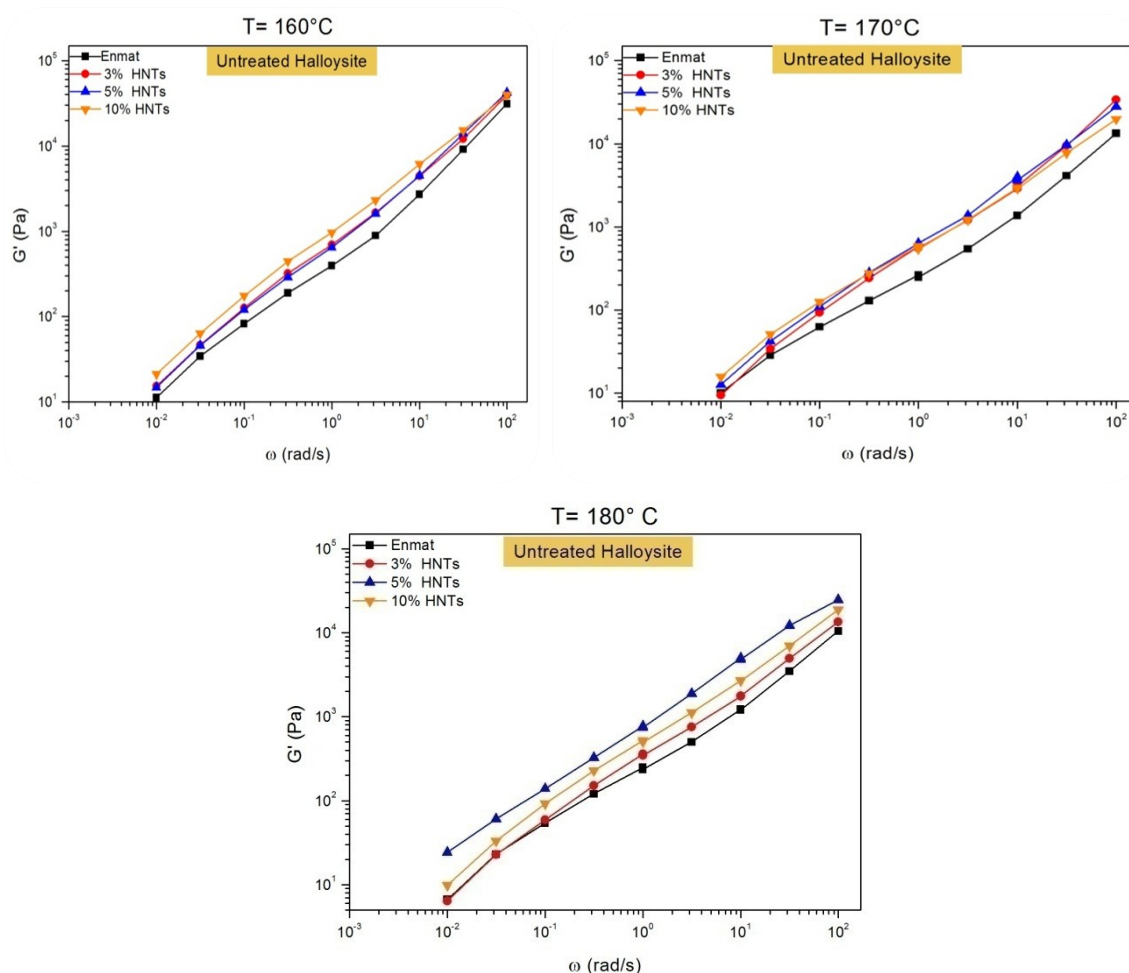


FIG. 5.5 Storage moduli of Enmat/HNTs as function of frequency at different temperatures

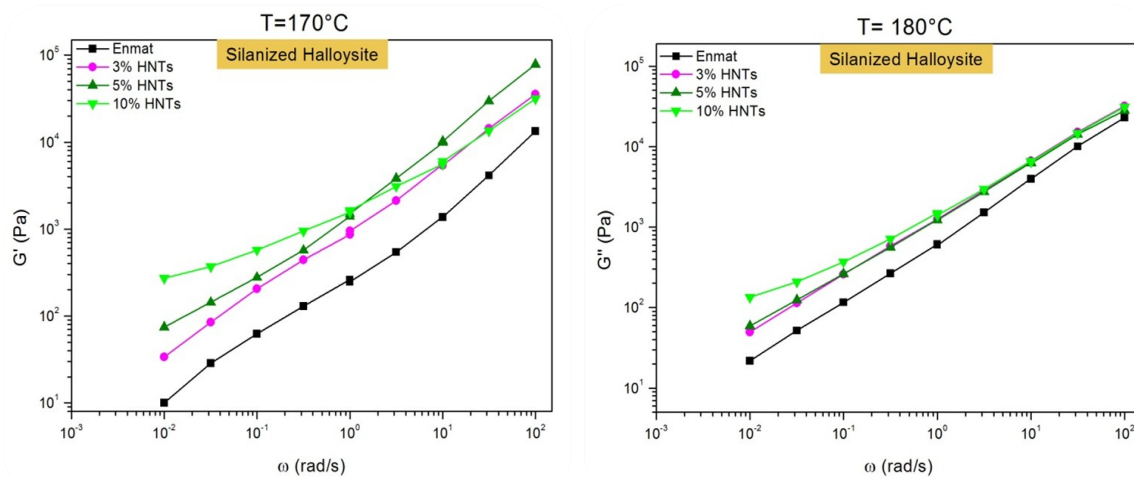


FIG. 5.6 Storage moduli of Enmat/ f-HNTs as function of frequency at different temperatures

The rheological behaviour of polymer composites depends, among other things, on the material microstructure, the fillers dispersion, the aspect ratio and orientation of the fillers, the interaction polymer-filler interaction and as well as filler-filler interactions[45,46]. The temperature can influence the rheological properties of the matrix changing the particle–particle interactions and the wettability of the fillers with the matrix [46].

Analyzing the curves in fig.5.5-5.6 , it can be seen that the incorporation of halloysites induces an increase of the storage modulus of the neat matrix all over the considered range of oscillation frequency. This effect is not monotonous with the filler content with a trend varying with the testing temperature probably for the occurrence of different level of filler distribution leading different extent of interaction with the surrounding matrix. . It is clearly seen that silanized Halloysites influence the storage modulus and this effect is pronounced especially at low frequencies.

The slopes of  $G'(\omega)$  curves in the terminal zone were calculated and listed in tables 5.1-5.2. With the inclusion of clay nanotubes, a slight increase of the slopes of the low frequency region of  $G'$  is observed, as listed in the table 5.1. This trend, usually ascribed to the occurrence of microstructural changes, seems to reach the maximum extent at the temperature of 170 °C.

Moreover, even at the largest filler fraction so far investigated, no indication of a solid

## Chapter V

like behavior (plateau of  $G'$  at low frequencies) can be noted. The absence of a percolating network can be attributed to the low initial aspect ratio of the halloysite nanotubes, usually further reduced by shear in melt processing steps.

Sample	Low-frequency slop of $G'$ vs $\omega < 0.1$		
	160 °C	170 °C	180 °C
Pure Enmat	0.87	0.82	0.90
Enmat/3 wt% HNTs	0.92	0.99	0.96
Enmat/5 wt% HNTs	0.91	0.93	0.75
Enmat/10 wt% HNTs	0.92	0.89	0.96

TAB.5.1 terminal slope of  $G'$  at different temperatures for different amounts of HNTs loadings

But it can be also seen from table 5.2 that, when modified halloysite is used, the nanocomposites have smaller low-frequency slope of storage modulus  $G'$  versus frequency  $\omega$ .

Sample	Low-frequency slop of $G'$ vs $\omega < 0.1$	
	170 °C	180 °C
Pure Enmat	0.82	0.90
Enmat/3 wt% Silanized HNTs	0.78	0.79
Enmat/5 wt% Silanized HNTs	0.57	0.67
Enmat/10 wt% Silanized HNTs	0.31	0.35

TAB.5.2 terminal slope of  $G'$  at different temperatures for different amounts of f-HNTs loadings

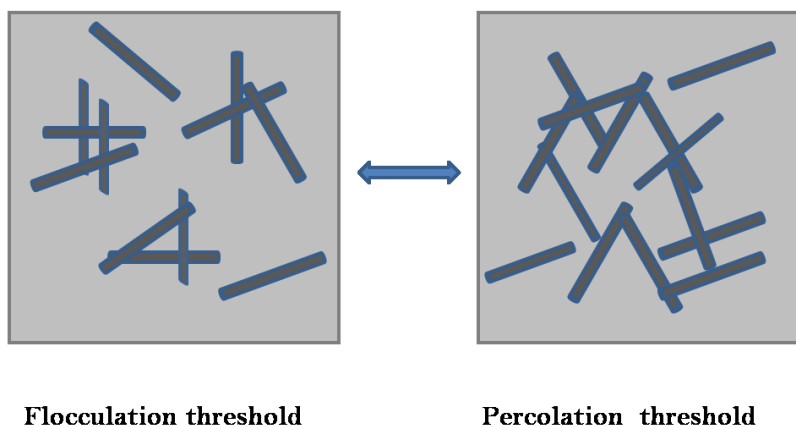
The dependence of  $G'$  on  $\omega$  at low frequencies becomes very weak.

Nevertheless no indication of a solid-like behavior (plateau of  $G'$  at low frequencies) can be observed.

At this regard, it is well know that for nano-structured systems two critical concentrations

accounting for structural transitions of nanodispersions with increasing nanofiller content are verified. These latter are best known as *flocculation threshold* and *percolation threshold* and described as follows:

1. The rheological flocculation threshold expresses the critical nanofiller concentration, where the short-range connectivity of the nanofiller particles becomes significant resulting in flocculation. The fractal flocs consist of near uniform nanofiller agglomerates penetrated with a matrix polymer.
2. The rheological percolation threshold represents the long-range connectivity of the fractal flocs within the polymer matrix, resulting in the formation of a three-dimensional (network) supramolecular structure [47].



In light of the above considerations, for systems containing silanized clay nanotubes the occurrence of **flocculation** rather than percolation phenomena can be assumed.

Figures 5.7 and 5.8 represent the loss modulus  $G''$  of neat Enmat and composites containing as received and silane-treated HNTs, respectively.

The trend of the loss modulus can not indicate more useful information. As expected, it can only show, also in this case, values of the slopes of the curves at low frequencies

lower than the theoretical one usually valid for linearly homo-dispersed polymer melts.

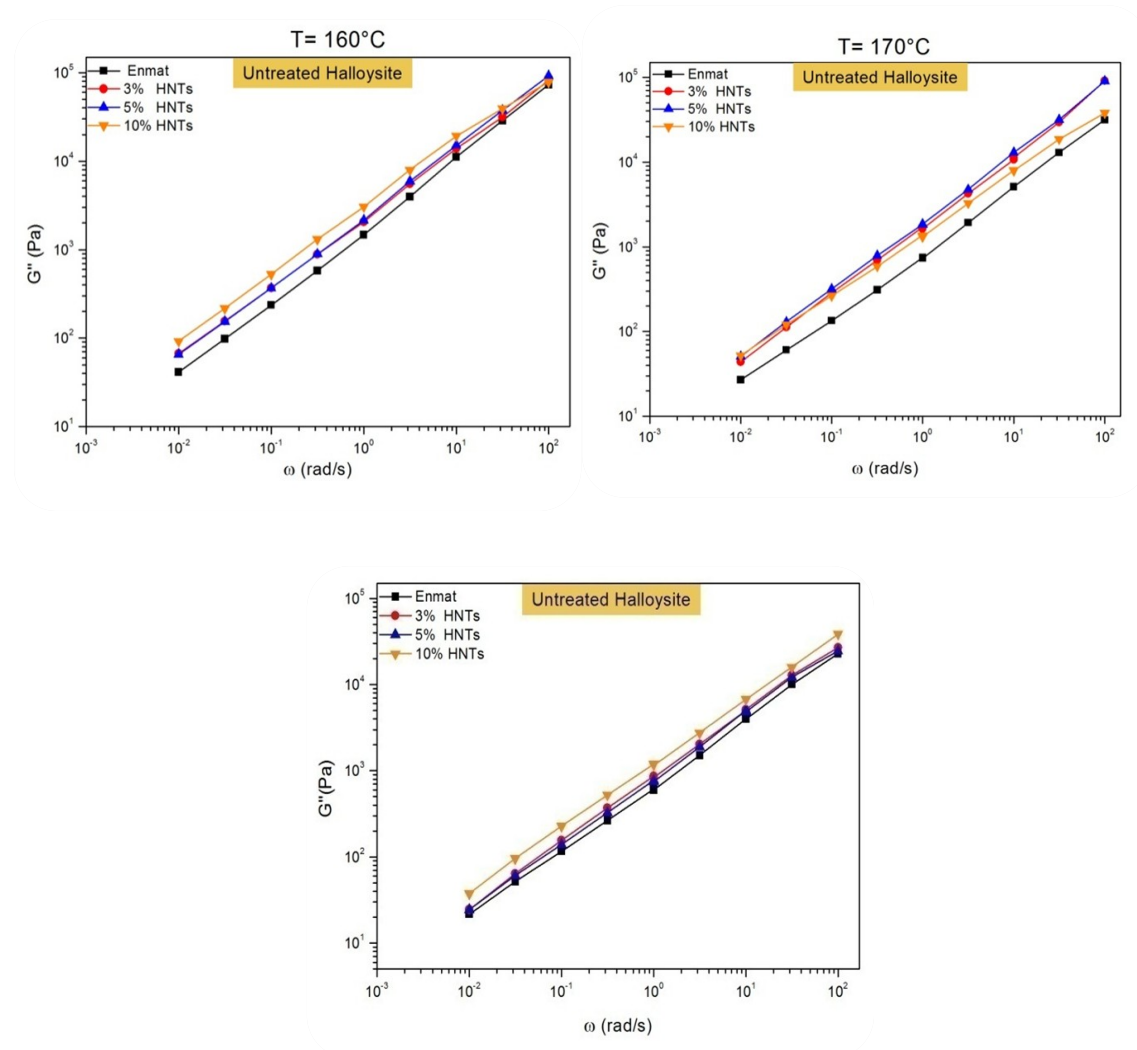


FIG.5.7 The variation in loss modulus with frequency for Enmat/HNTs nanocomposites at different temperatures.

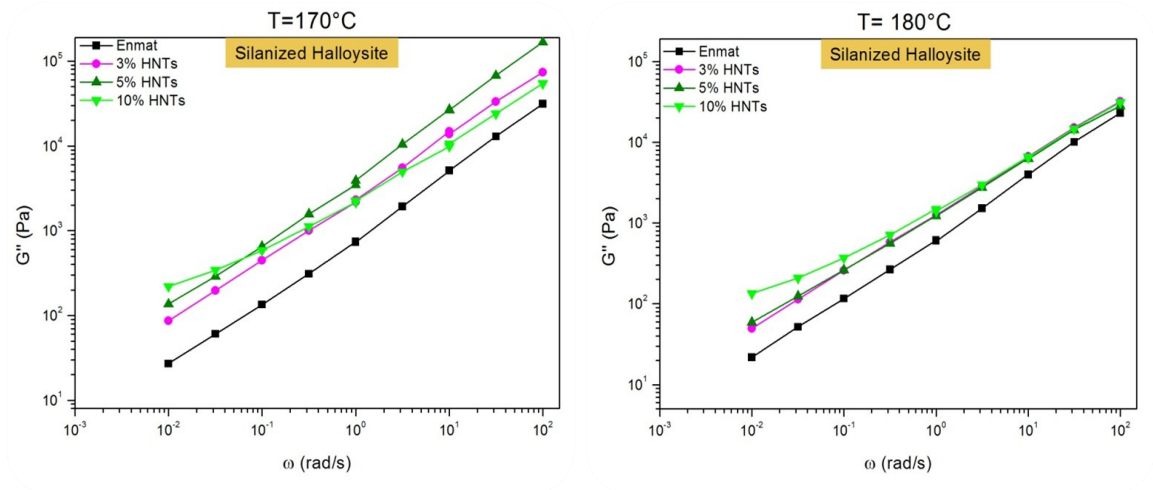


FIG.5.8 The variation in loss modulus with frequency for Enmat/ f-HNTs nanocomposites at different temperatures.

In fig. 5.9 comparisons of investigated materials in terms of loss modulus are depicted. As expected, the loss tangent,  $\tan \delta$ , where  $\delta$  is the phase angle is shown Figure 5.9 to be very sensitive to the structural change of the materials.

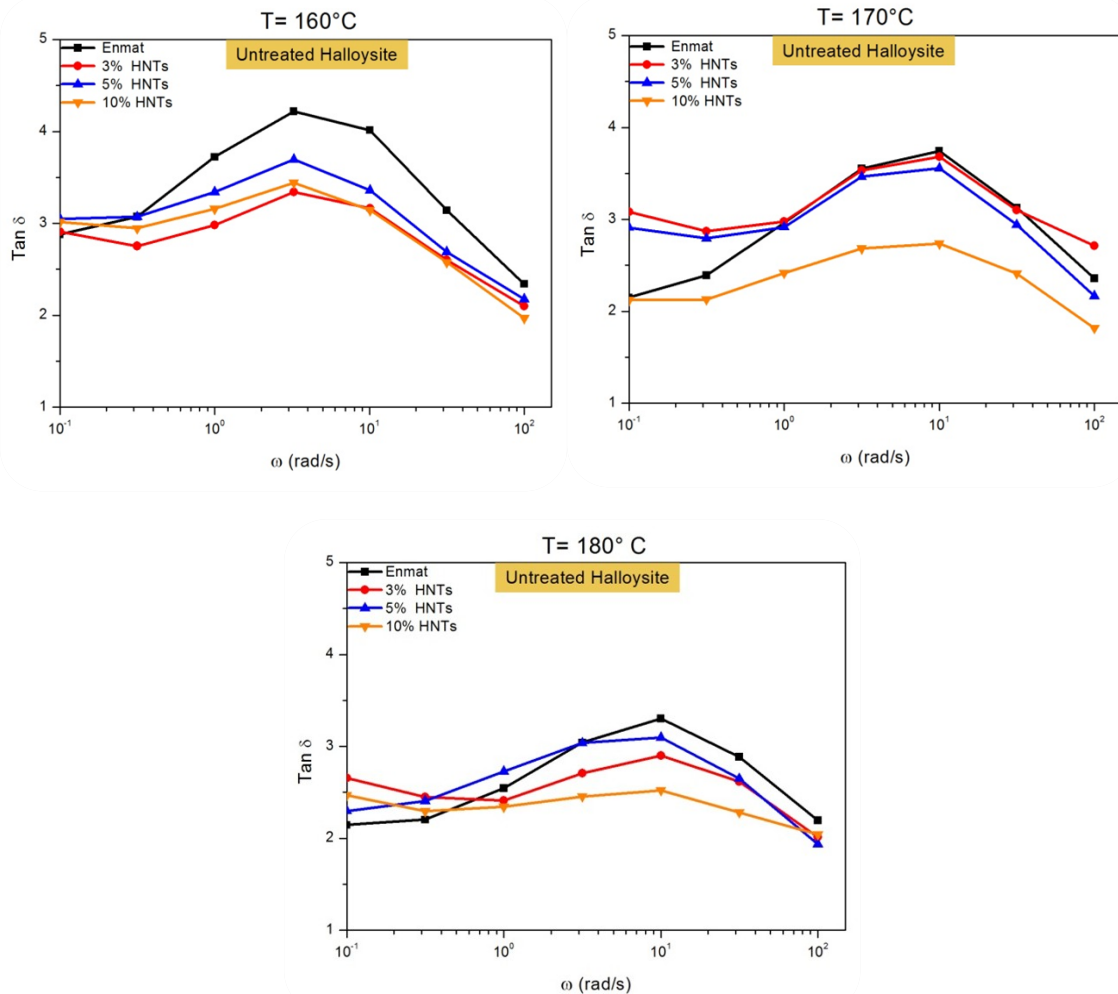


FIG. 5.9  $\tan \delta$  of HNTs nanocomposites as functions of the frequency at different temperatures

The damping intensity is lowered by increasing the clay nanotube concentration with an effect further emphasized by increasing the temperature of the test.

This behavior confirms that the nanocomposites are more elastic than the reference extruded matrix over all frequency range at molten state and that both energy dissipation and relaxation of the matrix chains are increasingly hindered as the filler loading increases.

The influence of the temperature may be explained assuming the achievement of different filler distribution and, consequently, by the enable of various extent of filler matrix interactions.

As highlighted in fig.5.10, the above mentioned effects are further enhanced with the improvement of the filler-matrix interface.

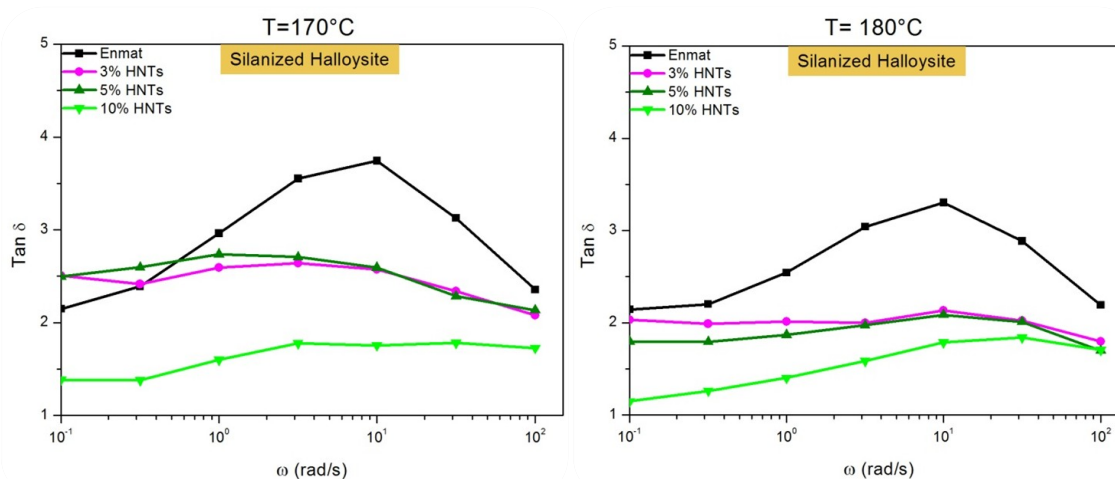


FIG. 5.10  $\tan \delta$  of nanocomposites containing functionalized Halloysite as functions of the frequency at different temperatures

The peaks occur at the frequency of about 10 rad/s and almost disappear with increasing nanotube content, showing that the material becomes more elastic.

The change in complex viscosity of the neat Enmat and Enmat/HNTs nanocomposites is shown in figures 5.11.

All materials containing untreated halloysites show a shear thinning behavior over all the analyzed oscillation frequency range.

An increase of the complex viscosity is verified for formulations including HNTs with respect to the reference matrix.

The extent of this effect varies with the testing temperature and the filler content.

For systems with improved interfacial regions(Fig. 5.12) a slight drift of the viscosity curve is observed for the highest filler content in the low frequency zone: behavior in line with the assumed occurrence of flocculation phenomena.

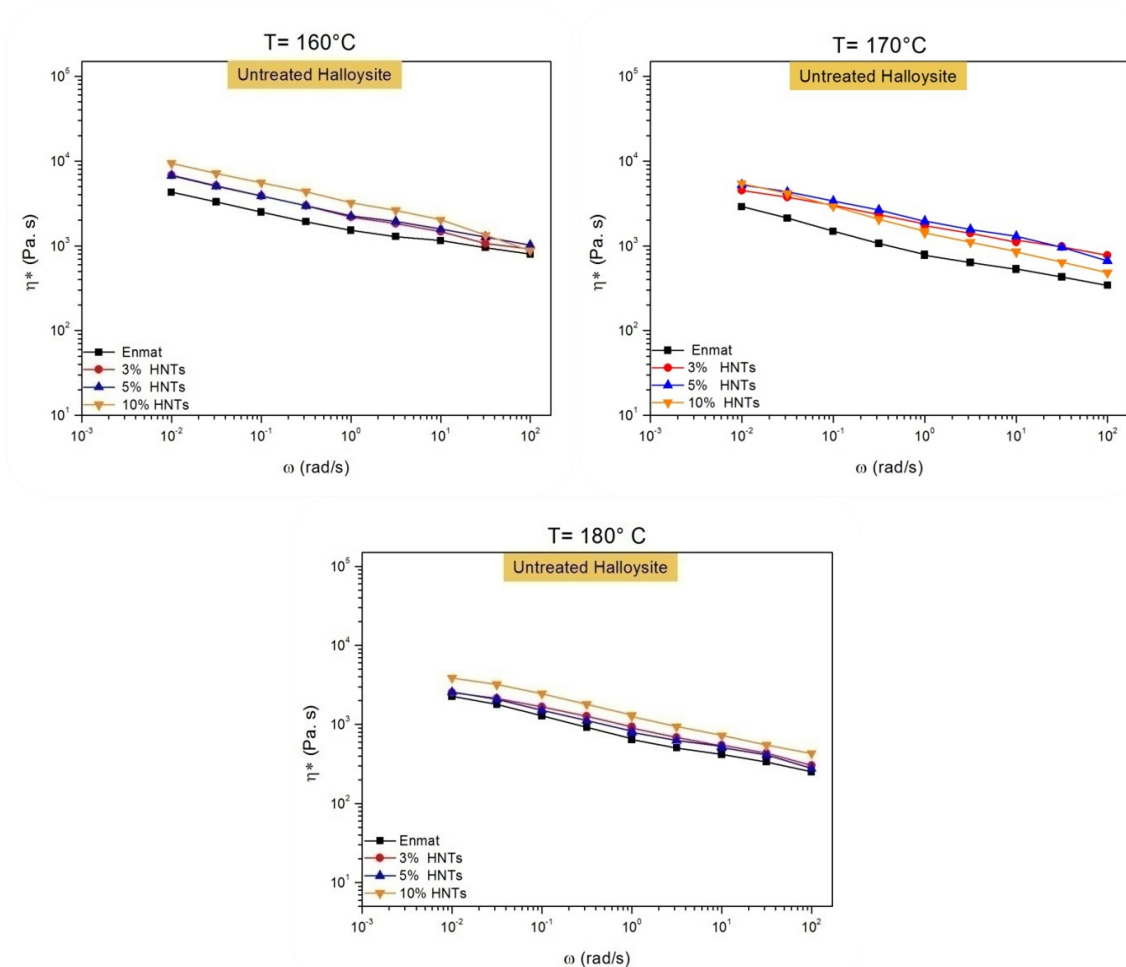


FIG.5.11 Frequency dependence of complex viscosity  $\eta^*$  at different temperatures for Enmat/HNTs nanocomposites

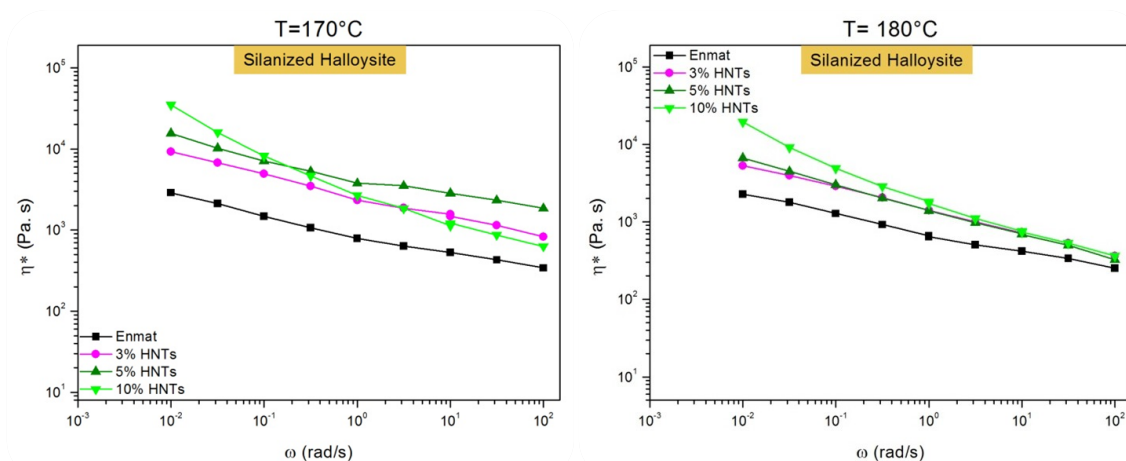


FIG.5.12 Frequency dependence of complex viscosity  $\eta^*$  at different temperatures for Enmat/f-HNTs nanocomposites

The interesting thing to note is that, unlike the previous case, the complex viscosity increases with the addition of modified nanotubes to the pure blend as better emphasized in graphs 5.13 and 5.14. In these plots the complex viscosity as a function of the filler content at various frequencies is reported.

The complex viscosity clearly depends on the filler content especially at low frequencies as well as on the testing temperature.

The effect, essentially related to the predominance at low frequencies of physical filler-filler and/or filler-matrix interactions, is emphasized by reducing the testing temperature. In other words, as expected, the wettability of clay nanotubes by the hosting matrix is reduced by increasing temperature.

The effect of the filler loading on the viscosity of the matrix becomes, as expected, particularly marked at low frequencies if the interface is improved by adequate pre-treatments of the included particles.

Clearly at 170 ° C there is an increase of an order of magnitude of the viscosity at 0.01 Hz: effect reduced by about 50% at 180 °C due to the increased mobility of macromolecules constituting the matrix and, consequently, to the lower wettability of included clay nanotubes.

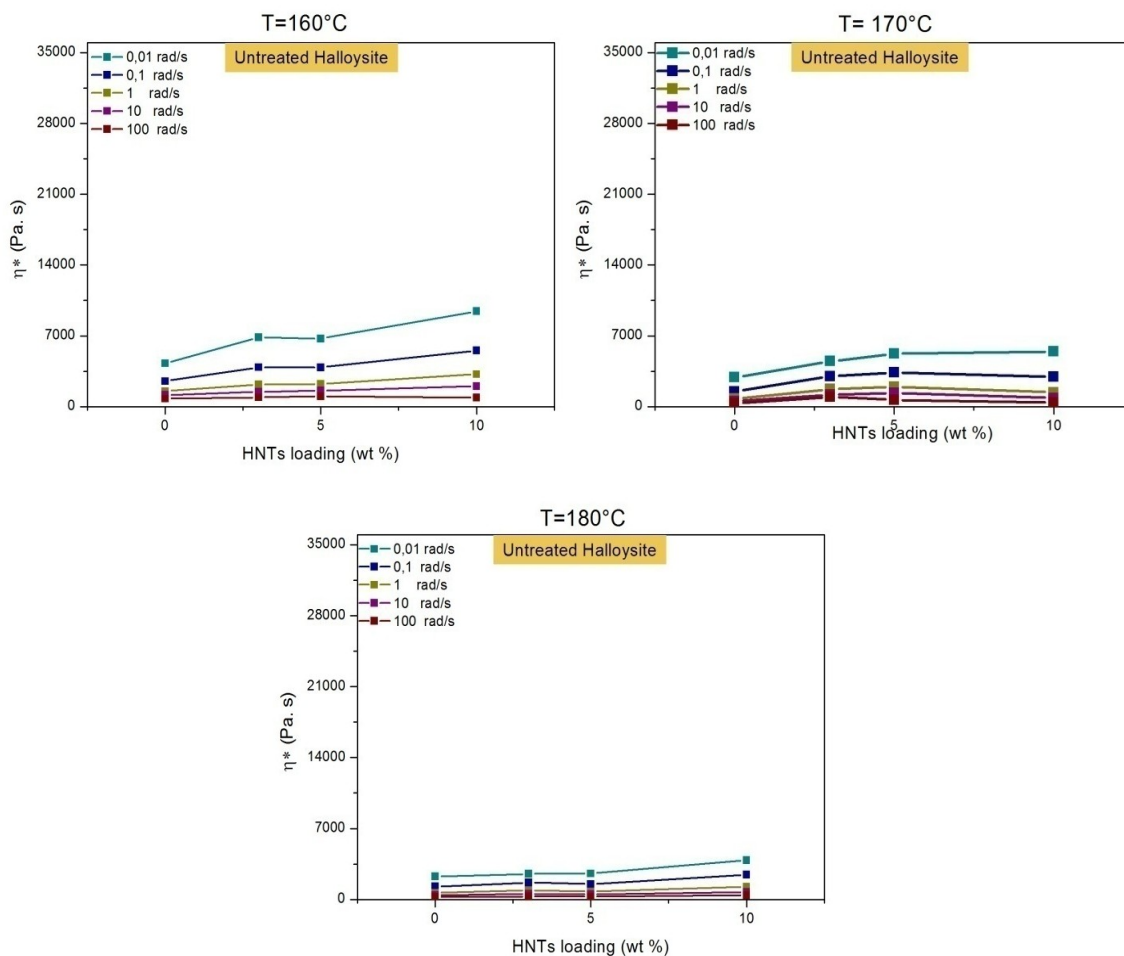


FIG 5.13 Complex viscosity  $\eta^*$ : effect of HNTs content at various frequencies

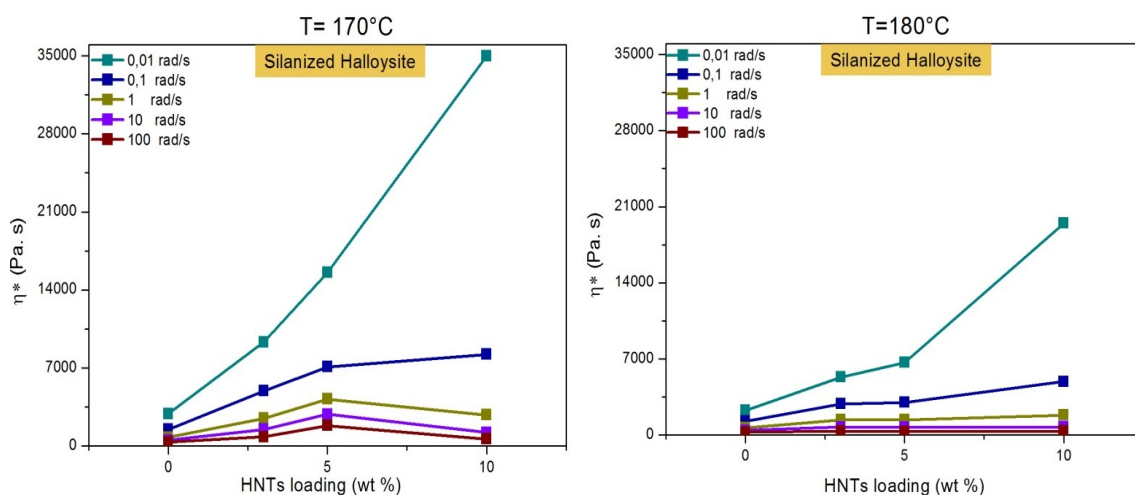


FIG 5.14 Complex viscosity  $\eta^*$ : effect of silanized HNTs content at various frequencies

## Chapter V

In order to understand the effect of temperature on the rheological properties the Andrade-Eyring equation defined for the complex viscosity [48] has been employed in which:

$$\eta^* = B \cdot e^{\frac{E_a}{RT}}$$

$E_a$  is the flow activation energy and  $R$  is the universal gas constant equal to 8.314 J/n K. In the case of nanocomposites,  $E_a$  can be related to the interactions between polymer chains and fillers. The value of  $E_a$  thus depends on the ease with which the fillers move through the polymer chains. The plot (fig. 5.15-5.16) of the values of  $\ln \eta^*$  (determined at 1 rad/s) as a function of  $1/RT$  makes to estimate the activation energy of the nanocomposites, given by the slope of this curve. Table 5.3 and 5.4 report the values of  $E_a$  for different nanotube loadings.

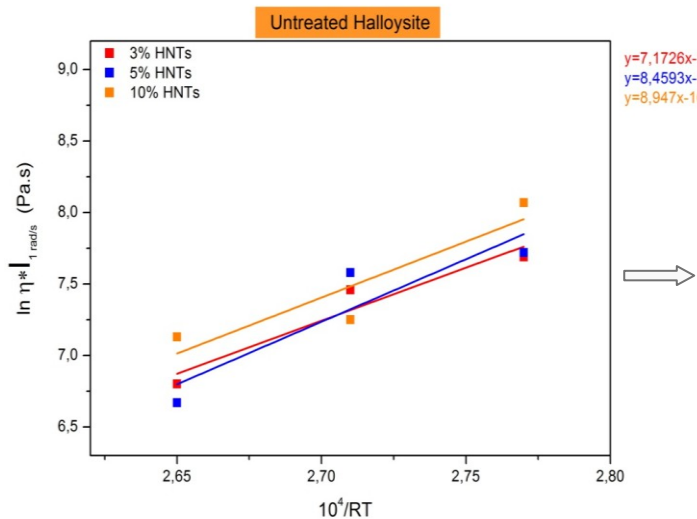


FIG.5.15 Linearized Andrade-Eyring relationship

Filler content	B (Pa s) $10^6$	Ea (J/n)
3 wt%	5,25	7,17
5 wt%	0,16	8,46
10 wt%	0,048	8,95

TAB.5.3 Activation energy values for systems containing pure HNTs

The activation energy increases with the clay nanotube loading. The influence is explainable assuming that the higher filler concentrations, the more constrained is the flow of compound melts.

Although in the case of organo- modified fillers it is improper to speak about data fitting because, given the particularly high viscosity of the system at 160 °C, there are only two points (fig. 5.16), it seems that in this case the activation energy values are higher than those evaluated for analogous materials containing as received clay nanotubes.

In other words, as expected, the improvement of the filler-matrix interface induces further constraints to the flow of the host matrix macromolecules.

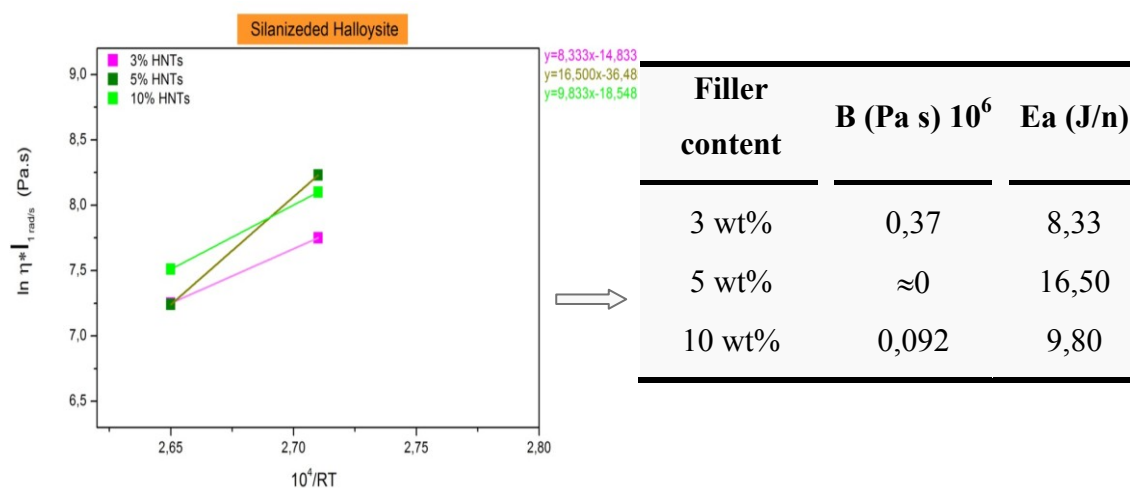


FIG.5.15 Linearized Andrade-Eyring relationship

TAB.5.3 Activation energy values of systems containing modified HNTs

The steady shear behavior of polymer/clay nanocomposites usually allows to obtain useful information on processability of the material [49]

In Fig. 5.16 the steady-shear rheological behavior of neat Enmat and its nanocomposites with Halloysite are reported.

Each flow curve shows two distinct regions: the first one with shear viscosity almost constant with the shear rate (at low shear) rates and the second one at higher shear rates where the shear viscosity decreases with an increasing shear rate. There is a transition from a Newtonian region to a power-law region.

To investigate the dependence of the viscosity on the shear rate, Carreau model [50] was employed to fit the non-Newtonian viscosity curve (square symbols) for neat Enmat and its nanocomposites, as shown in Figure 5.17 (solid lines).

## Chapter V

The equation used to fit this model to experimental results was the following:

$$\eta = \frac{\eta_0}{[1 + (\lambda\dot{\gamma})^2]^{(1-n)/2}}$$

where  $\eta_0$  is the zero shear rate viscosity,  $\lambda$  is the relaxation time (which characterizes the onset point of shear thinning), and  $n$  is the power-law index. Table 5.4 summarized the collected rheological parameters (  $\eta_0, n, \lambda,$  )

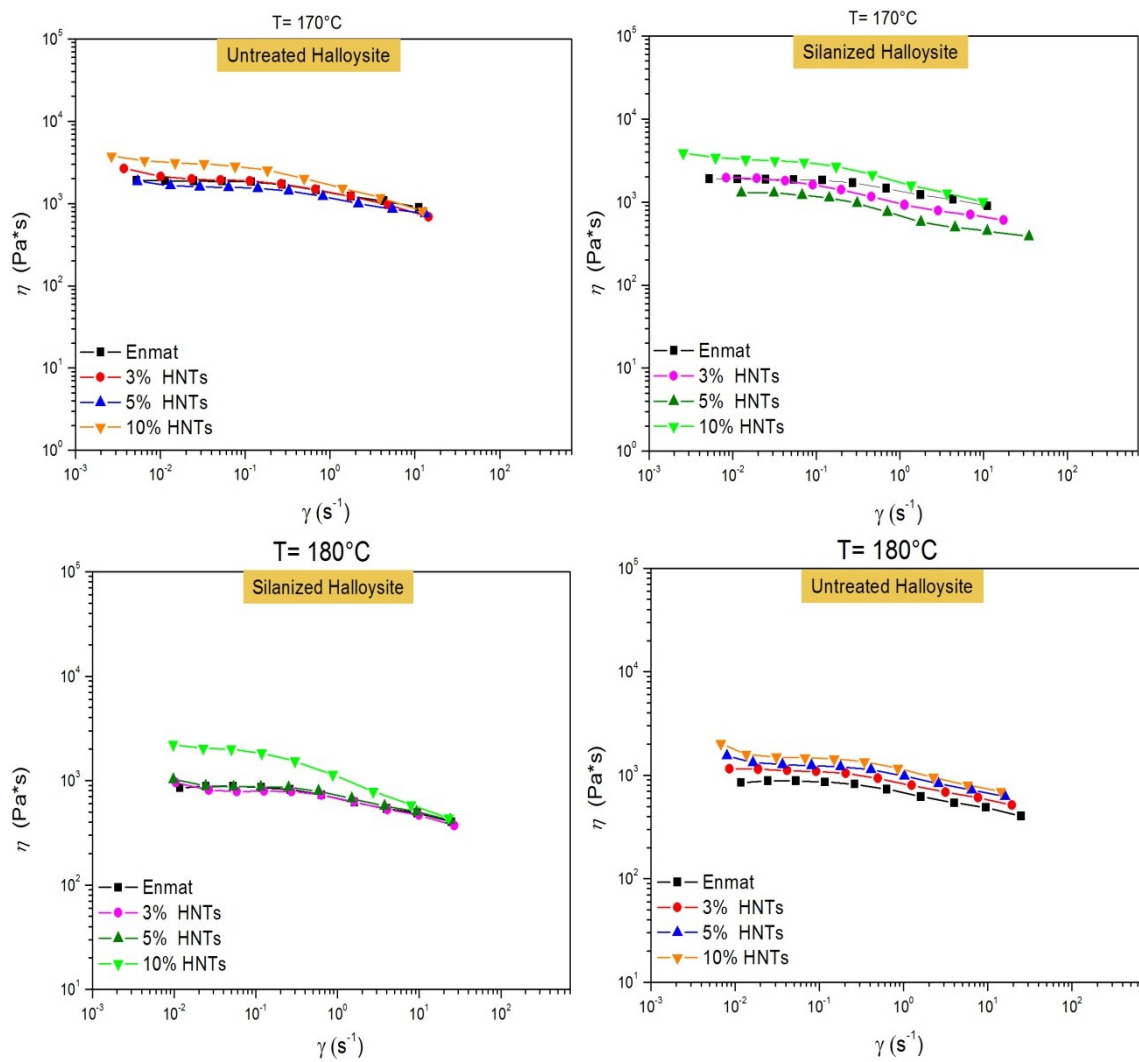


FIG.5.16 Steady shear viscosity of the nanocomposites at different temperatures.

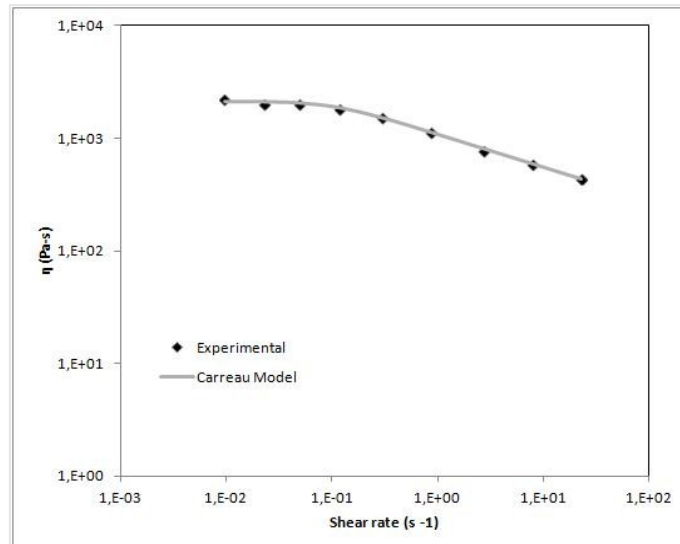


FIG.5.17 Example of comparison of the Carreau model fit to the experimental data

170°C					180°C				
Sample	$\eta_0 \times 10^{-3}$ (Pa.s)	$\lambda$ (s)	n	$\dot{\gamma}_c$ (s <sup>-1</sup> )	Sample	$\eta_0 \times 10^{-3}$ (Pa.s)	$\lambda$ (s)	n	$\dot{\gamma}_c$ (s <sup>-1</sup> )
Enmat	1,9	5,9	0,82	0,16	Enmat	0,87	4,5	0,84	0,11
3%HNTs	2,1	7,5	0,77	0,13	3%HNTs	1,1	7,1	0,84	0,14
5%HNTs	1,7	8,4	0,83	0,12	5%HNTs	1,3	8,8	0,84	0,11
10% HNTs	3,3	13,6	0,73	0,07	10% HNTs	1,6	11,1	0,83	0,09
3%f- HNTs	2,0	30,3	0,80	0,03	3%f- HNTs	0,83	3,0	0,82	0,12
5%f- HNTs	1,5	20,0	0,80	0,05	5%f- HNTs	0,81	4,0	0,82	0,25
10%f- HNTs	3,4	18,1	0,75	0,05	10%f- HNTs	2,1	10	0,70	0,1

TAB. 5.4 Parameters in Carreau model

Clearly at 170° the degree of shear thinning ( $1 - n$ ) and  $\lambda$  increases with the clay content. the critical shear rate  $\dot{\gamma}_c$  is defined as the onset point of shear-thinning transition and is approximately equal to the inverse of  $\lambda$ [51].

Hence, considering the values in table 5.4, the addition of clay shifts the transition from the Newtonian plateau region to shear-thinning region occurring at lower critical shear rate with increasing the clay concentration. This might suggest that the fillers are ease of orientation in response to externally applied stress.

Regarding results at 180° for systems containing surface modified clay nanotubes significant benefits are shown only by the 10% by weight loaded system. Probably this decrease in viscosity is caused by thermal degradation of the material that occurs during the testing. However, the parameter  $\lambda$  decreases with increasing temperature. The decrease in relaxation time with increasing temperature is due to the increased mobility of the polymer chains and the lower wettability of included clay nanotubes. The Newtonian plateau is extended at higher frequencies.

### *5.4.2.2 Steady shear capillary measurements*

Capillary experiments allow to determine the flow properties at large share rates. Shear rate in an extrusion can be determined by the following equation[51]:

$$\dot{\gamma} = \frac{\omega R}{H} = \frac{(2\pi v/60)}{R/10} \approx v$$

where  $v$  is the screw speed in RPM, H is of the order of one tenth of the barrel radius( $R$ ), the angular velocity  $\omega$  in rad/s is  $2\pi v/60$ .

Therefore, to verify the extrudability of the investigated nanocomposite systems, three temperatures were selected for each set measure, each of them including the range temperature used during extrusion.

Figures 5.18 and 5.19 present the results of the capillary measurements of the studied samples at the three different temperatures.

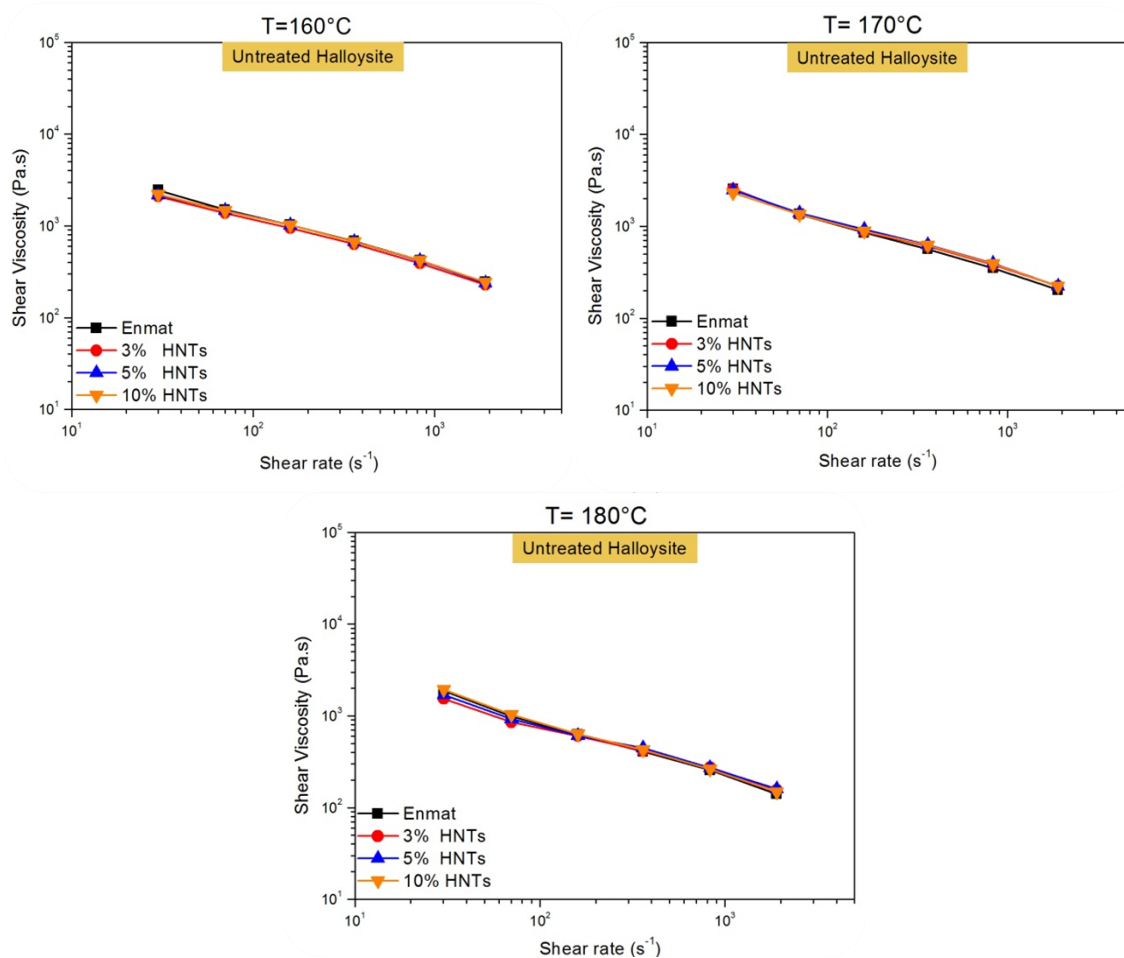


FIG.5.18 Comparison of viscosities of Enmat/HNTs composites

Nanocomposites show a flow behavior, at high share rate, not influenced by the presence of filler with respect to the reference pure matrix even in case of improved filler-matrix interface (fig.5.19).

The viscosity of nanocomposites does not increase with the content of nanotubes but it is within the order of magnitude of polymer matrix.

The processability of nanocomposites is not altered also with functionalized halloysite, so nanocomposites could be still processed in the same way as the raw materials.

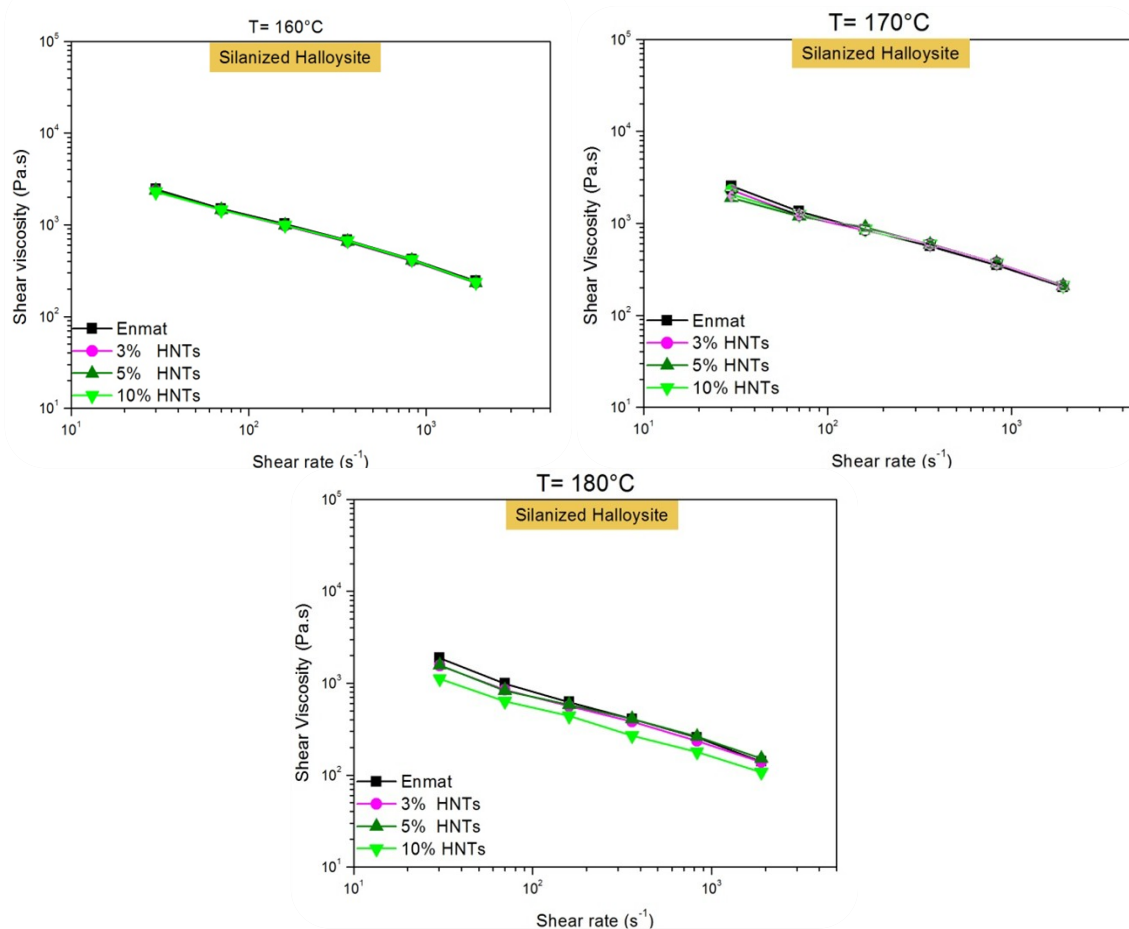


FIG.5.19 Comparison of viscosities of Enmat/f-HNTs composites

## Conclusions

Completely biodegradable systems based on a commercial PHBV/PBAT blend and natural clay nanotubes were prepared by melt blending and investigated from a rheological point of view at 160, 170 and 180 °C.

The effects of filler on viscoelastic behavior of composite systems are emphasized by improving the filler-matrix interface. In particular, in presence of the highest loading of silanized halloysite incipient flocculation phenomena seems to occur.

## Chapter V

---

The inclusion of halloysites result in increases of both the elastic modulus and the complex viscosity even if no percolating phenomena seems to occur on the filler loading range considered so far.

Regardless the surface treatment of nanoclay, the filler does not appear to alter the extrudability of the hosting matrix, remaining the measured viscosity in the same order of magnitude of pure Enmat.

The choice of processing temperature may be exclusively related to the level of filler distribution able to ensure optimal viscoelastic behavior of the melts.

## Bibliography

---

- [1] Bokobza L. *Polymer*;48(17), 4907 (2007).
- [2] Fornes TD, Paul DR. *Polymer*, 44:3945 (2003).
- [3] Mittal V. *J Thermoplast Compos Mater*, 20:575 (2007).
- [4] Mittal V. *Materials*, 2:992 (2009).
- [5] Utracki LA, Sepehr M, Boccaleri E. *Polym Adv Technol*, 18:1 (2007).
- [6] Bokobza L. *Polymer*, 48(17):4907 (2007).
- [7] Handge UA, Pötschke P. *Rheol Acta*, 46:889 (2007).
- [8] Giannelis, E. P. *Adv. Mater*, 8, 29 (1996).
- [9] Moniruzzaman, M.; Winey, K. L. *Macromolecules*, 39, 5194 (2006).
- [10] Paul, D. R.; Robeson, L. M. *Polymer*, 49, 3187 (2008).
- [11] S.S. Ray and M. Bousmina, *Prog. Mater. Sci.*, 50, 962 (2005).
- [12] S.S. Ray and M. Okamoto, *Macromol. Rapid Commun.*, 24, 815 (2003).
- [13] J.W. Gilman, C.L. Jackson, A.B. Morgan, R. Harris Jr., E. Manias, E.P. Giannelis, M. Wuthenow, D. Hilton, and S.H. Phillips, *Chem. Mater.*, 12, 1866 (2000).
- [14] T. Kashiwagi, F. Du, J.F. Douglas, K.I. Winey, R.H. Harris Jr., J.R. Shields, *Nature Mater.*, 4, 928 (2005).
- [15] LeBaron P.C., Wang Z., Pinnavaia T.J *Appl. Clay. Sci.* 15, 11, (1999).
- [16] S.C. Tjong, *Mater. Sci. Eng. Res*, 53, 73 (2006).
- [17] Gilman J.W. *Appl. Clay. Sci.* 15 31-49 (1999).
- [18] A. Riva, M. Zanetti, M. Braglia, G. Camino, and L. Falqui, *Polym. Degrad. Stabil.*, 77, 299 (2002).
- [19] Messersmith P.B, Giannelis E.P. *J. Polym. Sci, Part A: Polym. Chem.*33 1047 (1995).
- [20] Yano K., Usuki A., Okada A., Kurauchi T., Kamigaito O. *J. Polym. Sci., Part A: Polym. Chem.* 31 2493-(1993) .
- [21] Fornes TD, Yoon PJ, Keskkula H, Paul DR. *Polymer*;42:9929 (2001).
- [22] Fornes TD, Paul DR. *Polymer*;44:3945 (2003).

## Bibliography

---

- [23] Jonathan N. Coleman, Umar Khan, Werner J. Blau, Yurii K. Gun'ko, *Carbon* 44 1624 (2006).
- [24] Joussein, E.; Petit, S.; Churchman, J.; Theng, B.; Righi, D.; Delvaux, B., *Clay Minerals*, 40, 383(2005).
- [25] Zia, Z.; Luo, Y.; Guo, B.; Yang, B.; Du, M.; Jia, D. *Polym. Plast. Technol. Eng.* 48, 607 (2009).
- [26] Du, M.; Guo, B.; Jia, D. *Eur. Polym. J.* 42, 1362 (2006).
- [27] Hedicke-Hochstotter, K.; Lim, G. T.; Altstadt, V. *Compos. Sci. Technol*, 69, 330 (2009).
- [28] Deng, S.; Zhang, J.; Ye, L.; Wu, J. *Polymer* 49, 5119 (2008).
- [29] Ismail, H.; Pasbakhsh, P.; Ahmad Fauzi, M. N.; Abu Kakar, A. *Polym. Test.*, 27, 841 (2008).
- [30] Qi, R.; Guo, R.; Shen, M.; Cao, X.; Zhang, L.; Xu, J.; Yu, J.; Shi, X. *J. Mater. Chem.*, 20, 10622 (2010).
- [31] Qi, R.; Cao, X.; Shen, M.; Guo, R.; Yu, J.; Shi, X. *J. Biomater. Sci. Polym. Ed.*, 23, 299 (2012).
- [32] K. Prashantha, B. Lecouvet, M. Sclavons, M.F. Lacrampe, P. Krawczak, *J. Appl. Polym. Sci.* 128: 1895 (2013).
- [33] C.J. Song, S.F. Wang, S. Ono, B.H. Zhang, C. Shimasaki, and M. Inoue, *Polym. Adv. Technol.* 14, 184 (2003).
- [34] L.L. Madison and G.W. Huisman, *Mol. Biol. Rev.* 63, 21 (1999).
- [35] Nanda, M. R., Misra, M. and Mohanty, A. K., *Macromol. Mater. Eng.*, 296: 719 (2011)
- [36] Chun YS, Kim WN. *Polymer*;41:2305 (2000).
- [37] N. Lotti and M. Scandola, *Polymer Bulletin* 29 407 (1992).
- [38] C. M. Buchanan, S. C. Gedon, A. W. White and M. D. Wood, *Macromolecules* 25 7373 (1992).
- [39] A. Javadi, A.J. Kramschuster, S. Pilla, J. Lee, S. Gong, and L.-S. Tung, *Polym. Eng. Sci.* 50(7), 1440 (2010).
- [40] A. Javadi, Y. Srithep, J. Lee, S. Pilla, C. Clemons, S. Gong, and L.-S. Tung, *Compos Part A: Appl. Sci. Manuf.* 41(8), 982 (2010).

## Bibliography

---

- [41] Vidhya Nagarajan, Manjusri Misra, Amar K. Mohanty, *Industrial Crops and Products*, 42, 461 (2013).
- [42] A. Javadi, Y. Srithep, C.C. Clemons, L-S. Turng, S. Gong, *J. Mater. Res.*, 27, 11, (2012)
- [43] Bhattacharya, S., Gupta, R. K. and Bhattacharya, S. N., "Rheology of polymeric Nanocomposites" in *Polymer Nanocomposites Handbook*, edited by R. K. Gupta, E. Kennel and K- J Kim, CRC Press (2010).
- [44] M. Pantoja, B. Diaz-Benito, F. Velasco, J. Abenojar, J.C. del Real. *Applied Surface Science* 255 6386 (2009).
- [45] M.Song, J. Jin, "Characterization of rheological properties of polymer nanocomposites" in *Characterization techniques for polymer nanocomposites*. (ed V. Mittal), Wiley-VCH Verlag GmbH & Co. KGaA, Weinheim, Germany.(2012)
- [46] M. Rahail Parvaiz, P. A. Mahanwar, Smita Mohanty and Sanjay K. Nayak *Journal of Minerals & Materials Characterization & Engineering*, 9, 11, 985, (2010).
- [47] R. Kotsilkova, E. Ivanov, E. Krusteva, C. Silvestre, S. Cimmino, and D. Duraccio "Evolution of Rheology, Structure, and Properties around the Rheological Flocculation and Percolation Thresholds in Polymer Nanocomposites" in *Ecosustainable Polymer Nanomaterials for Food Packaging*. Edited by [Clara Silvestre](#), [Sossio Cimmino](#), CRC Press (2013)
- [48] Mendelson, R. *Polymer Engineering Science*, 8, 235 (1968).
- [49] X. He, J. Yang, L. Zhu, B. Wang, G. Sun, P. Lv, In Yee Phang, T. Liu. *Journal of Applied Polymer Science*, 102, 542 (2006)
- [50] Carreau, P. J.; De Kee, D. C. R.; Chhabra, R. P. *Rheology of Polymeric Systems: Principles and Applications*; Hanser: Munich, 1997.
- [51] Vikas Mittal, *Characterization Techniques for Polymer Nanocomposites*, John Wiley & Sons, (2012)
- [52] Dealy, J. & Wissburn, K. *Melt Rheology and its Role in Plastics Processing*, New York, Van Nostrand Reinhold. (1990)

## Chapter VI

---

***Mechanical ,Dynamic-Mechanical properties  
and morphological issues of PHBV based  
blown films containing Halloysite***

### 6.1 Introduction

Today manufacturers of products and packages have to meet several requests, such as lowering costs, improving performance and enhancing environmental attributes. Plastic films comprise a wide category of materials with different properties depending on application to which they are assigned. Polymeric films may be used in combination with other materials, such as aluminum or paper, in order to impart special properties[1].

Although the employment of plastic films substantially reduce the amount of material needed to make a product or package, there are, however, environmental issues associated with the production and disposal of plastics.

Composting of mixed organics is a potential strategy for recovering large quantities of waste. Compostable plastics can replace the non-degradable one, making composting a significant tool to divert large amounts of otherwise non recoverable waste from landfills. Compostable plastics combine the utility of plastics with the ability to completely biodegrade in a compost facility without separating them from organic wastes, enabling composting of a much larger amount of solid waste.

In the last decade, polyhydroxyalkanoates (PHA) have attracted a special attention due to their full biodegradability, biocompatibility and natural origin. Among resins involved in this family, several research efforts have been focused on poly(hydroxybutyrate-co-hydroxyvalerate) PHBV copolymers having performances very similar to those of polyolefins and thus being a potential substitute to petroleum-based materials. In particular, investigations have been performed to overcome specific drawbacks such as its fragility, thermal degradability at temperature not far above the melting point, and its high price by their blending with polymers [2,3] or by including opportune inorganic fillers [4] respectively. At this regard, with the awareness that the type of filler surface treatment plays a key role in the mechanical performances of products, several studies about the influence of chemical functionalization of fillers have been carried out. Based on this features the aim of this study was to manufacture and investigate the performances of blown films of a biodegradable polymer blend filled with Halloysite nanotubes HNTs (aluminosilicates). The choice of the film preparation method (film blowing) derives by the possibility of a good alignment or straightening of the high aspect ratio particles in films made by this process rather than by techniques such as compression molding.

The selected matrix was a blend of two copolymers : PHBV and PBAT (30:70 wt %) which are both biodegradable and compostable. PBAT(poly (butylene adipate-co-terephthalate) is a

biodegradable, statistical, aliphatic-aromatic copolyester having properties similar to low density polyethylene (LDPE) because of its high molecular weight and its branched molecular structure [5]. Halloysite nanotubes, untreated and chemically modified, were added to polymer matrix with the aim of improving their mechanical properties. ‘Halloysite clay enhances biodegradable and biocompatible nanocomposites, increases strength and provides new capabilities for consumer product, packaging and other application’[6]. Because of its unique hollow tubular structure, HNTs can be used as a carrier for the controlled release of special additives in order to obtain biodegradable films with antibacterial, antifungal, antioxidant, antimicrobial properties for food packaging applications.

### Experimental section

#### 6.2 Materials

A commercially available grade of PBAT/PHBV blend, Enmat 6010 P (Ningbo Tianan Biologic Material Co. Ltd.), with 70:30 weight ratio, was used in this study. Halloysite nanotubes (HNTs), used as filler, with average sizes equal to: 0.25-4 nm (length), 30 nm (diameter), 64 m<sup>2</sup>/g (surface area) and a specific gravity 2.53 g/cm<sup>3</sup> were provided by Sigma-Aldrich.

As confirmed by X-ray diffraction analysis Halloysite was in the dehydrated state showing a diffraction signal at 12.138 corresponding to a (001) basal spacing of approximately 7.3Å.

In an attempt to improve the dispersion of nanotubes within the polymer matrix an organosilane has been employed to modify the pristine surface of the clay, as described in the previous chapter.

The ATR\_FTIR analysis confirmed the success of the surface chemical modification [8] by the appearance of characteristic absorption band at 1470, 1637 and 1720 cm<sup>-1</sup> attributed to CH<sub>2</sub> scissoring, C-C and C-O stretching vibration respectively.

### 6.3 Preparation of bio-nanocomposites

The bio-nanocomposite of Enmat with various organically modified and natural HNTs was prepared using melt blending technique in a co-rotating twin screw extruder (HAAKE PolyLab, L/D=40). The matrix was melt mixed with nanoclays at different weight percentage (3, 5, 10 wt%) at a temperature difference from feed to die zone between 150 °C and 165 °C and screw speed of 100 rpm. The materials, opportunely pre-dried in a vacuum oven at 70°C for 12 hr, were pre-mixed by tumbling them in a closed plastic container.

Pure Enmat was also extruded under the same conditions to use as reference material.

Systematic thermogravimetric measurements, shown in chapter IV, confirmed the good agreement between nominal and actual filler contents.

Table 6.1 summarizes the compositions of composites and the abbreviation used in this work.

Formulation	Abbreviation
PBAT/PHBV	Enmat
PBAT/PHBV+3% Halloysite	3%HNTs
PBAT/PHBV+5%Halloysite	5%HNTs
PBAT/PHBV+10%Halloysite	10%HNTs
PBAT/PHBV+3% silanized Halloysite	3% f-HNTs
PBAT/PHBV+5% silanized Halloysite	5% f-HNTs
PBAT/PHBV+10%silanized Halloysite	10% f-HNTs

TAB. 6.1 Enmat/HNTs nanocomposite systems

### 6.4 Preparation of blown films

Film blowing of all extruded materials was accomplished using COLLIN single screw extruder (25:1 L/D) with three individually controlled temperature zones. The extruder was equipped with a COLLIN TEACH LINE BL50T with a diameter die of 30 mm, and a die-

gap of 0.8 mm was used. The velocity of the take-off rolls and the pressure inside the film “bubble” were adjusted in order to achieve a stable process and to avoid a double-walled

## Chapter VI

film impossible to separate after passage through the take up roll (blocking). The screw rotation speed was 27 rpm and the temperature profile equal to 160–175–175–165–160°C from the hopper to the die. Films having a thickness approximately equal to 35  $\mu\text{m}$  were manufactured with a blow up ratio (BUR) of 3.3 and maintaining the longitudinal draw ratio (DR) of 7. The homogeneity of the thickness of the film were quantitatively measured by cutting a 1m long film for all materials and measuring the thickness on at least five positions every 20 cm.

Optically the clarity of the films was not compromised by the addition of the fillers both untreated and modified ones(Fig.6.1).

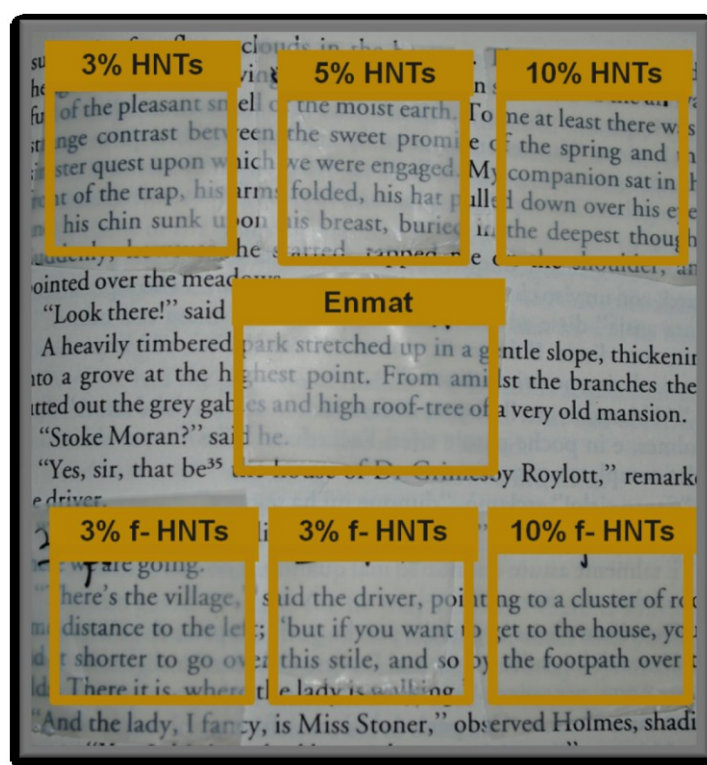


FIG.6.2 Film samples at different percentages of Halloysites

### 6.5 Characterization Techniques

#### 6.5.1 Tensile test

Tensile tests were performed at room conditions using a 5 kN load cell on a *Thensometer 2020 Alpha Technologies*. All measurements were carried out according to the ASTM D882-02. Tensile specimens, rectangular strips, were cut both in the flow direction of the extruder (MD) and in the perpendicular direction (TD). The gauge length was set at 50 mm and the deformation of specimens was set to a double speed, 25 mm/min for the determination of modulus and then 200 mm/min. At least five samples were tested for each investigated materials. Results reported in terms of tensile strength, yield stress, elongation at break and tensile modulus were always averaged on at least five tests.

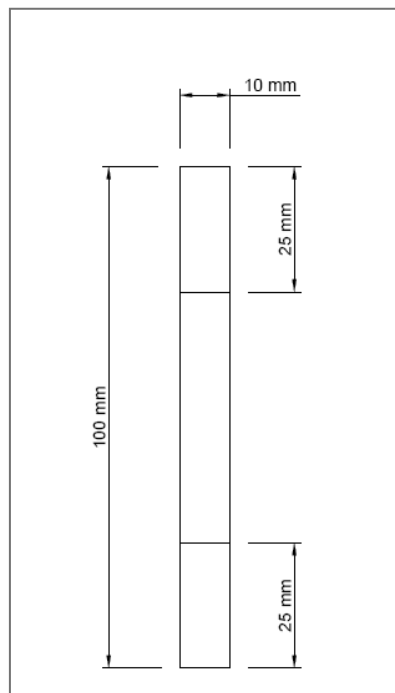


FIG 6.3 Shape of the tensile test sample.

### 6.5.2 Dynamic-Mechanical Analysis (DMA)

Dynamic mechanical analysis were assessed using a *DMA TRITEC 2000* over the temperature range from  $-80^{\circ}\text{C}$  to  $100^{\circ}\text{C}$  ( heating rate  $4^{\circ}\text{C}/\text{min}$ ) at an applied frequency of 1 Hz and strain amplitude of 0,01 mm.

A strain amplitude sweep test at 1 Hz frequency was carried out to assure that the tests were in the linear viscoelasticity region.

The tension mode method was used to measure storage modulus ( $E'$ ), loss modulus ( $E''$ ) and  $\tan \delta$  parameter of each sample.

The effective specimen size was  $5 \times 10 \times 0,035 \text{ mm}^3$ . A pre-tension of 1 N was applied on the specimens to avoid its slackening during the vibration.

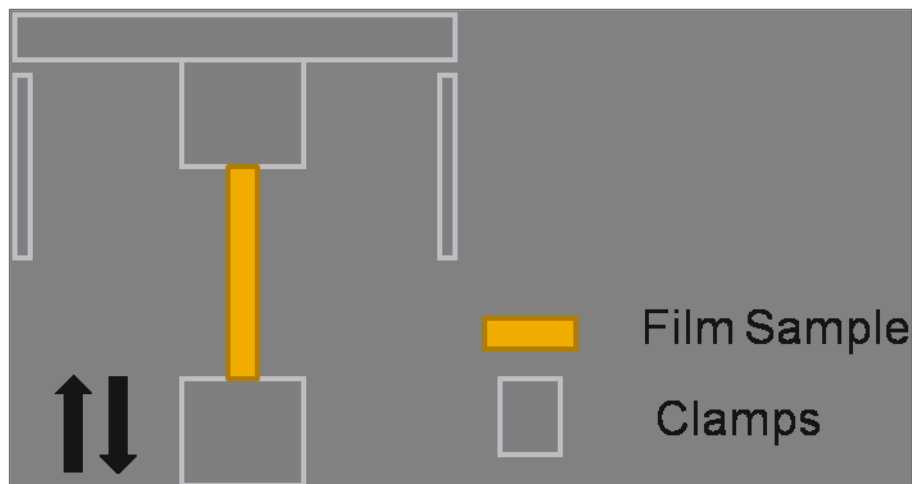


FIG.6.4 Illustration of a tension mode clamp in DMA

### 6.6 Morphological analysis

Morphological features of films were highlighted by using a Scanning Electron Microscope (Philips XL 20 Series , with an accelerating voltage of 30.0 kV).

6.7 Results and discussion

6.7.1 Tensile test

Figures 6.5 and 6.6 report typical stress-strain curves of all composite blown films stretched along machine (MD) and transverse (TD) direction, respectively.

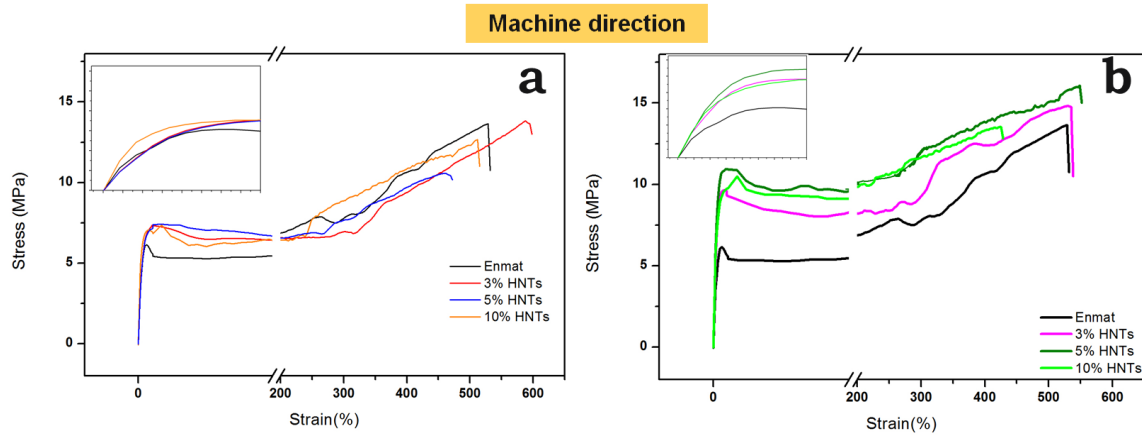


FIG.6.5 Representative curves of tensile test in MD of composite films containing a) as received and b) modified Halloysite

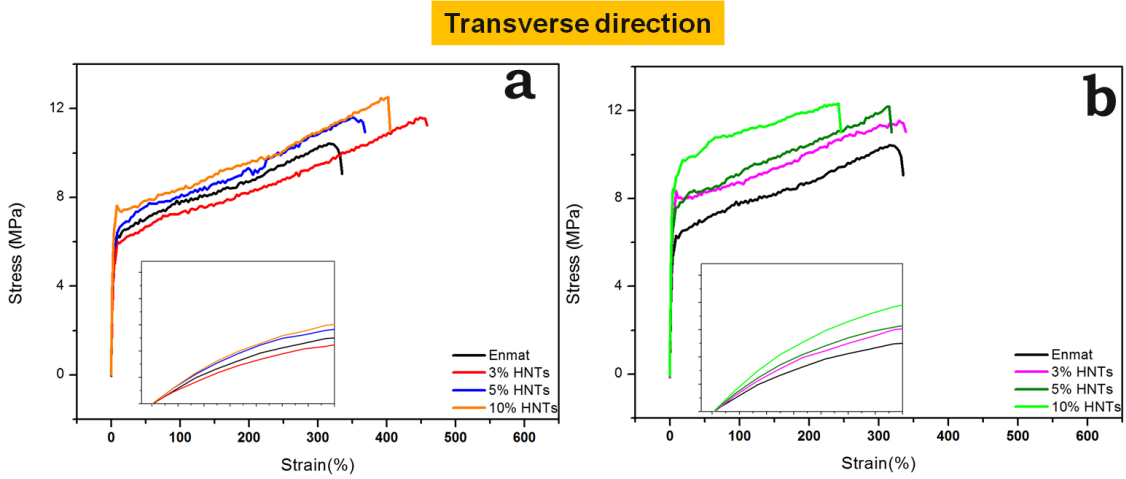


FIG.6.6 Representative curves of tensile test in MD of composite films containing a) as received and b) modified Halloysite

## Chapter VI

---

MD stress –strain curves showed a necking behavior which gradually propagates until all the material is cold drawn. Finally, the stress increased until failure takes place and a strain hardening was observed .

About TD tests, instead, the necking disappeared, except in the specimens containing 10% HNTs and 3% f-HNTs.

It is evident that the inclusion of clay nanotubes induces an increase of the stress at yield, especially in presence of functionalized fillers. Analogously, an increase of the tensile strength and negligible effects on the elongation at break are observed for the composite systems with respect to the neat film . In particular, focusing the attention on samples containing untreated HNTs, the increase of yield stress verified by the addition of 5 wt% of nanotubes seems to be not further enhanced by increasing the filler loading (10 wt%). This behaviour has been attributed to probable agglomerations of nanotubes, reducing the effective surface area which can undergo filler-matrix interactions.

In terms of stiffness, as clearly highlighted by expanding the low-strain region of the stress-strain curve, as expected, the inclusion of rigid nanofillers results in an increasing of the tensile modulus of the composite film samples. This effect is not strictly proportional to the clay nanotubes content and it essentially occurs without detrimental effects on the ultimate mechanical properties. In general, the inclusion of nanotubes up to 10% leads to a stiffness increase of the film samples, especially in presence of silanized ones. In particular, in MD, at equal filler content, the Young's modulus of the composite films with functionalized HNTs was increased approximately 60% with respect to the neat matrix, while in TD this benefit was more restrained. At this regard, considering that preliminary calorimetric investigations (chapter IV) have shown a negligible influence of the clay nanotubes on the hosting matrix crystallinity, the improvement of the tensile strength and modulus, without a significant loss in ductility, has been essentially ascribed to a satisfactory adhesion between the clay nanotubes and the matrix and the occurrence of an adequate distribution of the inorganic phase. As a consequence, an efficient stress transfer at the matrix-filler interface is obtained. Mechanical properties are higher in the MD than in the TD. This is attributable to orientation of the clay in the plane of the film (as confirmed by XRD analysis in the chapter 4).

Figures 6.7 and 6.8 show the evolution of the yield stress and Young's modulus (determined from the initial slope of the stress-strain curves) as a function of the halloysite content comparing systems containing untreated and functionalized nanotubes.

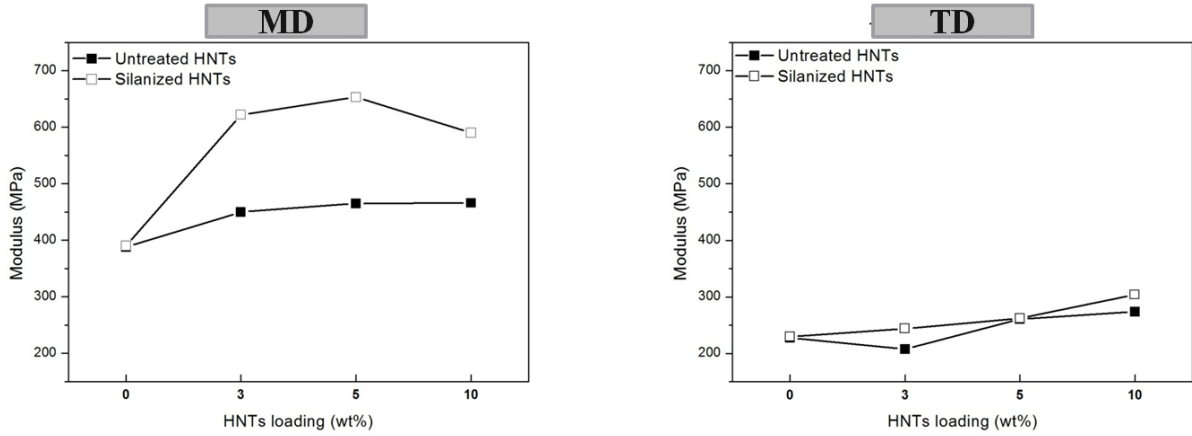


FIG. 6.7 Modulus as function of HNTs loading in machine (MD) and transverse (TD) direction

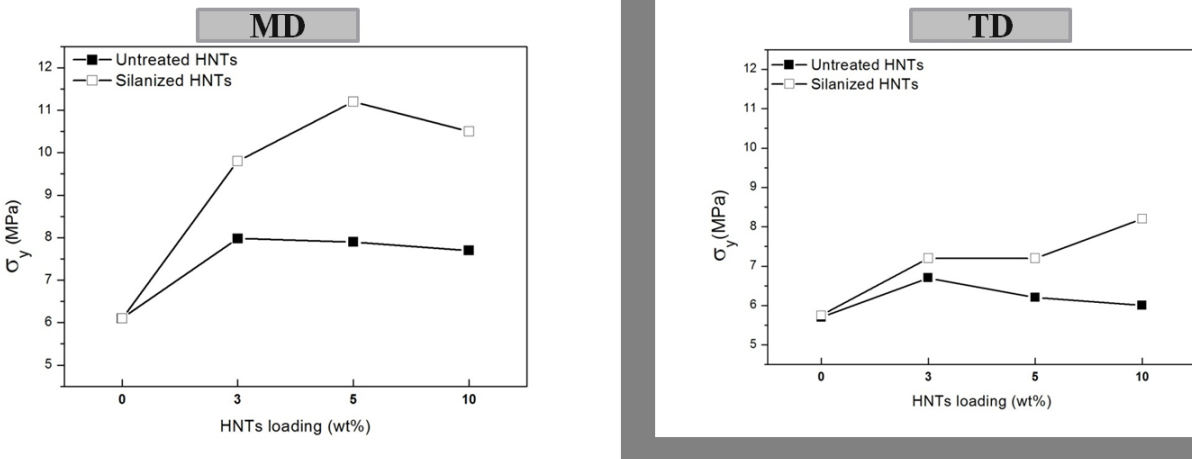


FIG. 6.7 Stress at yield as function of HNTs loading in machine (MD) and transverse (TD) direction

## Chapter VI

In table 6.2 the tensile parameters of composite films are summarized.

<b>Filler content</b>	<b>E (MPa)</b>	<b><math>\sigma_y</math> (MPa)</b>	<b><math>\sigma_b</math> (MPa)</b>	<b><math>\epsilon_b</math> (%)</b>	<b>Direction</b>
<b>0</b>	228 ( $\pm 21$ )	5,7 ( $\pm 0,4$ )	10,3 ( $\pm 0,5$ )	313( $\pm 65$ )	<b>TD</b>
	398 ( $\pm 42$ )	6,1 ( $\pm 0,3$ )	12,4 ( $\pm 1,0$ )	536 ( $\pm 22$ )	<b>MD</b>
<b>3% HNTs</b>	208 ( $\pm 19$ )	6,7 ( $\pm 0,8$ )	11,2 ( $\pm 0,4$ )	401 ( $\pm 60$ )	<b>TD</b>
	450 ( $\pm 27$ )	7,9 ( $\pm 0,4$ )	14,3 ( $\pm 0,6$ )	565 ( $\pm 15$ )	<b>MD</b>
<b>5% HNTs</b>	261( $\pm 10$ )	6,2 ( $\pm 0,3$ )	10,6 ( $\pm 0,8$ )	366 ( $\pm 15$ )	<b>TD</b>
	465 ( $\pm 36$ )	7.9 ( $\pm 0,2$ )	11,3 ( $\pm 0,9$ )	533 ( $\pm 61$ )	<b>MD</b>
<b>10% HNTs</b>	274 ( $\pm 18$ )	6,0 ( $\pm 0,4$ )	11,8 ( $\pm 0,6$ )	414 ( $\pm 39$ )	<b>TD</b>
	466 ( $\pm 10$ )	7,7 ( $\pm 0,3$ )	12,6 ( $\pm 0,4$ )	540 ( $\pm 40$ )	<b>MD</b>
<b>3% f-HNTs</b>	244 ( $\pm 15$ )	7,2( $\pm 0,6$ )	11,5 ( $\pm 0,3$ )	368 ( $\pm 42$ )	<b>TD</b>
	622 ( $\pm 41$ )	9,8 ( $\pm 0,5$ )	14,1 ( $\pm 0,6$ )	569 ( $\pm 26$ )	<b>MD</b>
<b>5% f-HNTs</b>	262( $\pm 15$ )	7,2 ( $\pm 0,5$ )	10,8 ( $\pm 0,3$ )	321 ( $\pm 32$ )	<b>TD</b>
	653( $\pm 23$ )	11,2( $\pm 0,4$ )	16,3 ( $\pm 0,9$ )	629 ( $\pm 27$ )	<b>MD</b>
<b>10% f-HNTs</b>	304 ( $\pm 32$ )	8,2 ( $\pm 0,6$ )	11,0 ( $\pm 0,9$ )	265 ( $\pm 47$ )	<b>TD</b>
	590 ( $\pm 16$ )	10,5( $\pm 0,3$ )	12,5 ( $\pm 0, 4$ )	436 ( $\pm 66$ )	<b>MD</b>

TAB.6.2 Tensile parameters of Enmat/HNTs composite films

The interfacial interaction between the fillers and matrix is an important factor affecting the mechanical properties of composites. The behaviour of the tensile yield strength has been modelled in terms of adhesion. At this regard the Nicolais-Narkis model [9], predicting the tensile strength of nanocomposites without adhesion between the matrix and the nanoparticles, has been considered . In this case the interfacial layer would be unable to transfer stress.

The general expression of the model is the following:

$$\sigma_{y,c} = \sigma_{y,m} (1 - \alpha \varphi^\beta)$$

where  $\sigma_{y,c}$  and  $\sigma_{y,m}$  are the yield stress values of the composite and of the neat matrix, respectively;  $\varphi$  is the volume fraction of the filler while  $\alpha$  and  $\beta$  are constants related to filler-matrix interaction and geometry of the filler, respectively. In the absence of interfacial adhesion, the model may be expressed by this simple expression:

## Chapter VI

$$\frac{\sigma_{y,c}}{\sigma_{y,m}} = 1 - 1.21\varphi^{2/3}$$

The volume fraction of the filler determined by the following:

$$\varphi = \rho_m W_f / [(\rho_m - \rho_c)W_f + \rho_c]$$

where  $\rho_m$  is matrix density (1,25 g/cm<sup>3</sup>) and  $\rho_c$  is filler one (2,53 g/cm<sup>3</sup>).

In table 6.3 are reported the values of volume fractions of halloysite nanoparticles.

TAB. 6.3 Volume fraction of HNTs

<b>W<sub>f</sub> (wt%)</b>	<b>φ (vol%)</b>
<b>3,00</b>	<b>1,50</b>
<b>5,00</b>	<b>2,53</b>
<b>10,00</b>	<b>5,20</b>

The plot of the experimental and theoretical tensile yield stress ratio of the composite and matrix versus HNTs content is shown (Figure 6.8).

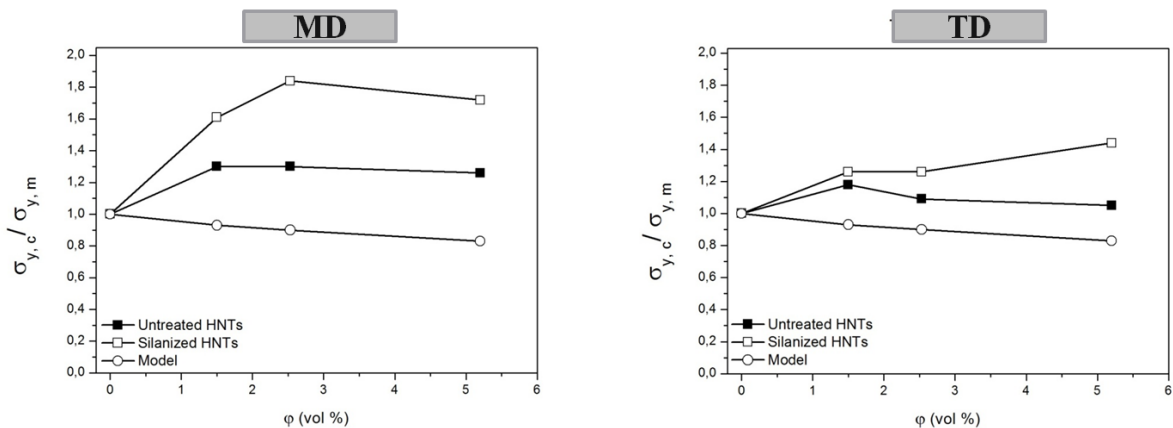


FIG 6.8 Comparison of experimental and theoretical tensile yield stress ratio of the composites and matrix.

Clearly, the experimental values are always higher than the theoretical ones: sign of the presence of a certain level of interfacial adhesion between the clay nanotubes and the hosting matrix. This effect is more pronounced in presence of functionalized filler especially in MD. Consequently, the applied stress can be easily transferred from the polymer matrix to the halloysite nanoparticles.

On the other hand, to quantify the level of adhesion at the filler-matrix interface, yield strength values have been also modelled by the Pukanszky model [10,11].

This model assumes that an interphase forms spontaneously in composites and that the yield stress changes proportionally to its actual value as a function of filler volume fraction according to following equation:

$$\frac{\sigma_{y,c}}{\sigma_{y,m}} = \left( \frac{1-\varphi}{1+2.5\varphi} \right) \exp(B\varphi)$$

where  $\sigma_{y,c}$  and  $\sigma_{y,m}$  are the yield stress of the composite and the matrix, respectively,  $\varphi$  is the volume fraction of the filler in the composites, and B is a parameter related to the macroscopic characteristics of the filler-matrix interface and interphase.

$$B = (1 + A_f \rho_f t) \ln(\sigma_{y,i} / \sigma_{y,m})$$

t,  $\sigma_{y,i}$ ,  $A_f$ ,  $\rho_f$  are the thickness of the interface, the strength of interaction, the specific surface area and density of the filler, respectively.

Generally, if the value of “B” is zero, the filler acts as a void, and the value of “B” depends on the factor influencing the load bearing capacity such as strength and thickness of the interface.

Otherwise, the higher the “B” value, the stronger are the surface interactions (via thickness and/or strength). As reported in literature, the “B” value for polymer nanocomposites ranges between 2 and 15 depending on the interaction level [12].

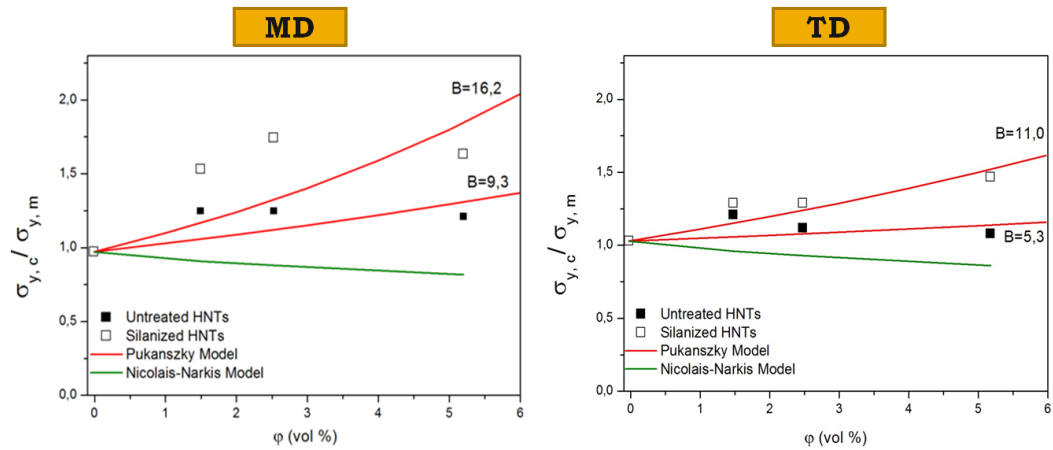


FIG. 6.9 B parameter for different nanocomposite films evaluated in machine (MD) and transverse (TD) direction

Comparing the measured tensile yield stress values with those calculated using Pukanszky model along the transverse (TD) direction, the surface treatment of halloysites leads to the highest value of the B parameter as a sign of strongest surface interactions. Experimental values match Pukanszky predictions quite well.

In machine (MD) direction, instead, considering systems with modified HNTs, the calculated B parameter is 16,2 which indicates a considerable load transfer mechanism. The model fit leads to lower  $\sigma_y$  values. However, the mechanical properties of composite materials are strongly influenced by anisotropy and orientation of the nanofillers and these issues are not evaluated in the model.

## 6.7.2 Dynamic-Mechanical properties

The storage modulus ( $E'$ ) and the loss factor ( $\tan \delta$ ) peaks were recorded as a function of temperature for both Enmat/HNT and Enmat /f-HNT nanocomposites along machine (MD) and transverse (TD) direction (Fig. 6.10-6.11).

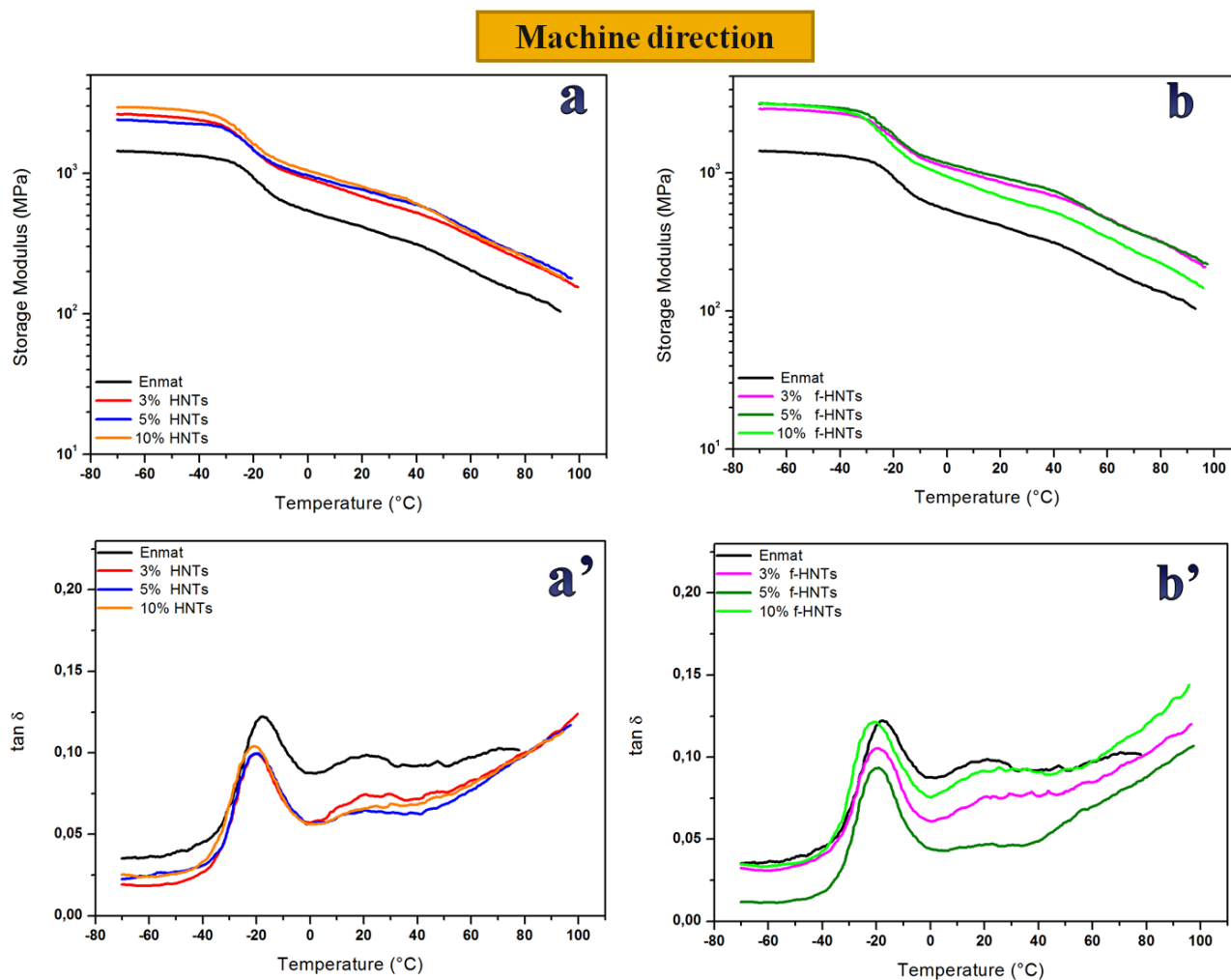


FIG.6.10 Storage modulus and  $\tan \delta$  versus temperature for Enmat/HNTs (a, a'), and Enmat/f-HNTs (b,b') nanocomposite films tested along the machine direction.

For the nanocomposite films, there was a significant enhancement of the modulus over the investigated temperature range, with respect to the neat film. Moreover, the modulus increased by increasing the filler content because of the strengthening effect of the clay nanotubes. A further increase of the storage modulus was observed for the Enmat/f-HNTs nanocomposites indicating the better interactions and compatibility between Enmat and HNTs.

## Chapter VI

When the modified clay content is 10% wt, the agglomeration of HNTs weakens the interaction between the matrix and the nanoparticles so the storage modulus increases but to a lesser extent.

Noticeable difference was not seen between the properties in the machine direction and the transverse direction for the blown films. In the cross direction the filler effects on the storage modulus are less pronounced than those shown before. This could be a further validation of the orientation of clay nanotubes along the machine direction.

Nevertheless, the decrease of the storage modulus with increasing temperature is less pronounced in all the examined nanocomposite films.

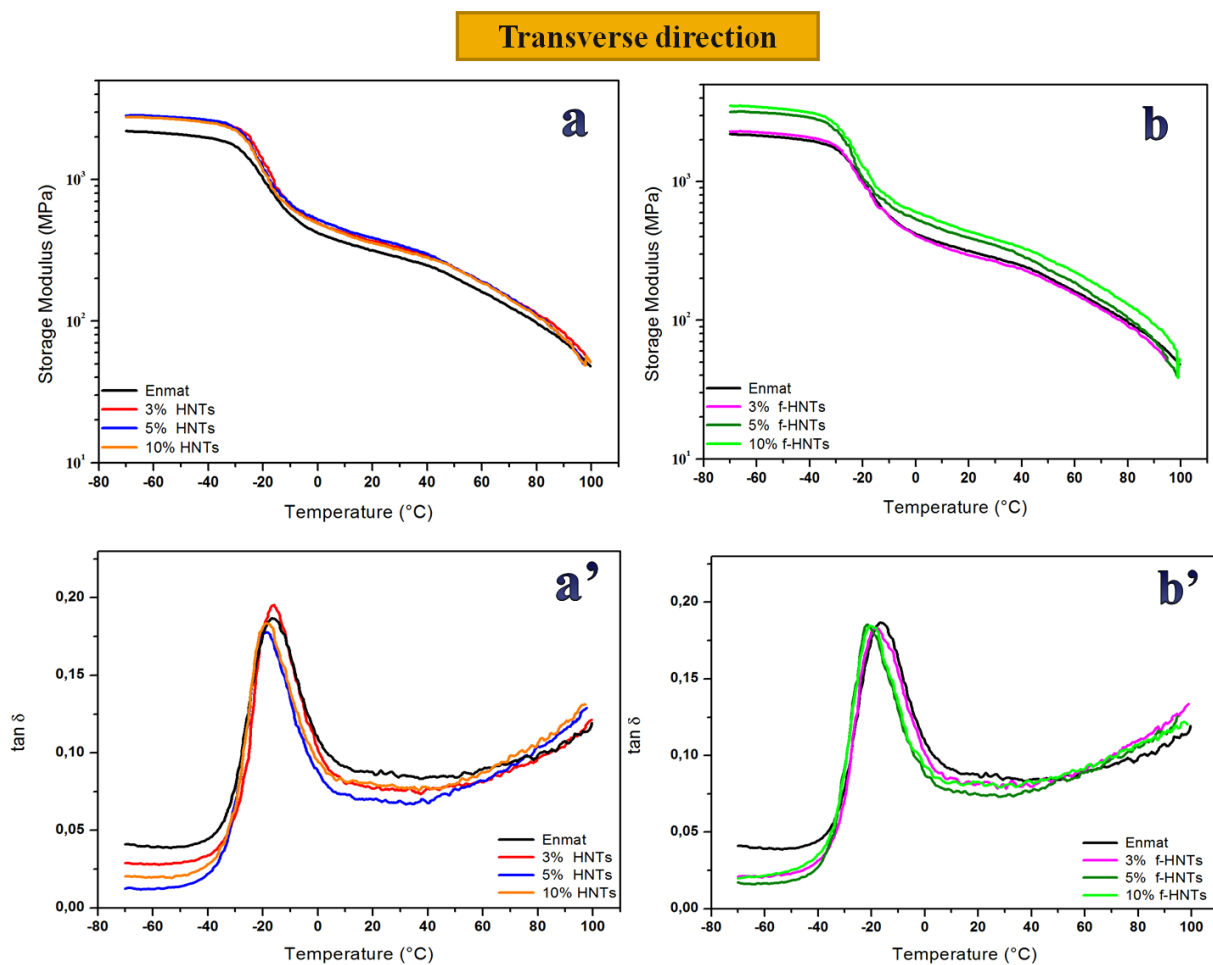


FIG.6.10 Storage modulus and  $\tan \delta$  versus temperature for Enmat/HNTs (a, a'), and Enmat/f-HNTs (b,b') nanocomposite films tested along the transverse direction.

The elasticity of a material is measured by  $\tan \delta$ , which is the ratio of energy dissipated to

## Chapter VI

energy stored per cycle. Thus, elasticity is inversely proportionate to  $\tan \delta$  [13].

In the machine direction nanocomposite films were more elastic than neat Enmat as shown by lower  $\tan \delta$  (fig.6.9 a',b'). The height of the damping peaks of nanocomposite films, in fact, was lower than those of PHBV/PBAT matrix. This is a consequence of the reduced matrix molecular mobility caused by the nanotubes which affect the polymer chain relaxation. The values of glass transition temperature ( $T_g$ ) were obtained from the temperature corresponding to  $\tan \delta$  peak. As it can be seen from the fig. 6.9 (b,b'), the pure Enmat showed two distinct transitions: one at  $\sim -20^\circ\text{C}$ , which corresponds to the glass-rubber transition of PBAT and the other at  $20^\circ\text{C}$ , related to the transition of the hard rigid PHBV phase.

The presence of HNTs significantly reduced the height of the peak related to the transition of PHBV.

To summarize, in the table 6.4 the glassy and rubbery storage modulus values for all investigated film samples are reported.

The data confirm the increase of the storage modulus by addition of halloysites especially for samples tested along the longitudinal direction. This effect, not proportional to the filler loading, appears to be more pronounced in presence of modified halloysites.

Filler content (wt%)	$E'_{\text{glassy state}}$ (MPa)	$E'_{\text{rubbery state}}$ (Mpa)	$T_g$ ( $^\circ\text{C}$ )	Direction
<b>0</b>	1996	308	-17,2	<b>TD</b>
	1430	430	-19,6	<b>MD</b>
<b>3% HNTs</b>	2316	320	-18,4	<b>TD</b>
	2486	672	-21,4	<b>MD</b>
<b>5% HNTs</b>	2470	344	-19,0	<b>TD</b>
	2300	798	-20,6	<b>MD</b>
<b>10% HNTs</b>	2404	320	-19,1	<b>TD</b>
	2793	751	-20,3	<b>MD</b>
<b>3% f-HNTs</b>	2046	299	-17,9	<b>TD</b>
	2773	829	-21,1	<b>MD</b>
<b>5% f-HNTs</b>	2785	347	-18,8	<b>TD</b>
	2847	832	-20,6	<b>MD</b>
<b>10% f-HNTs</b>	2700	397	-19,9	<b>TD</b>
	2855	657	-19,5	<b>MD</b>

TAB. 6.4 Comparative DMA data of Enmat nanocomposites containing HNTs and f- HNTs

About the glass transition temperature, no significant variation can be observed.

### 6.8 Morphological analysis

A homogeneous dispersion of halloysites and strong interfacial interactions between polymer matrix and nanotubes can effectively improve the mechanical properties of polymer nanocomposites [16,17,18].

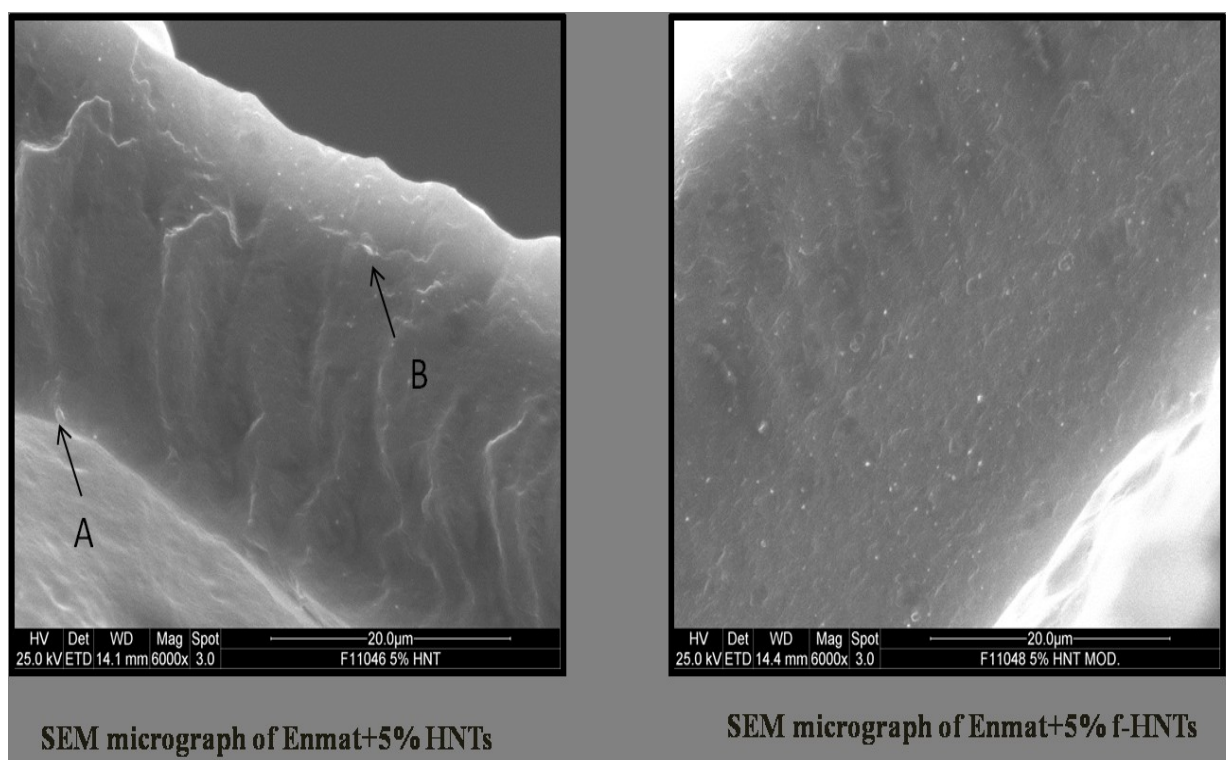
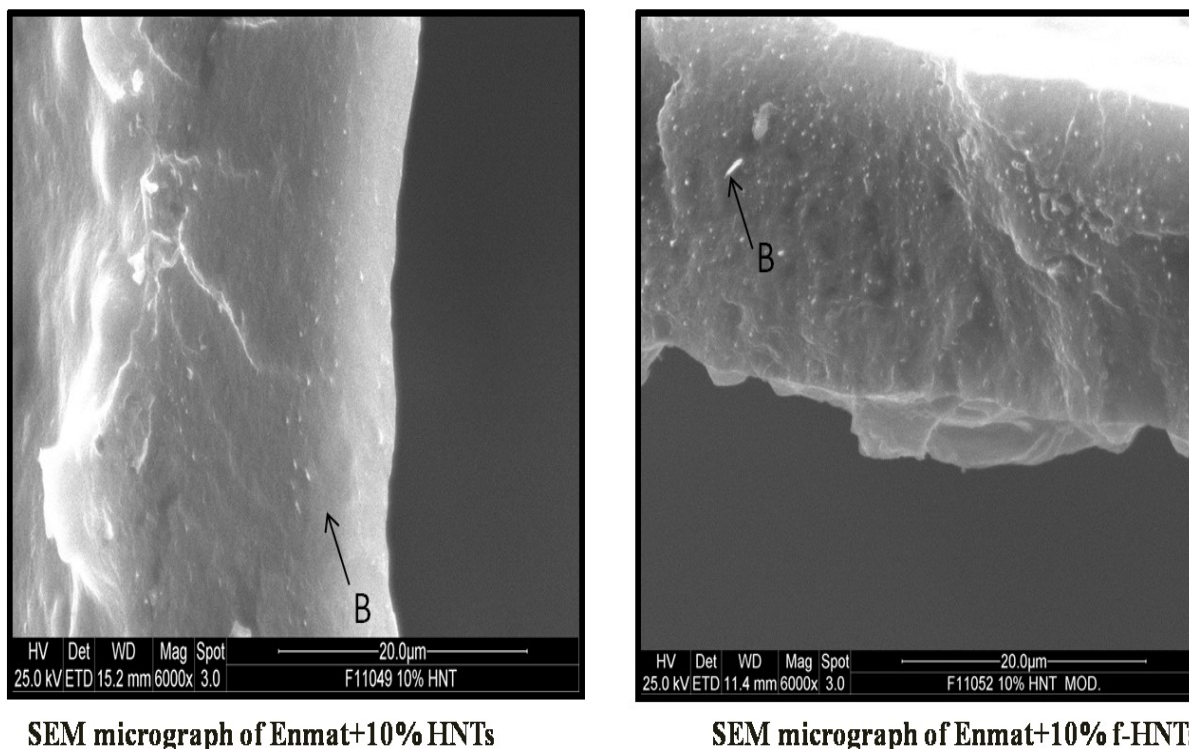


FIG.6.11 Comparison of SEM images of nanocomposite films containing 3 wt % of unmodified and functionalized halloysites



SEM micrograph of Enmat+10% HNTs

SEM micrograph of Enmat+10% f-HNTs

FIG.6.12 Comparison of SEM images of nanocomposite films containing 5 wt % of unmodified and functionalized halloysites

The SEM images of Enmat /HNTs and Enmat /f-HNTs nanocomposite films are shown in Figure 6.11-6.12. The dispersion of unmodified halloysites (HNTs) is not very good and whereas some aggregates are visible (marked as A). In case of nanocomposites with functionalized halloysites, the nanotubes are uniformly dispersed and distributed in the matrix even at high HNTs loading.

Moreover a good interface is observed between HNTs and Enmat matrix. Halloysite nanotubes (marked as B) appear to be not extensively debonded as well as visibly embedded in the Enmat matrix. Most HNTs are broken rather than pulled out from the polymer matrix .

### 6.9 Conclusion

Blown films of neat PHBV/PBAT 30/70 w/w blend and its composites containing up to 10 wt% of clay nanotubes have been characterized in terms of mechanical and dynamic mechanical properties. The influence of both unmodified (HNTs) and silanized halloysite nanotubes (f-HNTs) has been analyzed by tests performed in machine and transverse directions.

Mechanical tests have demonstrated that strength and modulus of nanocomposite systems significantly increase with addition of halloysites without significant loss of ductility.

Dynamic-mechanical analysis have evidenced a slight decrease in glass transition temperature as well as an improvement in storage modulus with the incorporation of halloysites especially in case of surface modified ones. A homogeneous dispersion of the modified nanotubes was obtained in the Enmat matrix.

## Bibliography

---

- [1] Understanding plastic film: Its Uses, Benefits and Waste Management Options Prepared for the American Plastics Council by Headley Pratt Consulting (1996) available at <http://plastics.americanchemistry.com/Understanding-Plastic-Film>
- [2] Nanda, M. R., Misra, M. and Mohanty, A. K., *Macromol. Mater. Eng.*, 296: 719 (2011)
- [3] J. Tao, C.Song, Mingfeng Cao, D. Hu, Li Liu, Na Liu, S. Wang, *Polymer Degradation and Stability*, 94, 4,575 (2009)
- [4] G. X. Chen, G. J. Hao, T. Y. Guo, M. D. Song, B. H. Zhang *Journal of Materials Science Letters* , 21, 20, 1587 (2002)
- [5] Smita Mohanty & Sanjay Kumar Nayak *Int J Plast Technol* 14, 2, 192 (2010)
- [6] Aaron L. Wagner, Sarah Cooper, and Michael Riedlinger. *Industrial Biotechnology*. Fall, 1,3 190 (2005).
- [7] M. Du, B. Guo, and D. Jia, *Eur. Polym. J.* 42, 1362 (2006).
- [8] N.N. Herrera, J.-M. Letoffe, J.-P. Reymond, and E. Bourgeat-Lami, *J. Mater. Chem.* 15, 863 (2005).
- [9] Nicolais L., Narkis M. *Polym. Eng. Sci.* 11, 194 (1971)
- [10] Pukanszky B. *New Polymeric Mater.* 3, 205 (1992)
- [11] Szazdi, L.; Pukanszky, Jr.; B.; Vancso, G. J. *Polymer*, 47, 4638 (2003).
- [12] Dayma, N.; Satapathy, B. K. *Mater. Des.* 31, 4693 (2010).
- [13] P. Pasbakhsh, H. Ismail, M.N Ahmad Fauzi, A. Abu Bakar. *Applied Clay Science*, 48, 3, 405 (2010).
- [14] Liu, X., Wu, Q.,. *Polymer* 42, 10013 (2001).
- [15] J.S. Shelley, P.T. Mather, K.L. DeVries , *Polymer* 42, 5849 (2001) .
- [16] Prashantha, K.; Soulestin, J.; Lacrampe, M. F.; Krawczak, P.; Dupin, G.; Claes, M. *Compos. Sci. Technol.*, 69, 1756 (2009).
- [17] Gupta B.; Lacrampe, M. F.; Krawczak, P. *Polym. Polym. Comp.* 14, 13, (2006).
- [18] Prashantha, K.; Soulestin, J.; Lacrampe, M. F.; Claes, M.; Dupin, G.; Krawczak, P. *Express Polym. Lett.* 2, 735,(2008).

## *Conclusions*

### Conclusions

The aim of this study was to develop biodegradable and compostable material with good performances that can be used in food packaging applications.

Nanocomposites, based on PBAT/PHBV blend and various concentrations of neat or silanized Halloysite nanotubes, were obtained using melt compounding technique and subsequently blown films were prepared.

The conclusions that could be drawn from this work are the following:

- ✓ From thermal analysis the simultaneous occurrence for the PHBV phase of both homogeneous crystallization and heterogeneous nucleation promoted by the included fillers was observed. These phenomena show effects of mutual entities depending on the quality of the filler–matrix interface and the applied cooling rate. On the contrary, for the PBAT phase, although the filler may alter kinetics and mechanisms of crystallizations, no effect is reported in terms of its degree of crystallinity. All these evidences have been supported by structural investigations. Moreover, X-ray diffraction analysis indicated that the process of film blowing enables the formation of more perfect crystals and, as expected, favors the orientation of the included nanotubes of clay.

An increase in thermal stability was observed after addition of both untreated and functionalized halloysites.

- ✓ From rheological measurements, increase in the complex viscosity and in the storage moduli of nanocomposites was shown. The effects of filler on viscoelastic behavior of composite systems are emphasized by improving the filler-matrix interface. In particular, in presence of the highest loading of silanized halloysite incipient flocculation phenomena seems to occur. The nanocomposites with the increasing Halloysites content exhibited higher zero shear viscosities and more rapid shear thinning behavior than pure matrix, which results from the reorientation of dispersed clay particles. Shear viscosities were well represented by the Carreau model.

The filler does not appear to alter the extrudability of the hosting matrix, remaining the measured viscosity in the same order of magnitude of pure blend.

The choice of processing temperature may be exclusively related to the level of filler distribution able to ensure optimal viscoelastic behavior of the melts.

- ✓ Mechanical tests have demonstrated that strength and modulus of nanocomposite systems significantly increase with addition of halloysites without significant loss of ductility. Good interfacial adhesion is required for the effective stress transfer between components in the multi-phase polymer blends. At this regard, in order to evaluate the interaction level between the filler and the matrix, two model were considered: the Nicolais-Narkis model and the Pukanszky model.
  
- ✓ Dynamic-mechanical analysis have evidenced a slight decrease in glass transition temperature as well as an improvement in storage modulus with the incorporation of halloysites especially in case of surface modified ones.

The obtained results showed that these composites films were promising materials for replacing non degradable materials in specific applications.

The nanocomposites investigated showed improved mechanical properties over that of the neat polymer. with no reduction in optical transparency. In addition, because of its unique hollow tubular structure, HNTs can be used as a carrier for the controlled release of special additives in order to obtain biodegradable films with antibacterial, antifungal, antioxidant, antimicrobial properties for food packaging applications.